New green solvents and additives for the industry of printing inks

Francesco Taddeo

NICL: Naples Industrial Chemistry Laboratory

Chemical Sciences Department

University of Naples Federico II

Naples, 2022

Supervised by

Professor Martino Di Serio
NICL: Naples Industrial Chemistry Laboratory
Chemical Sciences Department
University of Naples Federico II

Table of contents

Abstract

Biomass represents an extremely important alternative to the conventional raw materials derived from fossil resources. The growing attention towards environmental safety has led to the development of new processes starting from renewable resources.

The present thesis is devoted to the use of two different chemicals, pelargonic acid and levulinic acid, commercially available that can be obtained from biomass. In particular, this thesis can be theoretically divided into three main parts.

The first part is focused on the esterification reaction of pelargonic acid with 2-ethylhexanol. A batch and continuous kinetic study were performed in the presence of both homogeneous (sulfuric acid) and heterogenous catalysts. As for the heterogenous catalysts, different types were tested: among these Amberlyst-15 and Amberlite IR120 were tested both in batch and in continuous apparatus while a synthetic catalyst (H_2WO_4/SiO_2) was tested in batch reactor. In the case of the batch kinetic investigation different experimental conditions (stirring rate, temperature, reactants molar ratio and catalyst load) were varied in order to determine the kinetic and thermodynamic parameters. As for the continuous kinetic study, instead, temperature, reactants molar ratio and volumetric flowrate were varied. It was demonstrated that for the considered heterogeneous catalysts, an internal mass transfer limitation occurred. A kinetic model was elaborated obtaining a good agreement between the experimental data and the simulated curves. Overall, Amberlyst-15 showed a better behavior compared to Amberlite IR120 due to the different structure of the resins themselves and a more accessible pores in the case of Amberlyst-15 leading to a lower intraparticle mass transfer limitation.

The second part of the present thesis was focused on the synthesis of solvents to use in the formulation of printing inks through an esterification reaction of the pelargonic acid itself with 2-ethylhexanol. In this case, a different reactor

configuration was considered consisting in a loop reactor and for this purpose, Amberlyst-15 was chosen as heterogenous catalyst. The solvents synthesized in all these experiments were tested in formulations for printing inks investigating their characteristics and evaluating the rheological properties of the derived inks. The obtained results confirmed the excellent properties of these solvents compared to what is reported in the literature.

The third part of the thesis was devoted on the ketalization reaction: this part started with the batch kinetic study of the ketalization of acetone and glycerol and after that the attention was focused on ethyl levulinate ketalization with glycerol. Firstly, a catalytic screening was made to investigate the best catalysts for this reaction. Among these, different types of zeolites, ion exchange resins and a synthetic catalyst were tested. The most promising resulted to be Dowex 50WX8 among the resins and Y zeolite and beta zeolite. Based on these results, Y-zeolite was firstly chosen to perform a kinetic study and several tests were performed in different experimental conditions in order to evaluate their effect on the reaction rate and determine thermodynamic and kinetic parameters.

List of Publications

I. V. Russo, **F. Taddeo**, T. Cogliano, R. Vitiello, R. Esposito, R. Tesser, T. Salmi, M. Di Serio, Investigation of the intrinsic reaction kinetics and the mass transfer phenomena of nonanoic acid esterification with 2-ethylhexanol promoted by sulfuric acid or Amberlite IR120, *Chemical Engineering Journal* **2021**, 408, 127236.

II. **F. Taddeo**, R. Esposito, V. Russo, M. Di Serio, Kinetic Modeling of Solketal Synthesis from Glycerol and Acetone Catalyzed by an Iron(III) Complex, *Catalysts* **2021**, 11, 83.

III. **F. Taddeo**, R. Vitiello, R. Tesser, M. Melchiorre, K. Eränen, T. Salmi, V. Russo, M. Di Serio, Nonanoic acid esterification with 2-ethylhexanol: from batch to continuous operation, *Submitted to Chemical Engineering Journal*.

List of other Publications

I. Y. Meng, **F. Taddeo**, A.F. Aguilera, X. Cai, V. Russo, P. Tolvanen, S. Leveneur, The Lord of the Chemical Rings: Catalytic Synthesis of Important Industrial Epoxide Compounds, *Catalysts* **2021**, 11, 765.

II. R. Vitiello, **F. Taddeo**, V. Russo, R. Turco, A. Buonerba, A. Grassi, M. Di Serio, R. Tesser, Production of Sustainable Biochemicals by Means of Esterification Reaction and Heterogeneous Acid Catalysts, *ChemEngineering* **2021**, 5, 46.

Conference contributions

i. **F. Taddeo**, V. Russo, R. Esposito, R. Turco, R. Vitiello, R. Tesser, F. Ruffo, M. Di Serio, Kinetic study of solketal formation from glycerol and acetone, XXI Congresso Divisione Chimica Industriale, Salerno, August 27, 2019.

ii. **F. Taddeo**, Chemicals production from biosuccinic acid, XXI Congresso Divisione Chimica Industriale, Salerno, August 27, 2019.

iii. **F. Taddeo**, R. Vitiello, V. Russo, R. Esposito, M. Melchiorre, V. Benessere, F. Ruffo, M. Di Serio, Esters from pelargonic acid and their application as green solvents for printing inks, Chemistry meets Industry & Society (CIS2019), Salerno, August 28-30, 2019.

iv. **F. Taddeo**, R. Vitiello, V. Russo, R. Turco, R. Tesser, R. Esposito, V. Benessere, M. Melchiorre, M. Di Serio, Esters from pelargonic acid as green solvents for printing inks, International Congress on Catalysis for Biorefineries (Catbior), Turku/Åbo, September 23-27, 2019.

v. **F. Taddeo**, V. Russo, R. Vitiello, R. Turco, R. Tesser, M. Di Serio, About the Kintics of Pelargonic acid esterification with 2-Ethylhexanol, Merck Young Chemists' Symposium 2019, Rimini, November 25-27, 2019.

vi. **F. Taddeo**, R. Vitiello, V. Russo, R. Tesser, R. Turco, R. Esposito, F. Ruffo, M. Di Serio, Nonanoic acid esters as solvents for printing inks using zinc acetate as catalyst, XVII PhD Day of Consorzio Interuniversitario Reattività Chimica e Catalisi, Venezia_Webinar, April 29-30, 2021.

vii. **F. Taddeo**, V. Russo, R. Esposito, R. Vitiello, R. Turco, R. Tesser, F. Ruffo, M. Di Serio, Kinetics of solketal synthesis promoted by

Iron(III) complex, XXVII Congresso Nazionale della Società Chimica Italiana, September 14-23, 2021.

Chapter 1 – Introduction

1.1 Biomass

Nowadays great attention is focused on the valorization of biomass as a valid way to replace and minimize the use of toxic chemicals [1]. The growing use of renewable sources has numerous benefits in terms of environmental and human health thanks to the replacement of the classical products with alternatives such as biodegradable plastics [1]. Fossil sources are progressively decreasing due to the higher demand in the last period. For this reason limiting the negative effect connected with their use on the environment together with the emissions of carbon dioxide due to their combustion is of utmost importance today [2]. Biomass, in particular lignocellulosic biomass which is the most abundant on Earth, are considered a sustainable alternative to petroleum for the production of fuels and chemicals with no emission of carbon dioxide [3]. The use of biomass for the energy production lead to a lower emission of greenhouse gases since carbon dioxide produced during this process is requested for the growth of the biomass itself [4]. The most interesting feedstock in this field is represented by second generation biomass since the first-generation biomass can be considered suitable also for food [1,2]. The production of biomass is about 150 billion tonnes per year and only a small amount is used. Among these, agricultural wastes are favored since they cannot be used for food purposes [5].

Lignocellulosic biomass is constituted by a matrix of three different polymers which are cellulose (35-50%), hemicellulose (20-35%) and lignin (10-25%) [6].

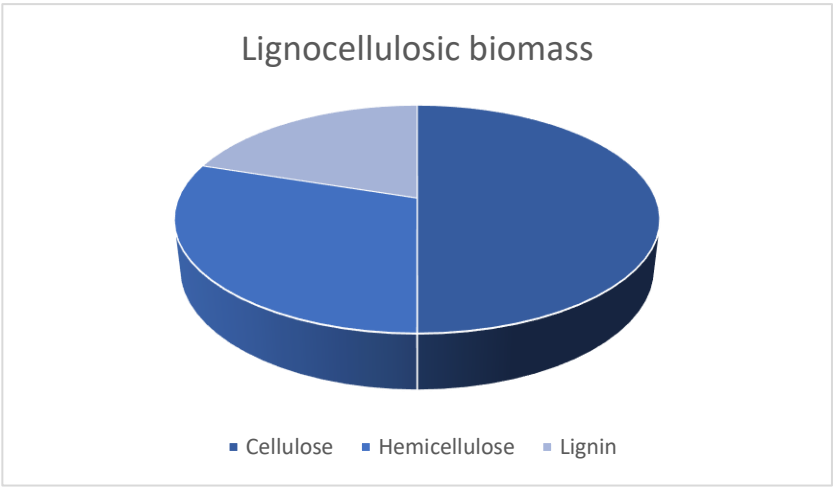

Figure 1. Lignocellulosic biomass composition.

In particular, cellulose and hemicellulose are presented in major amount and they are easily transformed in chemical compounds. Furthermore, lignocellulosic biomass contains a high amount of oxygen and lower amount of hydrogen and carbon compared to petroleum based sources and this difference in composition allows a greater amount of species obtainable from biomass respect to petroleum [6]. Cellulose is the most promising substitute to replace petroleum based polymers considering its bio-degradability and eco-friendly properties [7]. One of the most attractive products obtainable from the rehydration of 5-hydroxymethylfurfural derived from C6 carbohydrates by dehydration, is levulinic acid. Levulinic acid was included in the list of the top 12 most promising value-added chemicals from biomass by the Biomass Program of the US Department of Energy in 2004 [8] and it, together with its derivatives, finds applications in several fields such as lubricants, printing inks, corrosion inhibitors, products for the personal care and drug delivery [9]. The conversion of biomass in chemicals occurs through the depolymerization of the carbohydrates to sugars and the subsequent transformation to the chemicals themselves through several reactions, such as dehydration, hydrogenation and oxidation in the presence of different homogeneous (e.g. liquid mineral acids, such as HCl and H_2SO_4) and

heterogeneous catalysts (e.g. acids, bases and metal oxides) [4,10]. In particular, glucose is obtained from the cellulose degradation while even other types of sugars can be obtained from hemicellulose. Xylose and arabinose are examples of five membered while mannose and galactose of six membered sugars. The drawback of the conversion of lignocellulosic biomass to green chemicals is its resistance to the chemical and enzymatic degradation into cellulose, hemicellulose and lignin; the pyrolysis process is not sufficient and for this reason, the biomass needs to be pretreated with different types of mechanical, chemical or biological processes which are often economical and energetical expensive. At present, the most used method for the degradation of lignocellulosic biomass to sugars is the hydrolysis with HCl [6,11]. From biomass resources, great attention is devoted to the oleochemicals, in particular waste oils and non-edible oils to use for different types of reactions for the synthesis of attractive products in the industrial sector [12]. In the present thesis, pelargonic acid, a co-product of the azelaic acid derived from oleic acid oxidation, was used in order to obtain solvents with promising properties to use in the formulation of printing inks.

1.2 Pelargonic acid: general

Pelargonic acid, also known as nonanoic acid, with a chemical formula $C_9H_{18}O_2$, is a fatty acid derivable from biomass [13].

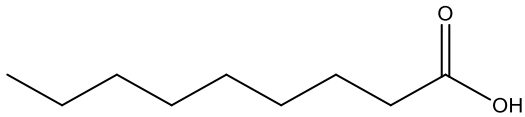

Figure 2. Pelargonic acid chemical structure.

It is usually contained in fruits, vegetables, cereals in a range from 0.2 to 400 mg/kg. Pelargonic acid is a weak organic acid (pKa = 4.95) and in aqueous

solution the acid itself is partially dissociated to give pelargonate anion and H_3O^+ species [13]. The main characteristics are reported in Table 1.

Table 1. Pelargonic acid chemical and physical properties [13,14].

Properties	Value
Molecular weight [g/mol]	158.24
Density at 20 °C /40 °C [g/mL]	0.9055
Water solubility at 25°C [mg/L]	210
Melting point [°C]	12.0
Boiling point at 760 Torr [°C]	254.4

Pelargonic acid is generally used as surfactant and emulsifying agent in the cosmetic industry, as lubricant and as herbicide with a rapid effect on green tissues causing the cell membranes destruction and the death of the tissues themselves. It was demonstrated that there are no risks on human health when pesticides based on pelargonic acid are used. On the bases of its properties, the U.S. Food and Drug Administration (FDA) authorized the use of pelargonic acid in food, cosmetic and products for the personal care [13–15].

One of the most interesting way to obtain pelargonic acid is the oxidation of oleic acid, obtainable from vegetable oils and particularly present in thistles and sunflowers. From the oleic acid oxidation, pelargonic acid and azelaic acid are produced (Figure 3).

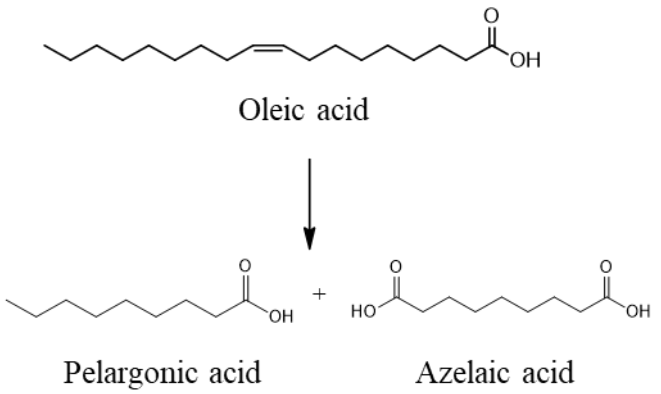

Figure 3. Oleic acid oxidation.

Different oxidants were proposed, such as chromic acid, nitric acid and peracids, but most of them are not convenient for an environmental point of view and due to the low yields, while using ozone as oxidant high yields can be reached but there are problems connected with the toxicity and possible explosions. The oleic acid ozonolysis represented the conventional way to produce pelargonic acid and azelaic acid. It was proposed by Santacesaria et al. [16,17] a process in which a first step was characterized by the reaction between the monoenic reagent with hydrogen peroxide catalyzed by pertungstic acid, followed by the oxidative cleavage of the derived diol with molecular oxygen in the presence of a catalyst obtained from the reaction between the pertungstic acid, used in the previous step, and cobalt acetate.

In recent years improvements in the process were proposed to make it more sustainable. In particular, Benessere et al. proposed to perform the oleic acid cleavage with H_2WO_4 as catalyst and H_2O_2 as oxidizing agent reaching yields higher than 90 % with a low catalyst amount. Another interesting advantage consist in a more eco-friendly properties of tungstic acid compared to other catalytic systems used in this process [18,19].

A promising application of pelargonic acid was found in recent years since it can be involved in esterification reaction with 2-ethylhexanol and its esters have

extremely interesting properties as solvents for varnishes [18,20].

1.2.1 Pelargonic acid: esterification reaction and catalysts

Esterification is one of the most important reactions involving carboxylic acids with alcohols often derived from renewable sources [14]. In the industrial processes, carboxylic acids esterification occurs in the presence of homogeneous mineral catalysts since they show a great activity. Examples of the most used catalysts can be sulfuric acid, *p*-toluenesulfonic acid and hydrochloric acid. At the same time, these catalysts suffer several drawbacks: (i) they are corrosive to the equipments; (ii) there are problems for the separation of the catalyst itself from the reaction mixture; (iii) the presence of side reactions and acid waste [21–23]. A different class of catalysts used in these reactions are biocatalysts (e.g. enzymes) but in this case the reaction rate is extremely slow and from two to three days are needed to reach the equilibrium [24]. The best alternative is represented by the heterogenous catalysts, for example supported heteropoly acids, zeolites and polystyrene-divinylbenzene resins. Several advantages in the use of this type of catalysts, in particular ion-exchange resins, can be found: (i) they are environmentally friendly; (ii) they can be separated from reaction mixtures without difficulties; (iii) they are not corrosive; (iv) there are not side reactions and byproducts; (v) they are reusable [21,22,25–28]. An important phenomenon occurring with resins is swelling in the presence of polar compounds. Hence, the composition inside catalyst particles can be different from the composition in the bulk. In a kinetic study with solid catalysts, particular attention has to be given to the swelling and on the water presence, since it can affect the conversion due to the adsorption on the catalysts active sites as well as the thermodynamic equilibrium [29].

1.2.2 Pelargonic acid: esters and uses

In the literature, some examples describing the reactions of pelargonic acid with different types of alcohols are found. A general reaction scheme is reported in Figure 4.

Figure 4. Pelargonic acid esterification reaction scheme.

One of these reactions is the esterification of pelargonic acid with methanol to obtain methyl pelargonate as product. This product is very interesting in the industrial sector since the several uses in which it can be involved. Among these uses, the principle ones are as plasticizers, lubricant oil, as component for environmentally friendly herbicides, intermediate for cosmetics and pharmaceutics [22,24]. Sharma et al. [24] studied the kinetics of the esterification reaction of pelargonic acid with methanol promoted by heterogenous catalysts, in particular Dowex 50Wx2, Amberlyst 35 and Amberlyst 15 evaluating the influence of different parameters on the reaction rate and the possible presence of mass transfer limitation. The authors estimated an activation energy of 47.6 kJ/mol. The same approach was used also for the reaction between pelargonic acid and ethanol promoted by Amberlyst 15. The ethyl pelargonate is generally used as intermediate in the synthesis of flavors, cosmetics, pharmaceuticals and corrosion inhibitors. The activation energy estimated for this reaction was equal to 53.7 kJ/mol [21]. The pelargonic esterification reaction was performed by Sharma et al. [29] also with 1-propanol with Amberlyst 15 as catalyst and the kinetics in a batch reactor was studied investigating the effect of operative parameters and external and internal mass transfer limitation on the reaction rate. In this case, the estimated activation energy value is similar to the previous cases and it is equal to

55.4 kJ/mol. The product obtained from this reaction can be used in a similar way, as intermediate in the synthesis of cosmetics and pharmaceuticals products [29]. Some examples of pelargonic acid esterification with 2-ethylhexanol can be found in the literature with different application of the obtained ester. In particular, it was reported the use of 2-ethylhexylpelargonate as bio-lubricant showing good properties in terms of viscosity better than commercial lubricant from both petrochemical and bio-based sources. The reaction was performed with Amberlyst-36 as heterogeneous catalyst reaching a conversion of 96% [30]. The same reaction was performed by Melchiorre et al. [12] in the presence of Zn(II) based catalyst reaching yield higher than 94% after a reaction time of 4h. The excellent properties of the 2-ethylhexylpelargonate as solvent in the formulation of varnishes was already discussed in section 1.2. In this context, a study was conducted by Benessere et al. [20] where these solvents were tested with a commercial resin managing to dissolve it at lower temperature, in less time and with results never reached before compared with common used solvents. Thanks to the observed results, one of the goals of this thesis was a detailed study of pelargonic acid esterification and the synthesis of solvents to use in the formulation of printing inks. This topic will be discussed in Chapters 2 and 3.

1.3 Levulinic acid: general

Levulinic acid, 4-oxopentanoic acid, is considered an attractive building block which can be used in a wide range of applications.

It is a colorless compound with a high solubility in hot water and other solvents such as ethanol, chloroform and acetone [9]. Some if its characteristics are reported in Table 2.

Table 2. Levulinic acid chemical and physical properties [9,31].

Properties	Value
Molecular weight [g/mol]	116.12
Density [g/mL]	1.13
pKa at 25°C	4.59
Melting point [°C]	37
Boiling point [°C]	245-246

The conventional way to produce levulinic acid using petrochemical raw material starts from maleic anhydride but this process leads to a high price of levulinic acid itself. A promising alternative from cheaper and renewable feedstocks involves lignocellulosic biomass and urban waste as sugar sources [5,32]. Through this process, levulinic acid is produced from the cellulose degradation to obtain glucose which is successively isomerized to fructose and then dehydrated to give different compounds, in particular HMF, formic acid and levulinic acid itself [33]. In order to catalyze the levulinic acid production, both homogeneous and heterogenous catalysts can be used. Sulfuric acid and hydrochloric acid are two examples of homogeneous catalysts which allowed a maximum yield of 73% mol and 81% mol, respectively, starting from fructose as feedstock, while a lower yield was obtained with glucose. Heterogeneous catalysts (e.g., zeolites and Amberlyst) received great interest thanks to their advantages, e.g., costs and equipments corrosion reduction thanks to the easy separation and reuse of the catalyst itself [5]. Futhermore, their good performance allows to reach a yield higher than 50% similar to those obtained with homogenous catalysts from both fructose and glucose [34].

A process for the levulinic acid production was proposed by Biofine Corporation starting from the hydrolysis of polysaccharides. This process improved the technology producing lower amounts of byproducts. It is based on two reactors plant and it starts with the mixing of the carbohydrates-based feedstocks with

sulfuric acid. They are fed to the first reactor at a temperature of 210-230°C for about 13-25 s. This first hydrolysis step produces hydroxymethylfurfural which are continuously fed to the second reactor operating at 195-215 °C for 15-30 min for a second step of hydration in order to produce levulinic acid, as liquid product, while formic acid and furfural are recovered in a vapor stream [34,35]. Another plant for the production of levulinic acid was proposed from Segetis in 2013 with the possibility to use a wide range of biomass as feedstock. In this case, the goal was the use of levulinic acid for the production of ketals through the reaction of levulinic acid esters with alcohols derived from vegetable oils, such as glycerol. In 2016 this plant, located in Caserta (Italy) started its production with a capacity of 2000 metric tons per year with the purpose to reach a production up to 10000 metric tons per year [34].

1.3.1 Levulinic acid: derivatives and uses

Thanks to its carboxylic and keto functional groups, levulinic acid can be involved in a wide range of chemical transformations to obtain several value-added chemicals. Among these, diphenolic acid (DPA), δ-aminolevulinic acid (DALA), γ-Valerolactone (GVL), levulinate esters and levulinate ketals are the main ones [8,34]. A schematic representation is reported in Figure 5.

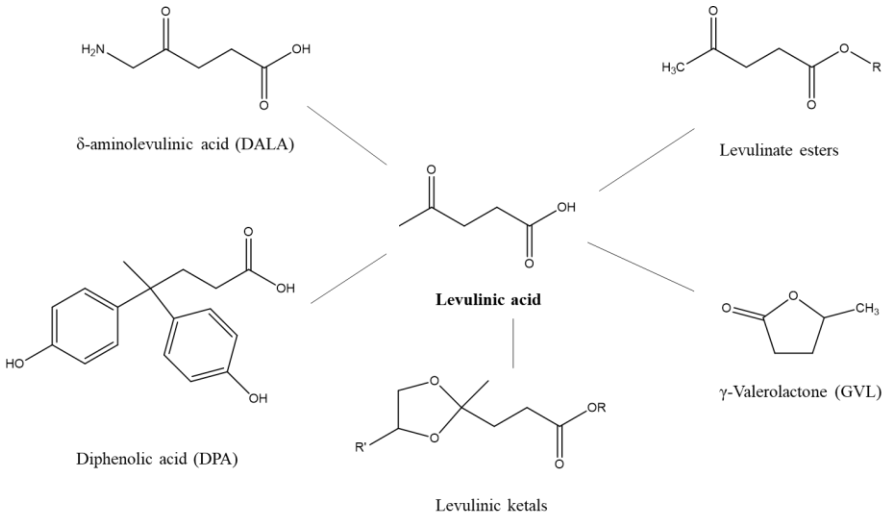

Figure 5. Levulinic acid derivatives. Adapted from Ref. 31.

In addition to the above-mentioned chemicals, other products obtainable from levulinic acid are succinic acid, pentanoic acid pyrrolidones finding several possible applications. The most interesting are plasticizers, food additives, cosmetics, fuel additives, pharmaceuticals, polymers, herbicides and solvents [8,32]. In particular, diphenolic acid (DPA) represents a green potential substitute to bisphenol A and it finds application in the polymer and polycarbonate productions[35,36]. δ-aminolevulinic acid (DALA), instead, has very interesting potentiality as it can be used as biodegradable herbicide and recently other applications were found, as insecticide and in the cancer therapy [35,36]. Among the principal derivative discussed at the beginning of this section, γ-Valerolactone (GVL) can be considered an attractive compound to produce chemicals such as α-methylene-γ-valerolactone which has a structure similar to methyl methacrylate and it can be also used as feedstock for adipic acid which is a precursor for nylon synthesis. Finally, levulinate esters can be produced from the reaction between levulinic acid and various types of alcohols. Levulinate esters show wide application possibilities in several fields, e.g. as fuel additives, flavors, in the polymers synthesis and an attractive alternative is their use as precursor for the

ketal synthesis [34,37]. Ketals started to be investigated by Segetis as biobased monomers for different applications as plasticizers, showing better performances compared to phthalates based commercial one, and solvents [6,38]. Levulinic acid ketals play a central role in this thesis work, so they will be discussed more in detail in section 1.3.2.

1.3.2 Levulinic acid: ketals and uses

Levulinic acid ketals are considered of great interest thanks to their proprieties such as high solvency and compatibility with several applications as lubricants, plasticizers and solvents [39]. Levulinic acid ketals are obtained from the reaction between levulinic acid itself or its esters with polyols promoted by acid catalysts. Also the transesterification reaction can occur leading to the formation of byproducts [40,41]. A general example of the two possible reactions are reported in Figure 6.

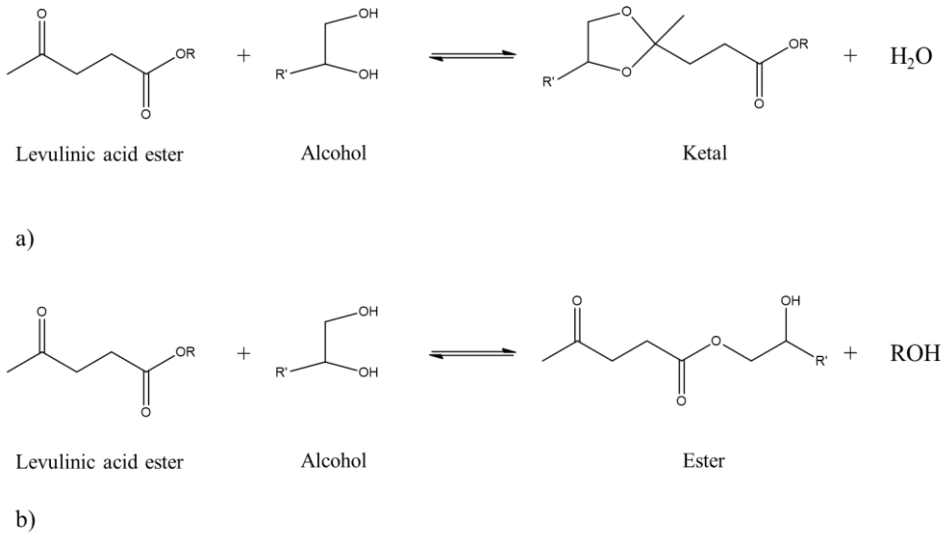

Figure 6. a) Levulinic acid ester ketalization reaction; b) Levulinic acid ester transesterification reaction. Adapted from Ref. [39]

Ketals from levulinic acid esters show excellent properties as solvents and they are thermally and chemically stable compounds [39]. In the literature, some examples can be found about the ketalization of levulinic acid and levulinic acid esters. Mullen et al. [42] studied the reaction between keto esters and polyols investigating the effect of different operative conditions such as catalyst type and their amount. In the work by Freitas et al. [40] the reaction of ethyl levulinate with ethylene glycol and 1,2-dodecanediol was investigated in the presence of both homogeneous and heterogeneous (e.g., Amberlyst 70, H-ZSM-5 zeolite and Niobium phosphate) catalysts. In particular, the product from ethyl levulinate and 1,2-dodecanediol showed good properties as green surfactant and in this case the authors obtained good conversions after a reaction time of 24 h removing water formed during the reaction.

An interesting study was conducted by Amarasekara et al. [43] on the reaction between levulinic acid and three different diols which are 1,2-ethanediol, 1,2-propanediol and 1,3-propanediol. Amberlyst-15 was chosen as heterogeneous catsalyst while *p*-toluenesulfonic as homogenous one and a comparison on their performance was made. They found a difference in the products obtained, in fact in the presence of Amberlyst-15 predominantly ketals and ketal esters were produced while with *p*-toluenesulfonic esters and ketal esters were found.

Among the polyols, glycerol is of utmost interest. It is obtained at high concentration as byproduct in the biodiesel synthesis. In recent years, the growing production of biodiesel from the transesterification reaction of vegetable oils with methanol has led also to an increase production of glycerol with costs decrease. For this reason, the conversion of glycerol in value-added chemicals, such as fuel additive is very attractive. In particular, glycerol acetals and ketals are particularly suitable for this purpose [44]. One of the example in this field is glycerol ketalization with acetone to obtain solketal which shows excellent properties as fuel additive [45]. Solketal synthesis can be promoted both by homogeneous (for example sulfuric acid or *p*-toluenesulfonic acid) and heterogeneous catalysts (e.g., zeolites,

heteropolyacids and ionic exchange resins). Ion exchange resins showed good results in their use in continuous operation for solketal synthesis [46].

The reaction between levulinc acid or levulinic acid esters with glycerol produces cyclic ketals with very interesting properties. In a study by Li et al. [47], the reaction between methyl levulinate and glycerol was investigated together with the application of the obtained ketal for the production of polyurethane foams. Due to the mass transfer limitation connected to the high viscosity of glycerol, an excess of methyl levulinate was used reaching a conversion of 72.7% and a yield of 69.1% with a methyl levulinate/glycerol molar ratio of 4.

Leibig et al. [39] investigated the ketalization of ethyl levulinate with glycerol in the presence of homogeneous catalysts (sulfuric acid and hydrochloric acid) and Amberlyst 15 as heterogeneous catalyst reaching conversions higher than 99% and selectivity >98% with a rection time of 1 h at a temperature between 80 and 120 °C removing the water formed during the reaction itself.

Some of the properties of ketals obtained from the reaction between ethyl levulinate and glycerol are reported in Table 3.

Table 3. Ketals properties [39].

Properties	Value
Viscosity [cP] at 25°C	37-40
Freeze point [°C]	-60
Boiling point [°C] at 1 atm	286

Ketals from ethyl levulinate with glycerol are widely soluble in water and some oils hence they are excellent solvents for both types of formulations (for example paints); furthermore they are considered an attractive alternative to replace the commonly used solvents in applications like coatings and adhesives [39].

1.4 Goals of the thesis

The present thesis work is mainly focused on the investigation of the pelargonic acid esterification with 2-ethylhexanol studying in depth the kinetics in order to determine the thermodynamic and kinetic parameters in the presence of different heterogeneous catalysts, both commercial and synthetic. At the present, few information can be found about this reaction in the literature but this process resulted to be particularly interesting since the obtained esters can be used as solvents in the formulation of printing inks leading to products environmentally friendly with very promising properties. Solvents will be synthesized and tested in the printing inks formulation in order to compare the obtained products with the commonly used ones. Furthermore, for similar purposes, the ketalization reaction, in particular from levulinic acid or its esters, is of huge interest and also in this case few works can be found in the literature. In this thesis, the ketalization reaction of ethyl levulinate with glycerol will be investigated focusing firstly on a catalytic screening testing different commercial and synthetic heterogeneous catalysts. The catalyst showing the most interesting properties will be chosen to be used in a kinetic study.

References

1. Sheldon, R. A. Green and sustainable manufacture of chemicals from biomass: State of the art. *Green Chem.* **16**, 950–963 (2014).

2. Lenk, F., Bröring, S., Herzog, P. & Leker, J. On the usage of agricultural raw materials - Energy or food? An assessment from an economics perspective. *Biotechnol. J.* **2**, 1497–1504 (2007).

3. Zhou, C. H., Xia, X., Lin, C. X., Tong, D. S. & Beltramini, J. Catalytic conversion of lignocellulosic biomass to fine chemicals and fuels. *Chem. Soc. Rev.* **40**, 5588–5617 (2011).

4. Chheda, J. N., Huber, G. W. & Dumesic, J. A. Liquid-phase catalytic processing of biomass-derived oxygenated hydrocarbons to fuels and chemicals. *Angew. Chemie - Int. Ed.* **46**, 7164–7183 (2007).

5. Rackemann, D. W. & Doherty, W. O. The conversion of lignocellulosics to levulinic acid. *Biofuels, Bioprod. Biorefining* **5**, 198–214 (2011).

6. Isikgor, F. H. & Becer, C. R. Lignocellulosic biomass: a sustainable platform for the production of bio-based chemicals and polymers. *Polym. Chem.* **6**, 4497–4559 (2015).

7. Ahn, Y., Lee, S.H., Kim, H.J., Yang, Y-H., Hong, J.H., Kim, Y-H. & Kim, H. Electrospinning of lignocellulosic biomass using ionic liquid. *Carbohydr. Polym.* **88**, 395–398 (2012).

8. Malu, T. J., Manikandan, K. & Cheralathan, K. K. Levulinic acid-a potential keto acid for producing biofuels and chemicals. *Biomass, Biofuels, Biochemicals* 171-197 (2020).

9. Mukherjee, A., Dumont, M. J. & Raghavan, V. Review: Sustainable production of hydroxymethylfurfural and levulinic acid: Challenges and opportunities. *Biomass and Bioenergy* **72**, 143–183 (2015).

10. Mamman, A. S., Lee, J-M., Kim, Y-C., Hwang, I. T., Park, N-J., Hwang, Y. K., Chang, J.S. & Hwang, J-S. Furfural: Hemicellulose/xylosederived biochemical. *Biofuels, Bioprod. Biorefining* **2**, 438–454 (2008).

11. Barakat, A., de Vries, H. & Rouau, X. Dry fractionation process as an important step in current and future lignocellulose biorefineries: A review. *Bioresour. Technol.* **134**, 362–373 (2013).

12. Melchiorre, M., Cucciolito, M. E., Di Serio, M., Ruffo, F., Tarallo, O., Trifuoggi, M. & Esposito, R. Homogeneous Catalysis and Heterogeneous Recycling: A Simple Zn(II) Catalyst for Green Fatty Acid Esterification. *ACS Sustain. Chem. Eng.* **9**, 6001–6011 (2021).

13. Pesticide Research Institute. Chapter 7 — Pelargonic Acid. *Mar. Munic. Water Dist. Herbic. Risk Assess.* (2010).

14. Johnson, W., Heldreth, B., Bergfeld W. F., Belsito, D. V., Klaassen, C. D, Hill, R., Liebler, D., Marks, J. G., shank, R. C., Slaga, T. J., Snyder, P. W. & Andersen, F. A. Final Report of the Cosmetic Ingredient Review Expert Panel on the Safety Assessment of Pelargonic Acid (Nonanoic Acid) and Nonanoate Esters. *Int. J. Toxicol.* **30**, 228S-269S (2011).

15. Ciriminna, R., Fidalgo, A., Ilharco, L. M. & Pagliaro, M. Herbicides based on pelargonic acid: Herbicides of the bioeconomy. *Biofuels, Bioprod. Biorefining* **13**, 1476–1482 (2019).

16. Santacesaria, E., Sorrentino, A., Rainone, F., Di Serio, M. & Speranza, F. Oxidative cleavage of the double bond of monoenic fatty chains in two steps: A new promising route to azelaic acid and other industrial products. *Ind. Eng. Chem. Res.* **39**, 2766–2771 (2000).

17. Santacesaria, E., Ambrosio, M., Sorrentino, A., Tesser, R. & Di Serio, M. Double bond oxidative cleavage of monoenic fatty chains. *Catal. Today* **79**–**80**, 59–65 (2003).

18. Benessere, V., Cucciolito, M. E., De Santis, A., Di Serio, M., Esposito, R., Ruffo, F. & Turco, R. Sustainable Process for Production of Azelaic Acid Through Oxidative Cleavage of Oleic Acid. *JAOCS, J. Am. Oil Chem. Soc.* **92**, 1701–1707 (2015).

19. Melchiorre, M., Benessere, V., Cucciolito, M. E., Melchiorre, C., Ruffo, F. & Esposito, R. Direct and Solvent-Free Oxidative Cleavage of Double Bonds in High-Oleic Vegetable Oils. *ChemistrySelect* **5**, 1396–1400 (2020).

20. Benessere, V., Cucciolito, M. E., De Santis, A., Di Serio, M., Esposito, R., Melchiorre, M., Nugnes, F., Paduano, L. & Ruffo, F. A Sustainable Process for the Production of Varnishes Based on Pelargonic Acid Esters. *JAOCS, J. Am. Oil Chem. Soc.* **96**, 443–451 (2019).

21. Sharma, M., Toor, A. P. & Wanchoo, R. K. Reaction kinetics of catalytic esterification of nonanoic acid with ethanol over amberlyst 15. *Int. J. Chem. React. Eng.* **12**, 451–463 (2014).

22. Kaur, K., Jain, P., Sobti, A. & Toor, A. P. Sulfated metal oxides: Eco-friendly green catalysts for esterification of nonanoic acid with methanol. *Green Process. Synth.* **5**, 93–100 (2016).

23. Altıokka, M. R. & Çıtak, A. Kinetics study of esterification of acetic acid with isobutanol in the presence of amberlite catalyst. *Appl. Catal. A Gen.* **239**, 141–148 (2003).

24. Sharma, M., Wanchoo, R. K. & Toor, A. P. Adsorption and kinetic parameters for synthesis of methyl nonanoate over heterogeneous catalysts. *Ind. Eng. Chem. Res.* **51**, 14367–14375 (2012).

25. Huang, Y.-S. & Sundmacher, K. Kinetics study of propyl acetate synthesis reaction catalyzed by Amberlyst 15. *Int. J. Chem. Kinet.* **39**, 245–253 (2007).

26. Ali, S. H. Kinetics of catalytic esterification of propionic acid with different alcohols over Amberlyst 15. *Int. J. Chem. Kinet.* **41**, 432–448 (2009).

27. Tejero, M. A., Ramírez, E., Fité, C., Tejero, J. & Cunill, F. Esterification of levulinic acid with butanol over ion exchange resins. *Appl. Catal. A Gen.* **517**, 56–66 (2016).

28. Maheria, K. C., Kozinski, J. & Dalai, A. Esterification of levulinic acid to n-butyl levulinate over various acidic zeolites. *Catal. Letters* **143**, 1220–1225 (2013).

29. Sharma, M., Wanchoo, R. K. & Toor, A. P. Amberlyst 15 catalyzed esterification of nonanoic acid with 1-propanol: Kinetics, modeling, and comparison of its reaction kinetics with lower alcohols. *Ind. Eng. Chem. Res.* **53**, 2167–2174 (2014).

30. Huai Ng, T. Synthesis of Bio-Lubricant By Esterification of Pelargonic Acid With 2-Ethylhexanol Over Amberlyst 36. (2015).

31. Liu, C., Lu, X., Yu, Z., Xiong, J., Bai, H. & Zhang, R. Production of levulinic acid from cellulose and cellulosic biomass in different catalytic systems. *Catalysts* **10**, 1–22 (2020).

32. Pratama, A. P., Rahayu, D. U. C. & Krisnandi, Y. K. Levulinic acid production from delignified rice husk waste over manganese catalysts: Heterogeneous versus homogeneous. *Catalysts* **10**, 327-339 (2020).

33. Yan, K., Jarvis, C., Gu, J. & Yan, Y. Production and catalytic transformation of levulinic acid: A platform for speciality chemicals and

fuels. *Renew. Sustain. Energy Rev.* **51**, 986–997 (2015).

34. Girisuta, B. & Heeres, H. J. Levulinic Acid from Biomass: Synthesis and Applications. *Biofuels and Biorefineries* **7**, 143–169 (2017).

35. Bozell, J. J., Moens, L., Elliott, D. C., Wang, Y., Neuenscwander, G. G., Fitzpatrick, S. W., Bilski, R. J. & Jarnedeld, J. L. Production of levulinic acid and use as a platform chemical for derived products. *Resour. Conserv. Recycl.* **28**, 227–239 (2000).

36. Rose, M. & Palkovits, R. Cellulose-based sustainable polymers: State of the art and future trends. *Macromol. Rapid Commun.* **32**, 1299–1311 (2011).

37. Pileidis, F. D. & Titirici, M. M. Levulinic Acid Biorefineries: New Challenges for Efficient Utilization of Biomass. *ChemSusChem* **9**, 562–582 (2016).

38. Bozell, J. J. & Petersen, G. R. Technology development for the production of biobased products from biorefinery carbohydrates—the US Department of Energy's "top 10" revisited. *Green Chem.* **12**, 539–55 (2010).

39. Leibig, C., Mullen, B., Mullen, T., Rieth, L. & Badarinarayana, V. Cellulosic-derived levulinic ketal esters: A new building block. *ACS Symp. Ser.* **1063**, 111–116 (2011).

40. Freitas, F. A., Licursi, D., Lachter, E. R., Raspolli Galletti, A. M., Antonetti, C., Brito, T. C. & Nascimento, R. S. V. Heterogeneous catalysis for the ketalisation of ethyl levulinate with 1,2-dodecanediol: Opening the way to a new class of bio-degradable surfactants. *Catal. Commun.* **73**, 84–87 (2016).

41. Amarasekara, A. S. & Hawkins, S. A. Synthesis of levulinic acid-glycerol ketal-ester oligomers and structural characterization using NMR

spectroscopy. *Eur. Polym. J.* **47**, 2451–2457 (2011).

42. Mullen, B. D., Badarinarayana, V., Santos-Martinez, M. & Selifonov, S. Catalytic selectivity of ketalization versus transesterification. *Top. Catal.* **53**, 1235–1240 (2010).

43. Amarasekara, A. S. & Animashaun, M. A. Acid Catalyzed Competitive Esterification and Ketalization of Levulinic Acid with 1,2 and 1,3-Diols: The Effect of Heterogeneous and Homogeneous Catalysts. *Catal. Letters* **146**, 1819–1824 (2016).

44. Trifoi, A. R., Agachi, P. Ş. & Pap, T. Glycerol acetals and ketals as possible diesel additives. A review of their synthesis protocols. *Renew. Sustain. Energy Rev.* **62**, 804–814 (2016).

45. Climent, M. J., Corma, A. & Iborra, S. Conversion of biomass platform molecules into fuel additives and liquid hydrocarbon fuels. *Green Chem.* **16**, 516–547 (2014).

46. Konwar, L. J., Samikannu, A., Mäki-Arvela, P., Boström, D. & Mikkola, J. P. Lignosulfonate-based macro/mesoporous solid protonic acids for acetalization of glycerol to bio-additives. *Appl. Catal. B Environ.* **220**, 314–323 (2018).

47. Li, P., Xiao, Z., Chang, C., Zhao, S. & Xu, G. Efficient Synthesis of Biobased Glycerol Levulinate Ketal and Its Application for Rigid Polyurethane Foam Production. *Ind. Eng. Chem. Res.* **59**, 17520–17528 (2020).

Chapter 2 – Pelargonic acid esterification: Kinetic investigation

2.1 Overview

A detail kinetic study of pelargonic acid esterification with 2-ethylhexanol is the main topic of this chapter.

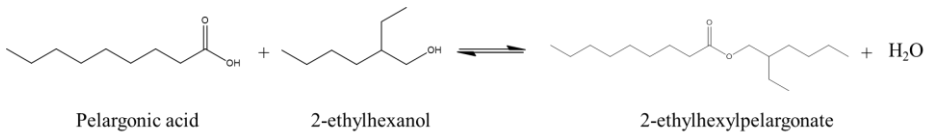

Figure 7. Pelargonic acid esterification with 2-ethylhexanol.

Firstly, the reaction was performed in a batch reactor in the presence of sulfuric acid as homogeneous catalyst followed by the investigation with different heterogeneous catalysts, in particular Amberlyst-15, Amberlite IR120 and a synthetic catalyst which is H_2WO_4/SiO_2. A comparison of these catalysts was made, and the two resins were tested also in a continuous apparatus. The effect of different experimental conditions on the reaction rate, such as temperature, stirring rate, catalyst load and reactants molar ratio in the case of the batch reactor and temperature, reactants molar ratio and volumetric flow in the case of the continuous apparatus, was evaluated and kinetic and thermodynamic parameters were estimated through a dedicated kinetic model.

2.2 Chemicals

Chemicals used in all the experiments are pelargonic acid (purity ≥ 96%) and 2-ethylhexanol (purity ≥ 99%). In the case of tests performed in the presence of H_2SO_4, sulfuric acid 98% w/w was used, and all the reactants were purchased by Merck while in the case of tests conducted in the presence of ion exchange resins, Amberlite IR120 was purchased by Rohm and Haas while Amberlyst-15 by Merck. Resins properties were taken from catalysts data sheet and are reported in Table 4.

Table 4. Amberlyst-15 and Amberlite IR120 properties.

	Amberlyst-15	**Amberlite IR120**
Particle size [μm]	300	620-830
Crosslinking degree [%]	20	8
Acid sites concentration [meq/g]	4.53	4.40
Surface area [m^2/g]	45	1.53
$R_{P,dry}$ [m]	$1.50 \cdot 10^{-4}$	$3.62 \cdot 10^{-4}$
$\mathcal{E}_P$ [-]	0.51	0.55
τ_P [-]	5.00	5.00
ρ_P [kg/m^3]	600	1518

2.3 Experimental setup

The experimental setup used for all the batch kinetic experiments consisted of a Hastelloy autoclave of 300 cm^3 equipped with a magnetically driven stirrer, a thermocouple connected to a thermoregulator in order to control the temperature inside the reactor and a controller to set the stirring rate. Furthermore, a syringe was connected to the batch reactor to load one of the reactants inside the reactor itself. A nitrogen cylinder was connected to the tank and it allowed the

pressurization of the reaction system to avoid the partition between the liquid and gas phases of the light components. In Figure 8 a scheme of the apparatus is reported followed by the real pictures in Figure 9.

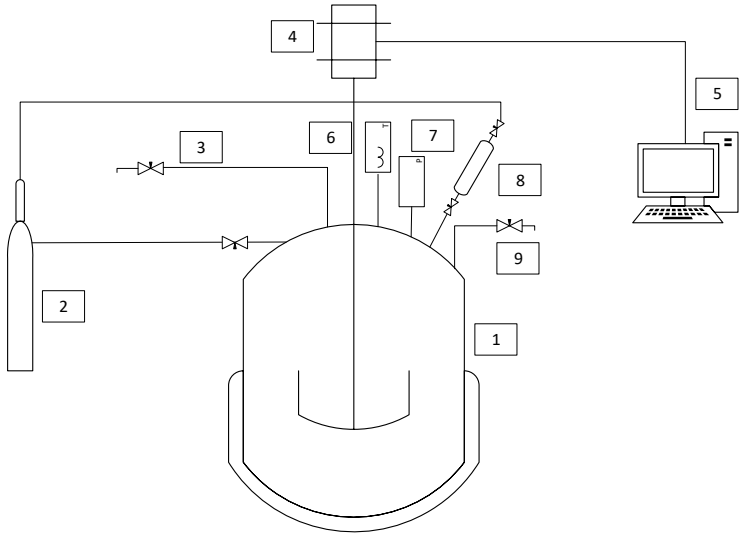

Figure 8. Reactor used for the batch tests scheme.

1. Stainless steel batch reactor;
2. Nitrogen cylinder;
3. Withdrawal valve;
4. Stirrer connected to the control system;
5. Control system;
6. Thermocouple connected to the control system;
7. Manometer connected to the control system;
8. Syringe for the reagent injection;
9. Pin valve.

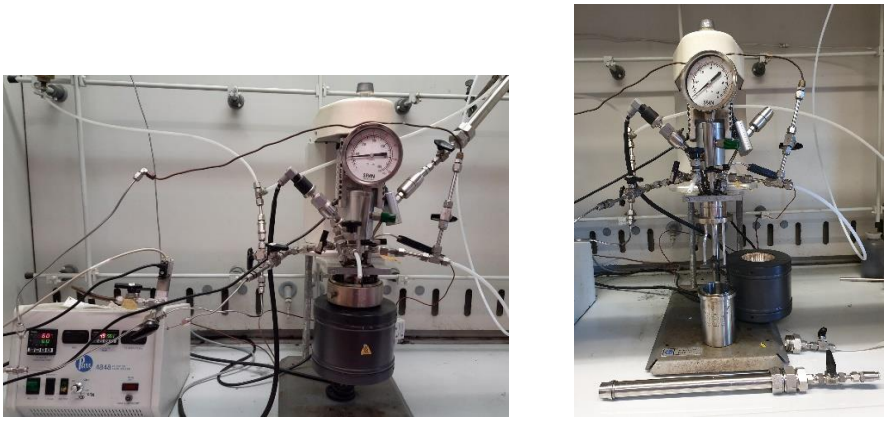

Figure 9. Reactor used for the batch tests pictures.

The experimental setup in the case of continuous experiments, instead, consisted of a packed tubular reactor (L = 66 cm, ID = 2.5 cm) equipped with two HPLC pumps in order to flow the acid and the alcohol separately and connected to a thermostat that ensured the heating of the reaction system. As it is possible to see from Figure 10, the tubular reactor was packed with five catalytic beds, containing 5 g both in the case of Amberlite IR120 and Amberlyst-15, interspersed with glass balls as inert material. Five different valves at different position along the reactor length allowed the samples collection in order to follow the pelargonic acid conversion after each catalytic bed.

A. 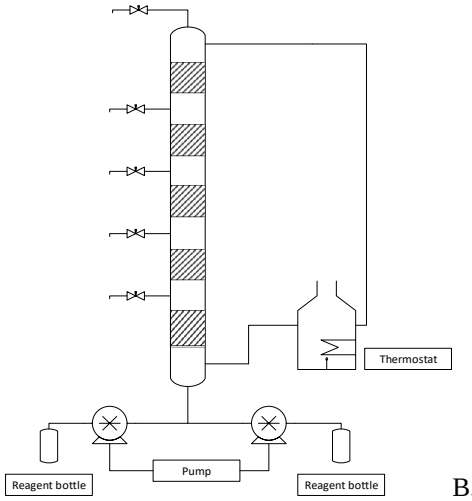

B. 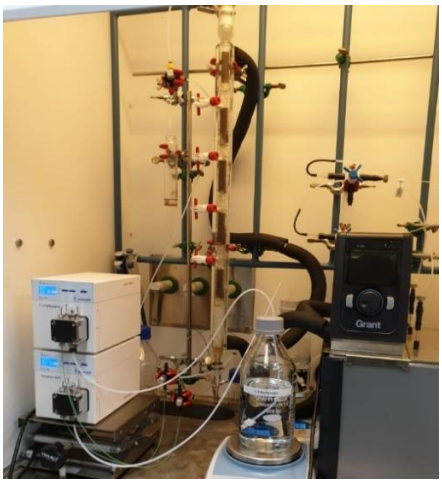

Figure 10. Continuous apparatus scheme (A) with related picture (B).

2.3 Reaction procedures

Different batch experiment sets were performed in the presence of both homogeneous (sulfuric acid) and heterogeneous (Amberlyst-15, Amberlite IR120 and H_2WO_4/SiO_2) catalysts. First of all, blank tests were made to evaluate the possible autocatalytic effect of the pelargonic acid itself and its contribution on the reaction rate. In the case of experiments with sulfuric acid, the reaction mixture was loaded in the reactor and the system was heated. After the heating, the catalyst was added using an external syringe connected to the batch reactor. In this way the reaction started when the catalyst was loaded in the system considering that the reaction did not take place without catalyst because of the negligible autocatalytic effect. The first sample was collected at $t = 0$ (it corresponded to the moment in which the system was at the desired temperature).

As for the experiments in the presence of heterogeneous catalysts, a similar procedure was followed. In particular, one of the two reactants were loaded in the reactor together with the catalyst and the system was heated up to the set value and when it was reached, the other reactant was added.

In all the tests samples were collected periodically and the experiments were prolonged overnight to measure the thermodynamic plateau.
Both resins, Amberlyst-15 and Amberlite IR120, were treated in an oven at 333 K before their use in order to remove water adsorbed in the pores.

2.4 Swelling tests

The dimension of the catalysts particles can influence the reaction rate due to the possible mass transfer phenomenon. The swelling involves heterogeneous catalysts and therefore it was considered for both resins and H_2WO_4/SiO_2 catalyst used in the kinetic tests.
The procedure followed to measure the swelling degree was the same in all the cases, so it will be described in a general way and it can be applied to the three different catalysts.
The catalyst (in the case of the resins it was previously dried) was placed into four different cylinders and the reactants and products (pelargonic acid, 2-ethylhexanol, 2-ethylhexylpelargonate and water) were added. The volume occupied by the catalyst itself was measured before and after adding the liquid in order to obtain the swelling degree. For Amberlite IR120, the radius of the wet catalyst was equal to the double of the radius of the dry one in the case of water while swelling degree with the other three liquids was next to zero. In the case of Amberlyst-15 it was about 50% with 2-ethylhexanol and water while about 5% with pelargonic acid and 2-ethylhexylpelargonate. Finally, for H_2WO_4/SiO_2 it was found a swelling degree of 20% only with 2-ethylhexanol and 2-ethylhexylpelargonate.

2.5 Analytical methods

Acid – base titration was chosen as analytical method using NaOH/EtOH 0.1 M solution and phenolphthalein as indicator. About 0.3 g of sample was dissolved in 25 mL of ethanol; phenolphthalein was added, and it was titrated with the NaOH/EtOH solution until a persistent pink color was obtained. In the presence of heterogeneous catalysts, the catalyst was separated from the reaction medium before the analysis while, in the case of sulfuric acid, the amount of catalyst was low and therefore it could be considered negligible.
The analysis was made three times to estimate an experimental error of 2.5%.

2.6 Fluid-dynamic characterization of the continuous apparatus

A study of the fluid-dynamic of the continuous reactor was made to investigate the residence time distribution (RTD), the bed void degree and the axial dispersion coefficient. Step experiments were made varying the volumetric flow and the temperature both for Amberlite IR120 and Amberlyst-15 (see Table 5 for the experimental conditions). Naphthol yellow was chosen as tracer because of its important properties: the size of its molecules is big enough to not enter inside the catalyst pores avoiding intraparticle diffusion phenomena and furthermore the presence of sulfonic group inhibited the adsorption of the molecules themselves on the resins. The solution containing the tracer was fed with an HPLC pump and at the reactor exit an online UV detector was placed.

Table 5. Fluid-dynamic tests conditions in the presence of Amberlyst-15 and Amberlite IR120.

Test	Q [m^3/s]	T [K]
1	$1.67 \cdot 10^{-8}$	298
2	$8.33 \cdot 10^{-9}$	298
3	$4.17 \cdot 10^{-9}$	298
4	$1.67 \cdot 10^{-8}$	313
5	$8.33 \cdot 10^{-9}$	313
6	$4.17 \cdot 10^{-9}$	313

The results of the step experiments allowed to determine the axial dispersion coefficient and the Péclet number. The behavior of a tubular reactor is directly connected to the axial dispersion D_z and a clear example is given by the two extreme values assumed by D_z: when it is 0, the reactor is a plug flow while when $D_z \rightarrow \infty$, it assumes the characteristics of a stirred tank reactor.

It is possible to write the mass balance as follows:

$$\frac{\partial c}{\partial t} = -u\frac{\partial c}{\partial z} + D_z\frac{\partial^2 c}{\partial z^2} \tag{1}$$

In order to solve the equation, two boundary conditions were adopted, and they were reported in Eqs. 2 and 3.

$$c\big|_{z=0} = c_0 \tag{2}$$

$$\left.\frac{\partial c}{\partial z}\right|_{z=L} = 0 \tag{3}$$

The solution of the mass balance equation gave the residence time distribution, (Eq. 4) while the Péclet number was obtained from Eq. 5.

$$F(t) = \frac{c}{c_0} = \frac{1}{2}\left[1 - erf\left(\frac{L-ut}{\sqrt{4D_z t}}\right)\right] \tag{4}$$

$$Pe = \frac{uL}{D_z} \tag{5}$$

From these experiments, reactor void degree, the axial dispersion coefficient (D_z) and the Péclet number were determined, and they are reported in Table 6.

Table 6. Fluid-dynamic characterization results.

Test	**Amberlite IR120**			**Amberlyst-15**		
	ε **[-]**	D_z **[m^2/s]**	***Pe*** **[-]**	ε **[-]**	D_z **[m^2/s]**	***Pe*** **[-]**
1	0.22	$5.40 \cdot 10^{-7}$	186.38	0.20	$1.57 \cdot 10^{-6}$	69.98
2	0.21	$2.50 \cdot 10^{-7}$	210.45	0.20	$1.20 \cdot 10^{-6}$	46.75
3	0.20	$1.00 \cdot 10^{-7}$	280.50	0.20	$8.00 \cdot 10^{-7}$	35.06
4	0.20	$5.40 \cdot 10^{-7}$	210.70	0.21	$1.57 \cdot 10^{-6}$	69.50
5	0.17	$2.50 \cdot 10^{-7}$	258.62	0.21	$1.20 \cdot 10^{-6}$	45.30
6	0.20	$1.00 \cdot 10^{-7}$	280.50	0.20	$8.00 \cdot 10^{-7}$	35.06

An average void degree value of 0.20 resulted for both Amberlyst-15 and Amberlite IR120.

In Figure 11, tests at $Q = 8.33 \cdot 10^{-9}$ m^3/s were reported where the good agreement between the experimental results and the simulated curves can be appreciated. The parameters, obtained from the fluid-dynamic characterization, were involved in the development of the kinetic model to interpret the experimental data collected in the continuous characterization tests.

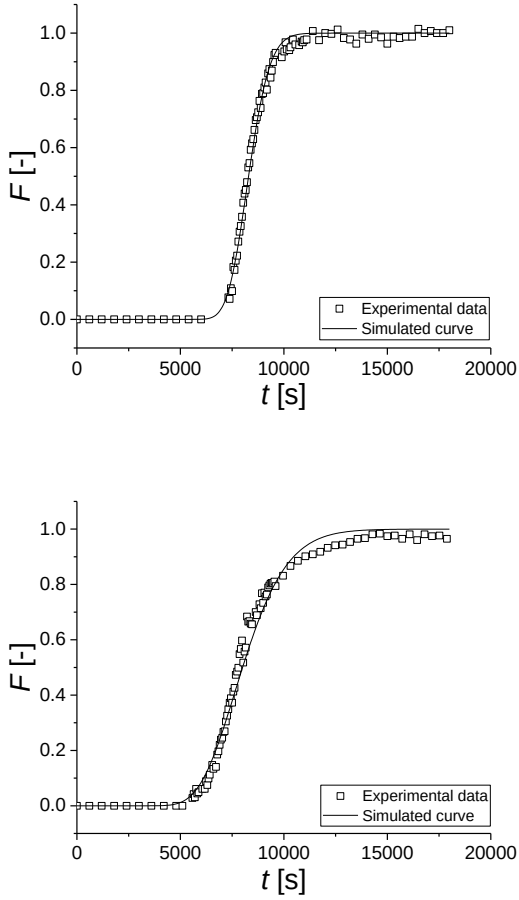

Figure 11. Fluid-dynamic characterization tests at $Q = 8.33 \cdot 10^{-9}$ m^3/s.
A. Amberlite IR120. B. Amberlyst-15.

2.7 Batch kinetic study

Experimental tests were performed with all the previously cited catalysts to study the kinetics of the pelargonic acid esterification varying different experimental conditions (e.g. stirring rate, temperature, catalyst load and reactants molar ratio).

2.7.1 Blank tests

A first set of blank tests were performed to evaluate the possible autocatalysis of pelargonic acid itself. These tests (summarized in Table 7) were made at different temperatures and reactants molar ratio.

Table 7. Blank tests conditions.

Test	*v* [rpm]	*T* [K]	EtHex/PA [mol/mol]
1	800	323	5:1
2	800	333	5:1
3	800	343	5:1
4	800	353	5:1
5	800	353	2.5:1
6	800	353	1:1

As it can be observed from Figure 12, the autocatalytic effect can be considered negligible as the reached conversion after 5 h of reaction was always less than 5%.

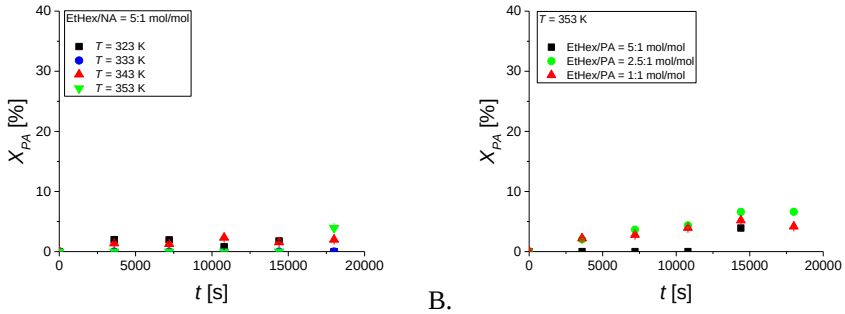

Figure 12. Blank tests. A. Temperature effect. B. Reactants molar ratio effect.

2.7.2 Tests promoted by sulfuric acid

A set of experiments were performed in the presence of the homogeneous catalyst (H_2SO_4) at different temperatures and catalyst load to investigate its effect on the reaction rate and to determine the equilibrium constant.

Table 8. Tests promoted by sulfuric acid.

Test	***v*** **[rpm]**	***T*** **[K]**	**EtHex/PA [mol/mol]**	**H_2SO_4 [mol %]**
1	800	313	5:1	1.0
2	800	323	5:1	1.0
3	800	333	5:1	1.0
4	800	343	5:1	1.0
5	800	333	5:1	0.5
6	800	333	5:1	0.25

In Figure 13 it is possible to observe that reaction rate increased by increasing the temperature and the equilibrium was reached at long reaction time, therefore tests were prolonged overnight to measure the equilibrium constant which is favored by increasing the reaction temperature.

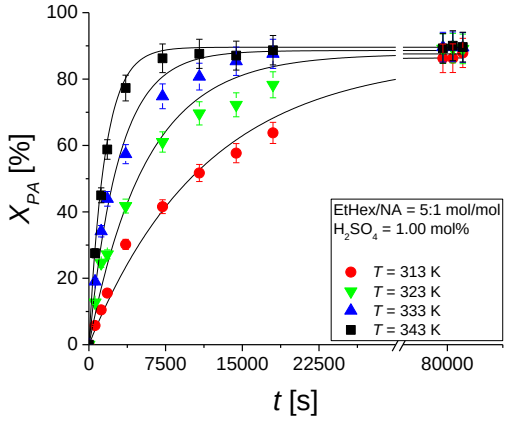

Figure 13. Temperature effect for tests promoted by sulfuric acid.

Also in the case of tests conducted at different catalyst load, by increasing sulfuric acid amount the reaction rate increased, too (Figure 14A).

Multiplying the reaction time for the catalyst percentage, as reported in Figure 14B, it is possible to see that experimental data overlap meaning that the proportionality coefficient is one respect to the catalyst concentration.

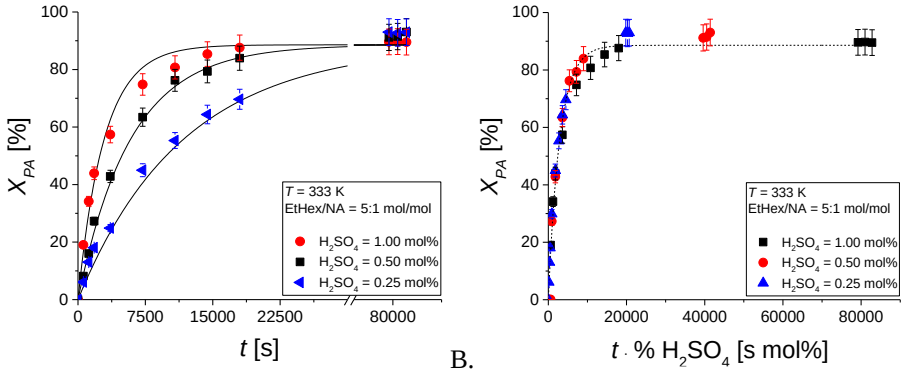

Figure 14. A. Catalyst load effect for tests promoted by sulfuric acid. B. Reaction time normalized per catalyst percentage.

The collected experimental data were interpreted by a kinetic model taking into account all the phenomena involved in the reaction network.

The dependence of density and viscosity with temperature is of crucial importance in the study of a reaction kinetics. No information about 2-ethylhexylpelargonate were reported in the literature and for this reason both density and viscosity were determined as function of temperature. More information can be found in publication **I** attached at the end of the thesis. In the case of pelargonic acid, 2-ethylhexanol and water, database available in the literature was used.

The reaction rate can be expressed as reported in Eq. 6.

$$r_H = k_H c_{H_2SO_4} \left(c_{PA} c_{EtHex} - \frac{1}{K} c_{EtHex-PA} c_{H_2O} \right) \tag{6}$$

A modified Arrhenius (Eq. 7) and van't Hoff (Eq. 8) equations were considered to express the dependency with temperature. In both equations T_{ref} was set at 333 K.

$$k_H = k_{H,ref} \exp\left(-\frac{Ea_H}{R} \left(\frac{1}{T} - \frac{1}{T_{ref}} \right) \right) \tag{7}$$

$$K = K_{ref} \exp\left(-\frac{\Delta_r H}{R} \left(\frac{1}{T} - \frac{1}{T_{ref}} \right) \right) \tag{8}$$

The mass balance equation used to consider the variation with time of the composition of each component is reported in Eq. 9.

$$\frac{dc_i}{dt} = \nu_i r_H \tag{9}$$

Kinetic and thermodynamic parameters resulted from the estimation are reported in Table 9. The results confirmed that the reaction is endothermic and the product formation is favored as indicated from the equilibrium constant.

Table 9. Parameter estimation results for tests promoted by sulfuric acid.

	Value	95 % CI	Units	Correlation matrix			
				$\Delta_r H$	Ea_H	K_{ref}	k_{ref}
$\Delta_r H$	10.3	0.2	kJ/mol	1			
Ea_H	60.8	0.1	kJ/mol	-0.2	1		
K_{ref}	1.69	0.01	-	+0.3	-0.1	1	
$k_{H,ref}$	$9.04 \cdot 10^{-10}$	$0.01 \cdot 10^{-10}$	$(m^3/mol)^2 s^{-1}$	-0.1	+0.4	-0.2	1

In the following Figure, an overall parity plot is reported where it can be seen that all the collected data are included in an error window of $\pm$10 %.

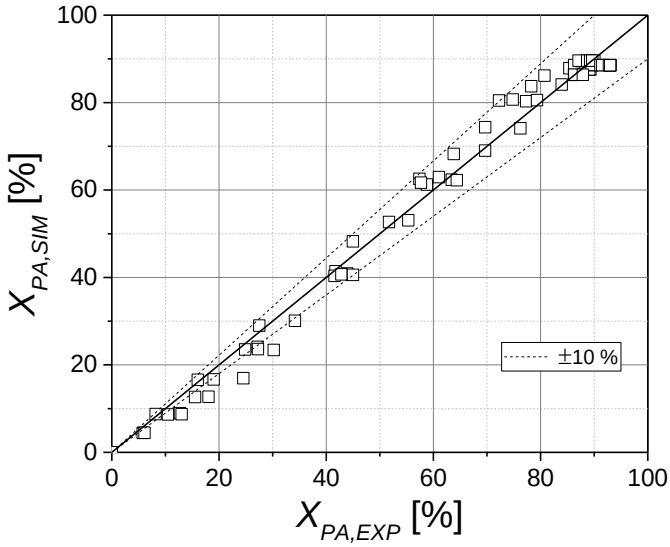

Figure 15. Parity plot for tests promoted by sulfuric acid.

2.7.3 Tests promoted by Amberlite IR120

Tests were performed in the presence of Amberlite IR120 as heterogeneous catalyst (Table 10). The effect of different experimental conditions on the reaction

rate (i.e. stirring rate, temperature, catalyst load and reactants molar ratio) was studied.

Table 10. Tests promoted by Amberlite IR120.

Test	***v*** **[rpm]**	***T*** **[K]**	**EtHex/PA [mol/mol]**	ρ_B **[kg/m^3]**
1	200	363	5:1	16.9
2	400	363	5:1	16.9
3	600	363	5:1	16.9
4	800	363	5:1	16.9
5	600	353	5:1	16.9
6	600	343	5:1	16.9
7	600	363	5:1	10.6
8	600	363	5:1	4.2
9	600	363	2.5:1	16.9
10	600	363	1:1	16.9

Tests at different values of stirring rate (Figure 16) were performed to investigate the possible presence of external mass transfer limitation. Similar results were obtained for the tests at 200, 400 and 600 rpm confirming the absence of fluid-solid mass transfer limitation, while lower conversion was reached at 800 rpm since the catalyst was confined on the reactor wall due to the high stirring rate.

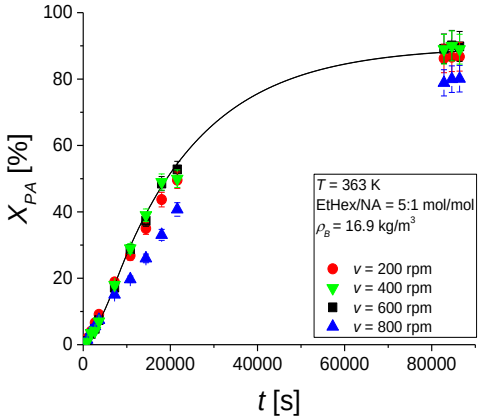

Figure 16. Stirring rate effect for tests promoted by Amberlite IR120.

Temperature effect was reported in Figure 17 where it can be seen that by increasing the temperature value also an increase in reaction rate was observed.

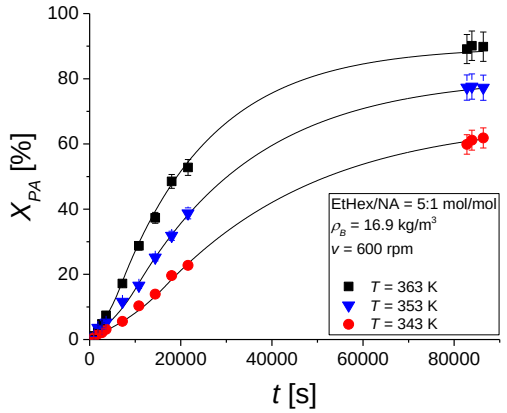

Figure 17. Temperature effect for tests promoted by Amberlite IR120.

The same effect was obtained also in the experiments conducted varying reactants molar ratio (Figure 18).

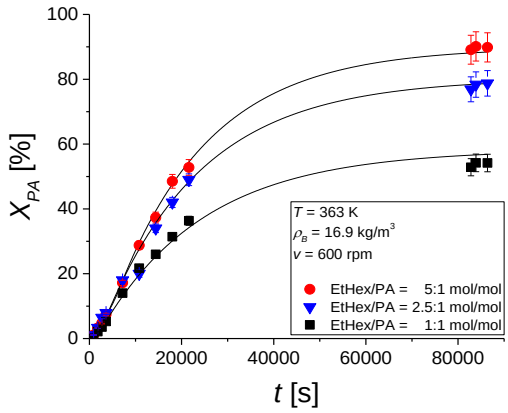

Figure 18. Reactants molar ratio effect for tests promoted by Amberlite IR120.

Other experiments were conducted to investigate the effect of the Amberlite IR120 load on the reaction rate. By increasing catalyst concentration, the reaction rate increased, too (Figure 19A).

Differently from sulfuric acid, in the case of Amberlite IR120, multiplying reaction time catalyst for bulk density raised to 0.5 experimental data overlap indicating that this value was the proportionality coefficient (Figure 19B).

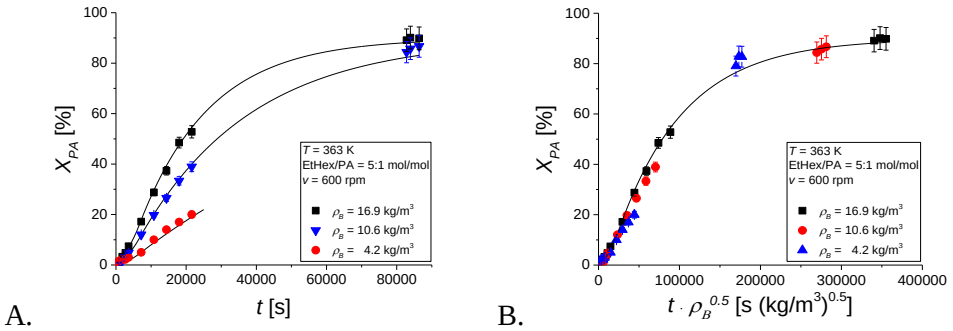

Figure 19. A. Catalyst load effect for tests promoted by Amberlite IR120.
B. Reaction time normalized per catalyst bulk density.

A value lower than one indicates that an internal mass transfer limitation occurred. The experimental data were elaborated with a kinetic model taking into account intraparticle diffusion phenomena.

As in the case of the sulfuric acid, the reaction rate was expressed as reported in Eq. 10.

$$r_A = k_A\left(c_{PA}c_{EtHex} - \frac{1}{K}c_{EtHex-PA}c_{H_2O} \right) \tag{10}$$

A modified Arrhenius equation (Eq. 11) was used as in the previous case while the enthalpy and the equilibrium constant values were the same of sulfuric acid as they don't change with the catalyst.

$$k_A = k_{A,ref}\exp\left(-\frac{Ea_A}{R}\left(\frac{1}{T} - \frac{1}{T_{ref}} \right) \right) \tag{11}$$

Also in this case T_{ref} was fixed at 333 K.

An intraparticle mass balance equation was used considering a spherical catalyst particle, as reported in Eq. 12.

$$\varepsilon_P \frac{\partial c_{i,s}}{\partial t} = \frac{D_{e,i}}{R_P^2}\left(\frac{\partial^2 c_{i,s}}{\partial x^2} + \frac{2}{x}\frac{\partial c_{i,s}}{\partial x} \right) + \nu_i r_A \rho_P \tag{12}$$

Effective diffusivity, was calculated with the following equation:

$$D_{e,i} = D_i \frac{\varepsilon_P}{\tau_P} \tag{13}$$

where the molecular diffusivity was calculated using Wilke and Chang equation for a multicomponent system (Eq. 14).

$$D_i = 7.4\cdot 10^{-12}\frac{T\left(\phi_{mix}M_i\right)^{0.5}}{\mu_{mix}V_{m,i}^{0.5}} \tag{14}$$

Two boundary conditions for the center and the surface of the catalyst particle were needed to solve the intraparticle mass balance equation, reported respectively in Eqs. 15 and 16.

$$\left.\frac{\partial c_{i,s}}{\partial x}\right|_{x=0} = 0 \tag{15}$$

$$\frac{D_{e,i}}{R_P}\frac{\partial c_{i,s}}{\partial x}\bigg|_{x=1} = k_s a_{sp}\left(c_i - m_i\, c_{i,s}\big|_{x=1}\right) \tag{16}$$

In Eq. 12, a mass balance equation is reported for the liquid bulk phase considering the accumulation as the mass transfer flux to the catalyst surface.

$$\frac{dc_i}{\partial t} = -k_s a_s\left(c_i - m_i\, c_{i,s}\big|_{x=1}\right)\frac{\rho_B}{\rho_P} \tag{17}$$

Further information about the kinetic model approach can be found in publication **I** where it is discussed more in detail.

All the experiments were elaborated with gPROMS Model Builder v.4.0 software and the results of the parameter estimation are reported in Table 11.

Table 11. Parameter estimation results for tests promoted by Amberlite IR120.

	Value	**95 % CI**	**Units**	**Correlation matrix**	
				Ea_A	$k_{A,ref}$
Ea_A	57.7	0.1	kJ/mol	1	
$k_{A,ref}$	$3.4\cdot10^{-11}$	$0.01\cdot10^{-11}$	$(m^3/kg)(m^3/mol)s^{-1}$	-0.5	1

The good agreement between the experimental and simulated data can be appreciated from the Figures previous reported and from the parity plot in Figure 20 where it can be seen that all the collected data are included in an error range of ±20 %.

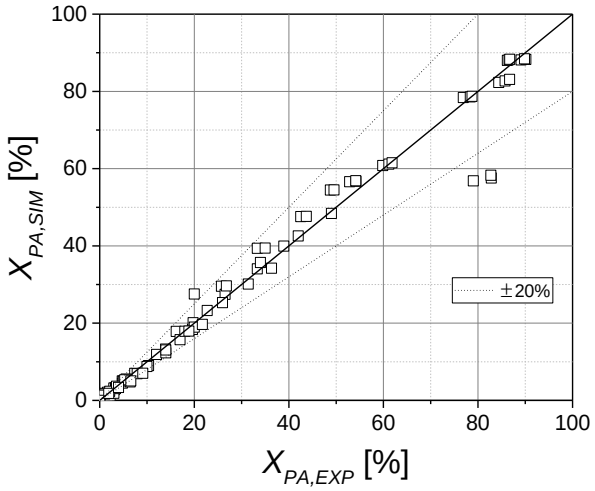

Figure 20. Parity plot for tests promoted by Amberlite IR120.

2.7.4 Tests promoted by Amberlyst-15

Experiments were also performed in the presence of Amberlyst-15 as heterogeneous catalyst. As in the case of Amberlite IR120, the effect of stirring rate, temperature, catalyst load and reactants molar ratio on the reaction rate was investigated. In Table 12 tests conditions are reported.

Table 12. Tests promoted by Amberlyst-15.

Test	v [rpm]	T [K]	EtHex/PA [mol/mol]	ρ_B [kg/m^3]
1	200	363	5:1	16.9
2	600	363	5:1	16.9
3	800	363	5:1	16.9
4	600	353	5:1	16.9
5	600	343	5:1	16.9
6	600	363	5:1	25.4
7	600	363	5:1	33.8
8	800	363	5:1	33.8
9	1000	363	5:1	33.8
10	600	363	2.5:1	33.8
11	600	363	1:1	33.8
12	600	353	5:1	33.8
13	600	343	5:1	33.8

A first set of experiments was conducted at different stirring rate to evaluate the possibility of external mass transfer limitation. Three tests were made by using a lower amount of catalyst (ρ_B = 16.9 kg/m^3) but with these conditions the equilibrium was not reached, as visible in Figure 21A, hence it was chosen to conduct the same experiments using a higher catalyst amount (ρ_B = 33.8 kg/m^3), as reported in Figure 21B.

Similar results were obtained in all the tests, so it possible to confirm the absence of external mass transfer limitation.

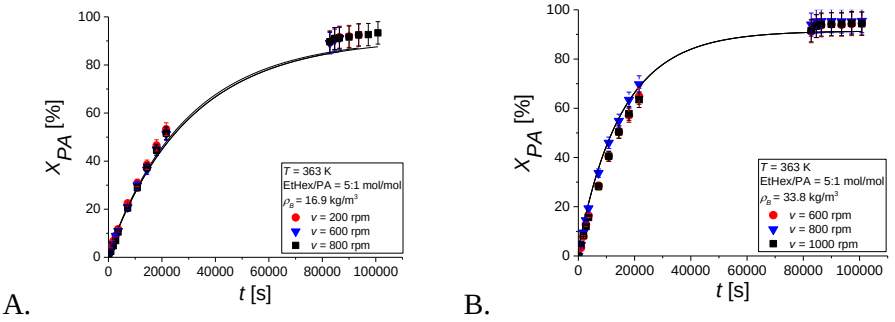

Figure 21. Stirring rate effect for tests promoted by Amberlyst-15 fixing: A. ρ_B = 16.9 kg/m^3. B. ρ_B = 33.8 kg/m^3.

The Amberlyst-15 load was varied in order to investigate its effect on the reaction rate. From Figure 22A it is possible to see that reaction rate increased by increasing the catalyst load. As in the case of Amberlite IR120, multiplying reaction time for catalyst bulk density raised to 0.5, experimental data overlap. This indicated that this value was the proportionality coefficient (Figure 22B). A value lower than one implies that an internal mass transfer limitation can occur, hence it was considered in the development of the kinetic model.

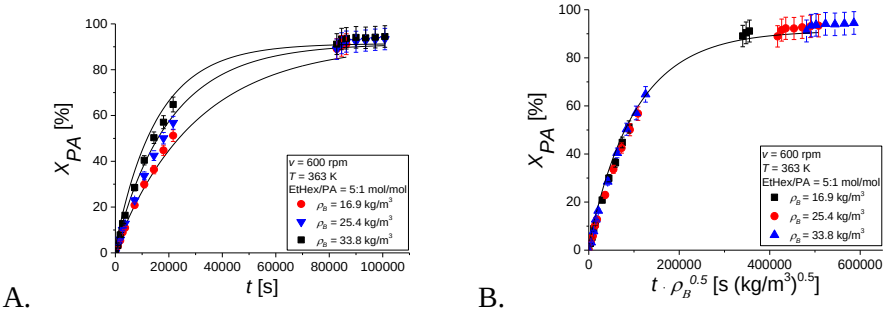

Figure 22. A. Catalyst load effect for tests promoted by Amberlyst-15. B. Reaction time normalized per catalyst bulk density.

Tests were performed at different alcohol/pelargonic acid molar ratio. By increasing the molar ratio, also the reaction rate increased, as showed in Figure 23.

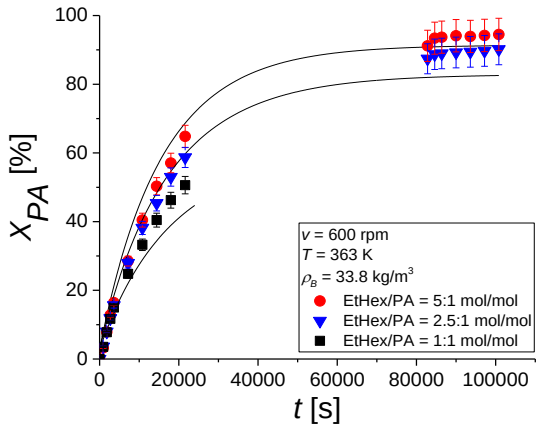

Figure 23. Reactants molar ratio effect for tests promoted by Amberlyst-15.

Two experiments sets were made to investigate the temperature effect. The first one was made at ρ_B = 16.9 kg/m^3 (Figure 24A) while the second one was made at ρ_B = 33.8 kg/m^3 (Figure 24B). As showed in Figure 24A, the equilibrium plateau was not reached, hence a higher amount of catalyst needed to reach the equilibrium in a lower reaction time. The same effect occurred in the test at 343 K with a bulk density of 33.8 kg/m^3. In both cases it is possible to note that by increasing the temperature, also an increase in reaction rate was observed.

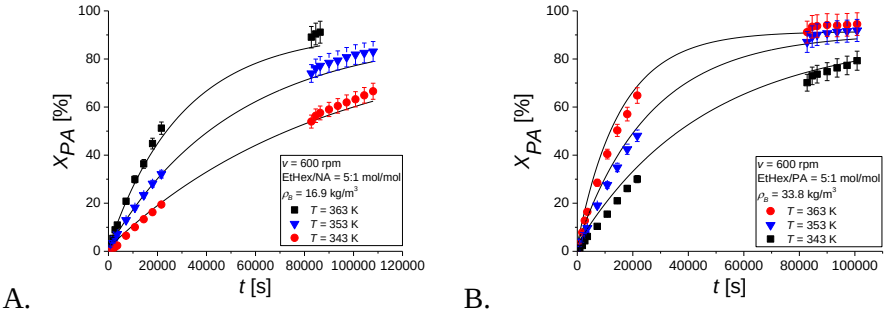

Figure 24. Temperature effect for tests promoted by Amberlyst-15 fixing: A. ρ_B = 16.9 kg/m^3. B. ρ_B = 33.8 kg/m^3.

The experimental data were interpreted with a reliable kinetic model using the same approach already reported for Amberlite IR120 catalyzed tests (section 2.6.3). From the elaboration of the kinetic model, the activation energy and the reference kinetic constant were estimated, and the results are reported in Table 13 together with the statistic information.

Table 13. Parameter estimation results for tests promoted by Amberlyst-15.

	Value	**95 % CI**	**Units**	**Correlation matrix**	
				$Ea_{A\text{-}15}$	$k_{A\text{-}15,\,ref}$
$Ea_{A\text{-}15}$	58.4	0.1	kJ/mol	1	
$k_{A\text{-}15,\,ref}$	$6.21\cdot10^{-11}$	$7.34\cdot10^{-14}$	$(m^3/kg)(m^3/mol)s^{-1}$	-0.9	1

Finally, a parity plot including all the collected experimental data was reported in Figure 25.

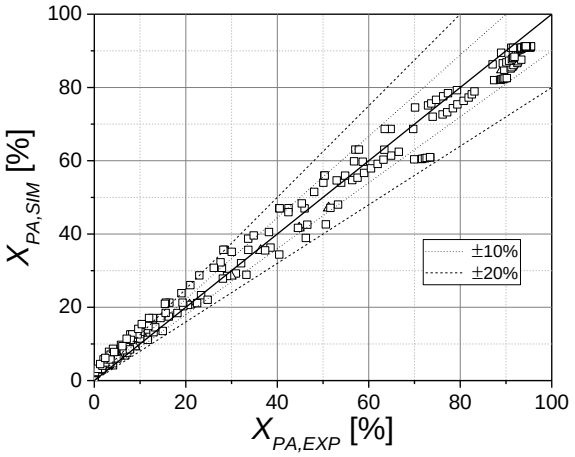

Figure 25. Parity plot including all the collected data for the tests promoted by Amberlyst-15.

All the collected experimental data are included in an error window of ±20 % confirming the good agreement between the experimental data and the simulated curves, already reported in Figures 21-24.

2.7.5 Tests promoted H_2WO_4/SiO_2

The results reported in the previous sections showed the good performances of both resins but despite this, they have the limit of not being able to be used at temperatures higher than 120 °C because of their degradation. For this reason, a H_2WO_4/SiO_2 based catalyst, suitable at high temperatures [1], up to 200 °C, was synthetized and tested in the batch kinetic study of the pelargonic acid esterification with 2-ethylhexanol.

2.7.5.1 Catalyst synthesis

The catalyst used in the kinetic tests contained 10 wt.% of H_2WO_4 supported on silica Aerolyst 355. It was synthesized according to a previous patent reported in the literature [2]. First, the silica was ground in order to obtain a powder and the incipient wetness was evaluated. This is an important operation because it allowed to evaluate the amount of H_2O_2 needed as solvent in the catalyst preparation. In the incipient wetness determination, distilled water was used and a value of about 180% was obtained. The catalyst was synthesized through the following steps: (i) dissolution of the tungstic acid in the previous determined amount of H_2O_2 (60 vol %) under magnetic stirring; (ii) the silica was impregnated with the solution of H_2WO_4 in H_2O_2 obtaining a yellow product; (iii) the supported catalyst was dried at 120 °C for 24 h and then (iv) it was calcinated in an oven at 300 °C for 2 h to obtain a better dispersion of the tungstic acid on the silica support. The pictures of the catalyst after each step are reported in Figure 26.

A. 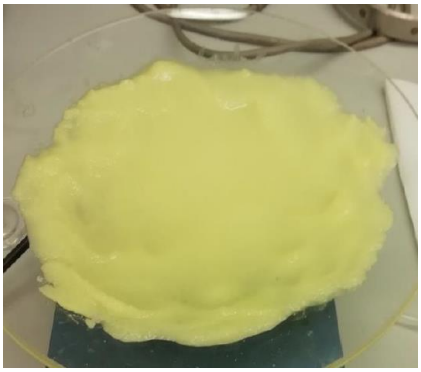 B. 

C. 

Figure 26. A. Silica impregnated with tungstic acid in H_2O_2 solution. B. Catalyst dried at 120 °C for 24 h. C. Catalyst after calcination at 300 °C for 2 h.

2.7.5.2 Batch kinetic tests

The catalyst synthetized as described in the previous section was tested in kinetic experiments. As in the case of Amberlite IR120 and Amberlyst-15, the effect of stirring rate, temperature, catalyst load and reactants molar ratio on the reaction rate was investigated. In Tables 14-17, a list of all performed tests are reported.

Table 14. Conditions of the tests promoted by H_2WO_4/SiO_2.

Test	***v* [rpm]**	***T* [K]**	**EtHex/PA [mol/mol]**	ρ_B **[kg/m^3]**
1	200	403	5:1	8.50
2	400	403	5:1	8.50
3	600	403	5:1	8.50
4	800	403	5:1	8.50
5	600	393	5:1	8.50
6	600	383	5:1	8.50
7	600	373	5:1	8.50
8	600	363	5:1	8.50
9	600	403	5:1	4.23
10	600	393	5:1	4.23
11	600	383	5:1	4.23
12	600	373	5:1	4.23
13	600	363	5:1	4.23
14	600	403	5:1	2.02
15	600	393	5:1	2.02
16	600	383	5:1	2.02
17	600	373	5:1	2.02
18	600	363	5:1	2.02
19	600	403	5:1	1.06
20	600	403	2.5:1	8.50
21	600	403	1:1	8.50
22	600	393	2.5:1	8.50
23	600	393	1:1	8.50
24	600	383	2.5:1	8.50
25	600	383	1:1	8.50

26	600	373	2.5:1	8.50
27	600	373	1:1	8.50

Also in this case, the first investigated parameter was the stirring rate to evaluate the existence of the external mass transfer limitation (Figure 27).

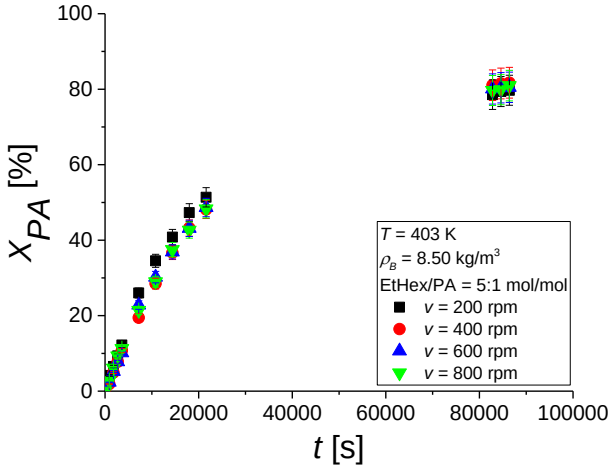

Figure 27. Stirring rate effect for tests promoted by H_2WO_4/SiO_2.

The similar results, obtained in each test, confirmed the absence of the external mass transfer limitation, hence 600 rpm was the rate adopted in all other tests.

In Figure 28, three sets of experiments loading different catalyst amount were showed to evaluate the temperature effect on the reaction rate where it was clear in all the three cases that reaction rate increased by increasing temperature value.

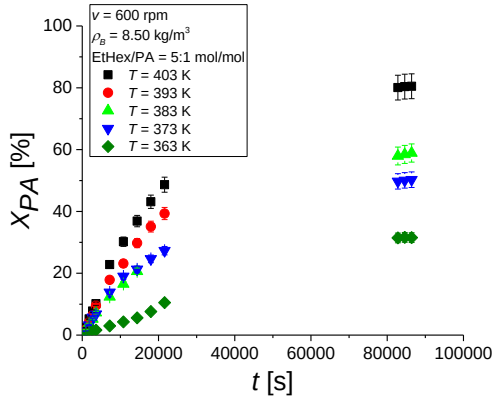
v = 600 rpm
ρB = 8.50 kg/m3
EtHex/PA = 5:1 mol/mol
T = 403 K
T = 393 K
T = 383 K
T = 373 K
T = 363 K
XPA [%]
t [s]
0
20
40
60
80
100
0
20000
40000
60000
80000
100000

A.

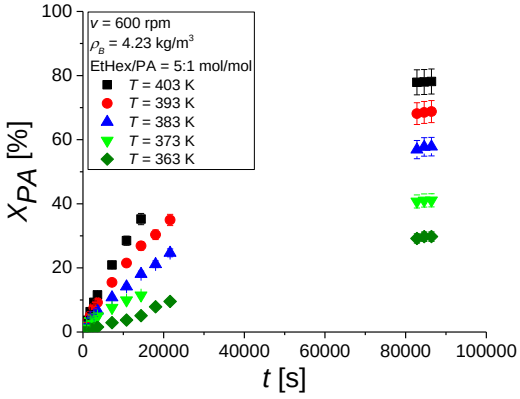
v = 600 rpm
ρB = 4.23 kg/m3
EtHex/PA = 5:1 mol/mol
T = 403 K
T = 393 K
T = 383 K
T = 373 K
T = 363 K
XPA [%]
t [s]
0
20
40
60
80
100
0
20000
40000
60000
80000
100000

B.

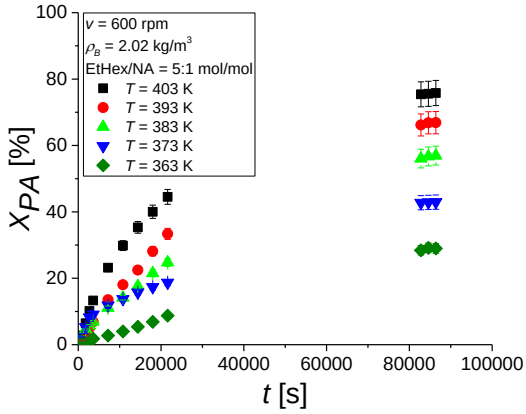

C.

Figure 28. Temperature effect for tests promoted by H_2WO_4/SiO_2 fixing: A. v = 600 rpm, ρ_B = 8.50 kg/m^3, EtHex/PA = 5:1 mol/mol, B. v = 600 rpm, ρ_B = 4.23 kg/m^3, EtHex/PA = 5:1 mol/mol, C. v = 600 rpm, ρ_B = 2.02 kg/m^3, EtHex/PA = 5:1 mol/mol.

From tests performed at different temperatures, an apparent value of the activation energy could be estimated using the linearized Arrhenius equation (Eq. 18).

$$\ln\left(k\right) = \ln\left(k_{ref}\right) - \frac{E_a}{RT} \tag{18}$$

The reaction enthalpy, instead, was evaluated using the linearized van't Hoff equation (Eq. 19).

$$\ln\left(K\right) = -\frac{\Delta_r H}{RT} + c \tag{19}$$

In the following Table, the apparent values of the activation energy for the three experiments sets at different catalyst load and the reaction enthalpy are reported. The apparent activation energy decreased by increasing the catalyst load and this was an expected result considering the presence of the intraparticle diffusion phenomenon. The enthalpy reaction didn't have consistent variations in the three cases, therefore an average value is reported.

Table 15. Parameter estimated for tests promoted by H_2WO_4/SiO_2.

Parameter	Value	Error	Unit
$E_{a,1}$	44	17	kJ/mol
$E_{a,2}$	55	12	kJ/mol
$E_{a,3}$	62	14	kJ/mol
$\Delta_r H$	89	5	kJ/mol

Different experiment sets were made to investigate the effect of catalyst load on the reaction rate. Tests experimental conditions are summarized in Table 14.
An interesting effect is visible from Figures 29-32 where increasing the catalyst amount, there was not an improvement in the reaction rate and this phenomenon was found in all the tested temperatures.

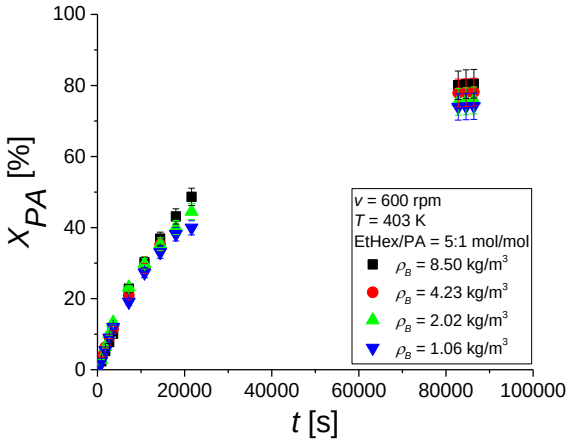

A.

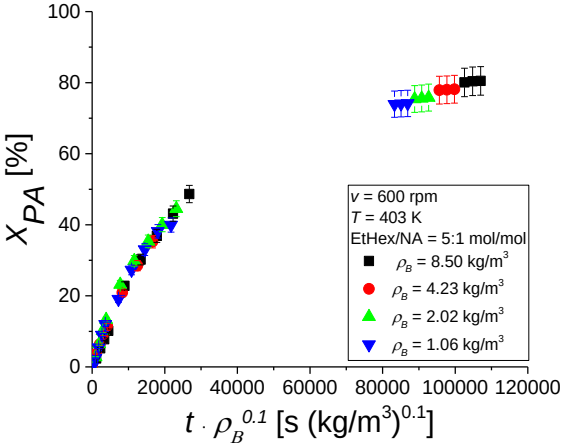

B.

Figure 29. A. Catalyst load effect for tests promoted by H_2WO_4/SiO_2 fixing T = 403 K. B. Reaction time normalized per catalyst bulk density.

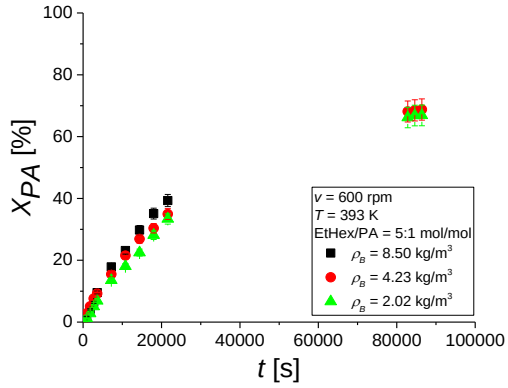

A.

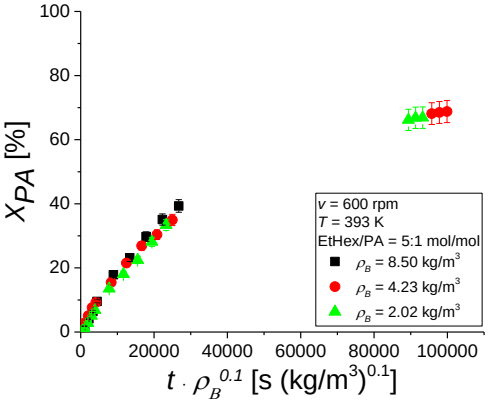

B.

Figure 30. A. Catalyst load effect for tests promoted by H_2WO_4/SiO_2 fixing T = 393 K. B. Reaction time normalized per catalyst bulk density.

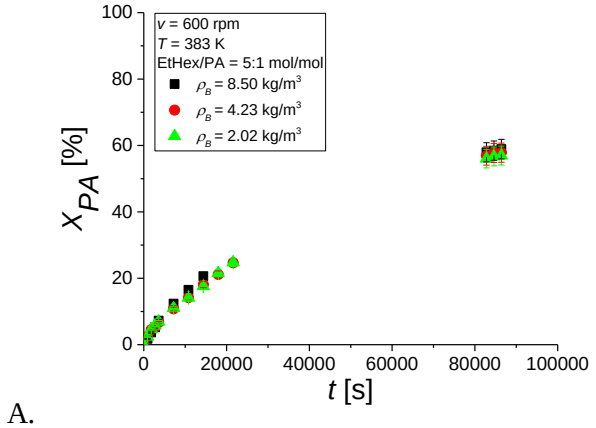

A.

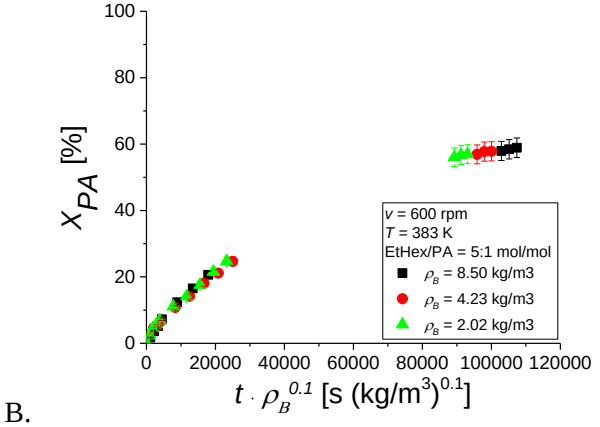

B.

Figure 31. A. Catalyst load effect for tests promoted by H_2WO_4/SiO_2 fixing T = 383 K. B. Reaction time normalized per catalyst bulk density.

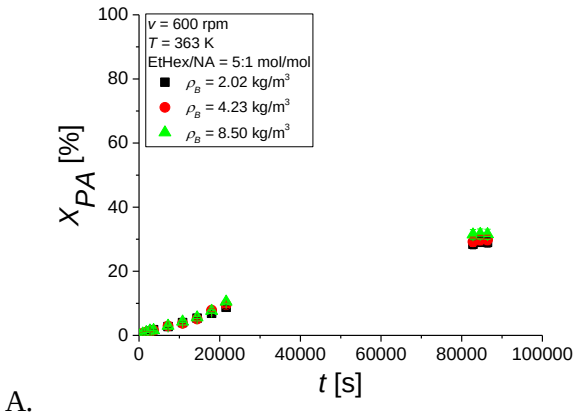

A.

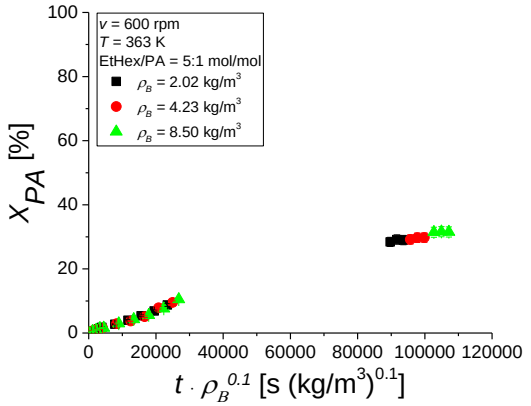

B.

Figure 32. A. Catalyst load effect for tests promoted by H_2WO_4/SiO_2 fixing T = 363 K. B. Reaction time normalized per catalyst bulk density.

A cause can be found in the intraparticle mass transfer limitation considered that the proportionality coefficient is equal to 0.1, much less than the unity. Further investigations are needed to understand this behavior, and, for this reason, other experiments are still ongoing to develop also a kinetic model that can interpret well the experimental data.

Different sets of experiments were made also to investigate the effect of the alcohol/acid molar ratio on the reaction rate. In particular, tests were conducted fixing catalyst bulk density (ρ_B = 8.50 kg/m^3) at different temperatures.

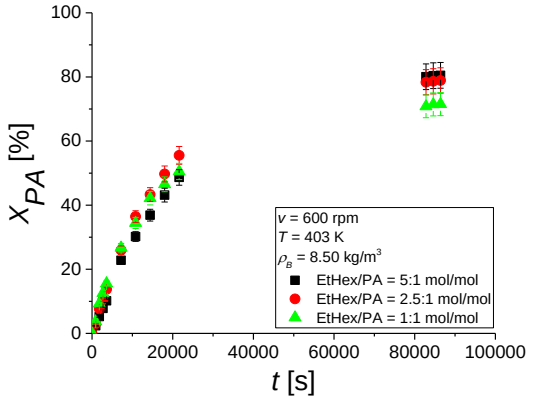
100
80
60
40
20
0
X_{PA} [%]
0
20000
40000
60000
80000
100000
t [s]
v = 600 rpm
T = 403 K
ρ_B = 8.50 kg/m^3
EtHex/PA = 5:1 mol/mol
EtHex/PA = 2.5:1 mol/mol
EtHex/PA = 1:1 mol/mol

A.

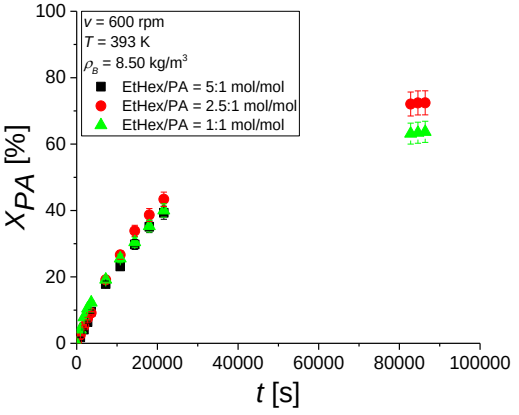
100
80
60
40
20
0
X_{PA} [%]
0
20000
40000
60000
80000
100000
t [s]
v = 600 rpm
T = 393 K
ρ_B = 8.50 kg/m^3
EtHex/PA = 5:1 mol/mol
EtHex/PA = 2.5:1 mol/mol
EtHex/PA = 1:1 mol/mol

B.

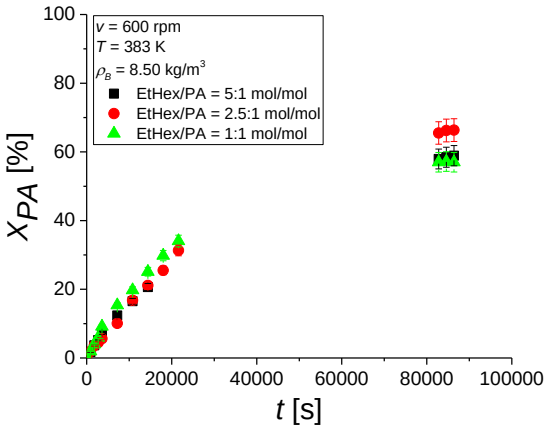

C.

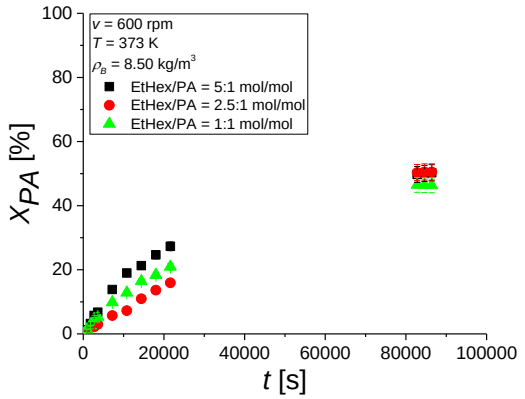

D.

Figure 33. Reactants molar ratio effect for tests promoted by H_2WO_4/SiO_2 fixing: A. T = 403 K. B. T = 393 K. C. T = 383 K. D. T = 373 K.

From Figure 33, an unconventional behavior can be seen. Experimental data followed an irregular trend, showing better results with a lower alcohol/acid molar ratio. Similar trend can be appreciated in all the four sets. Also in this case, as mentioned before, further investigations will need to better understand the reasons of the obtained results.

2.8 Continuous kinetic study

Experimental tests were performed in a continuous apparatus, packed respectively with Amberlite IR120 and Amberlyst-15, in order to validate the kinetics studied in the batch reactor. Different experimental conditions were varied, such as temperature, volumetric flow and reactants molar ratio.

2.8.1 Continuous tests promoted by Amberlite IR120

Tests in the continuous apparatus were made varying volumetric flow, temperature and alcohol/acid molar ratio. The list of the conditions of all performed experiments is reported in the following table.

Table 16. Experimental conditions for continuous tests.

Test	***T* [K]**	***Q* [m^3/s]**	**EtHex/PA [mol/mol]**
1	353	$4.17 \cdot 10^{-9}$	5:1
2	343	$4.17 \cdot 10^{-9}$	5:1
3	363	$4.17 \cdot 10^{-9}$	5:1
4	363	$8.33 \cdot 10^{-9}$	5:1
5	353	$8.33 \cdot 10^{-9}$	5:1
6	343	$8.33 \cdot 10^{-9}$	5:1
7	363	$1.67 \cdot 10^{-8}$	5:1
8	353	$1.67 \cdot 10^{-8}$	5:1
9	343	$1.67 \cdot 10^{-8}$	5:1
10	363	$4.17 \cdot 10^{-9}$	2.5:1
11	363	$4.17 \cdot 10^{-9}$	1:1

A first test (Test 1 in Table 16) was prolonged for 54 h to check the stability of the catalyst, in order to evaluate its applicability in the continuous operation. The results (Figure 34) showed that the catalyst was suitable for the purpose since the conversion in each bed was the same after a long reaction period.

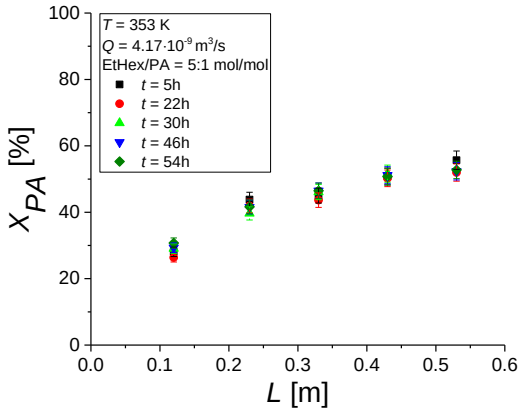

Figure 34. Stability test for Amberlite IR120 fixing T = 353 K, $Q = 4.17 \cdot 10^{-9}$ m^3/s, EtHex/PA = 5:1 mol/mol.

The experimental data, collected in the experiments reported in Table 16, were simulated with a reliable kinetic model. The mass balance in the liquid bulk was the following:

$$\frac{\partial c}{\partial t} = -u\frac{\partial c}{\partial z} + D_z\frac{\partial^2 c}{\partial z^2} - k_s a_{sp}\left(C - C_s\right) \tag{20}$$

where the superficial velocity, u, was calculated from Eq. 21.

$$u = \frac{Q}{A \cdot \varepsilon} \tag{21}$$

The mass balance on the catalyst surface, instead, was reported in Eq. 22.

$$k_s a_{sp}\left(C - mC_s\right) = \nu_i r \rho_B \tag{22}$$

The fluid-solid mass transfer coefficient ($k_s \cdot a_{sp}$) was estimated from the kinetic model and the resulted value is reported in Table 17.

Table 17. Parameter estimation result.

Parameter	Value	Unit
$k_s \cdot a_{sp}$	$5 \cdot 10^{-7}$	1/s

The kinetic model well described the collected data as it is possible to see from Figure 35, where the temperature effect and the good agreement between experimental and calculated data were showed and confirmed by the parity plot in Figure 36 in which the error range for all the experimental data is ± 20%.

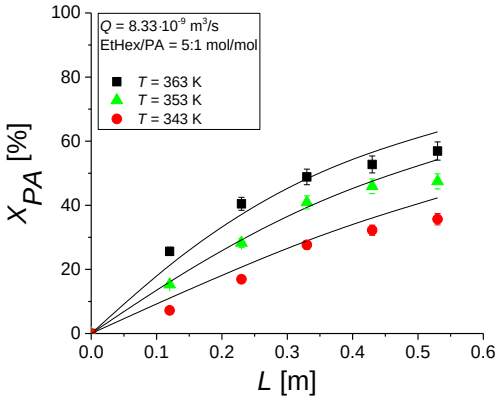

Figure 35. Temperature effect for tests catalyzed by Amberlite IR120 fixing Q = $8.33 \cdot 10^{-9}$ m^3/s and EtHex/PA = 5:1 mol/mol.

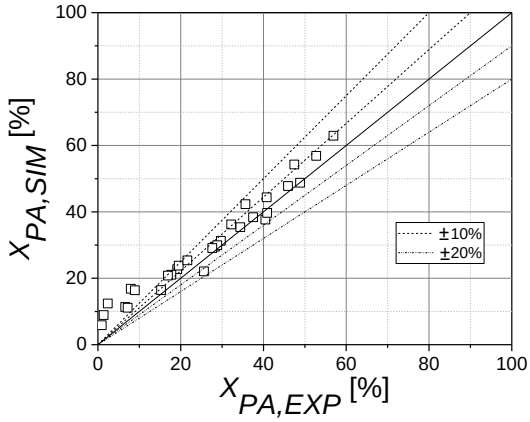

Figure 36. Parity plot considering all the collected experimental data for Amberlite IR120.

2.8.2 Continuous tests promoted by Amberlyst-15

Tests catalyzed by Amberlyst-15 were performed in the same conditions of Amberlite IR120, reported in Table 19 in section 2.8.1.

Also in this case, a first test (Test 1 in Table 16) was prolonged for 54 h to check the stability of the catalyst. This test confirmed its applicability in the continuous operation as appreciated from the results in Figure 37 where it can be seen that the conversion is stable for the whole test time.

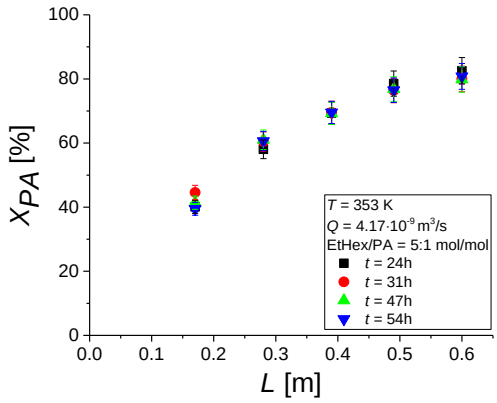

Figure 37. Stability test for Amberlyst-15 fixing T = 353 K, Q = 4.17·10^{-9} m^3/s, EtHex/PA = 5:1 mol/mol.

The same approach, already described in the section 2.8.1, in the kinetic model development was followed. Also in this case, the model interpreted in a good way the experimental data as shown in Figure 38, where the volumetric flow effect was reported together with the parity plot in Figure 39. From the parameter estimation, the fluid-solid mass transfer coefficient ($k_s \cdot a_{sp}$) was obtained (see Table 18).

Table 18. Parameter estimation result.

Parameter	Value	Unit
$k_s \cdot a_{sp}$	5·10^{-8}	1/s

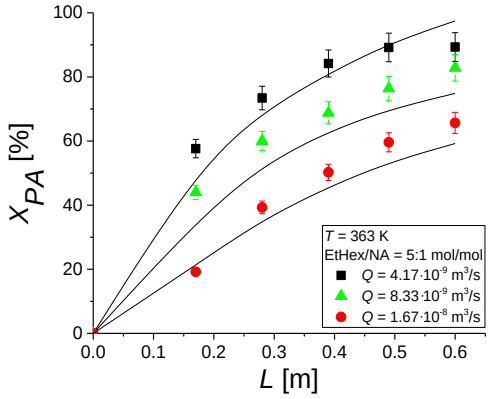

Figure 38. Volumetric flow effect for tests catalyzed by Amberlyst-15 fixing T = 363 K, EtHex/PA = 5:1 mol/mol.

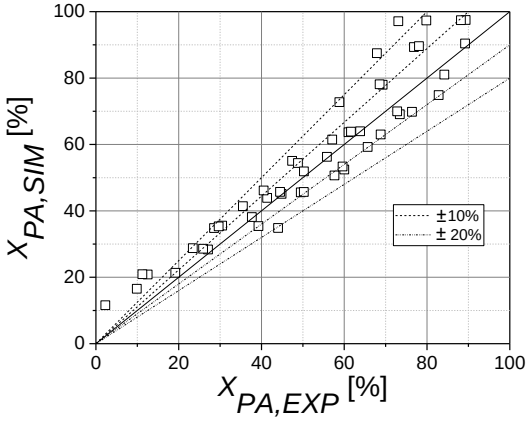

Figure 39. Parity plot including all the collected experimental data for Amberlyst-15.

References

1. Vitiello, R., Tesser, R., Russo, V., Turco R., Andini, S. & Di Serio, M. Loop reactor modeling for lubricant synthesis. *Chem. Eng. J.* **329**, 295-304 (2017).
2. Vairo, G., Di Serio, M., Santacesaria E., Tesser, R., Cammarota F. & Mandato, N. (DOW Italia srl) PCT Int. Appl. WO 2008037400 (A1) (2008).

Chapter 3 – Pelargonic acid esterification: Solvents synthesis and applications.

3.1 Overview

In this chapter the synthesis of solvents from pelargonic acid will be discussed. In the literature [1], solvents from pelargonic acid and 2-ethylhexanol were synthesized using zinc oxide as catalyst. In the present thesis, the goal was the synthesis of these solvents promoted by Amberlyst-15, already used in the kinetic investigation, in order to verify its applicability in this reaction.
For this reason, the esterification reaction of pelargonic acid with 2-ethylhexanol was performed in a loop reactor in the presence of Amberlyst-15 as catalyst. Several tests were conducted to verify the stability of the catalyst and finally, the synthesized solvents were tested in the formulation of printing inks and their properties were characterized.

3.2 Chemicals

Pelargonic acid (purity ≥ 96%) and 2-ethylhexanol (purity ≥ 99%) were used in all the experiments. All the reagents together with the catalyst, Amberlyst-15, were purchased by Merck. Amberlyst-15 properties were reported in Table 4 in section 2.2.

3.3 Experimental setup

The experimental apparatus used for the synthesis of the solvents consisted of a loop reactor. The scheme of the reaction system together with the related picture was represented in Figure 40.

A.

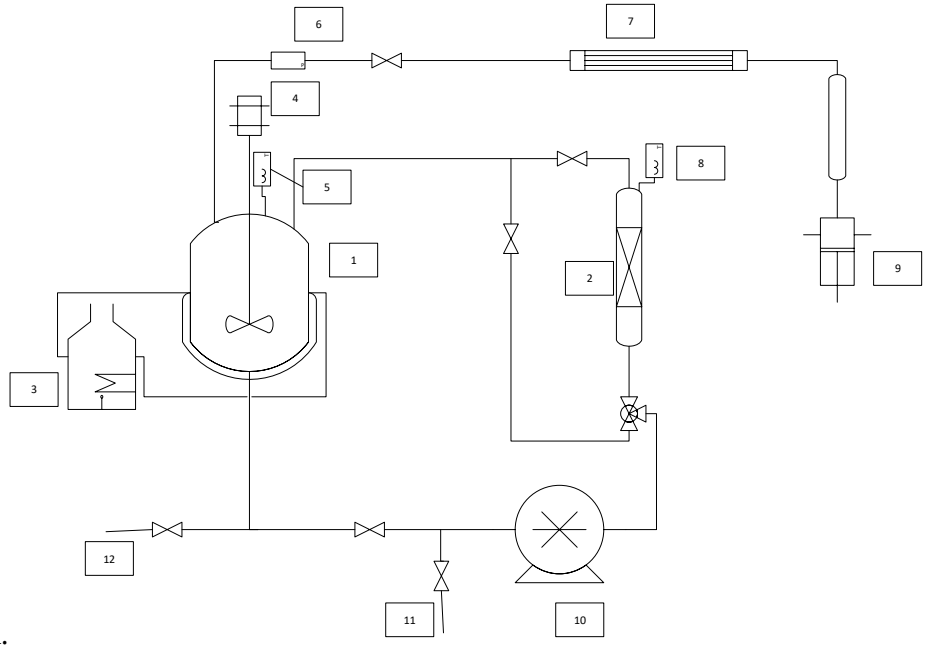

B.

Figure 40. Loop reactor scheme (A) with the related picture (B).

1. Stainless steel batch reactor;
2. Packed bed reactor;
3. Oil thermostat;
4. Stirrer connected to the inverter;
5. Batch reactor thermocouple;
6. Manometer connected to the vacuum pump;
7. Condenser;
8. Tubular reactor thermocouple;
9. Vacuum pump;
10. Pump;
11. Feed valve;
12. Withdrawal valve.

The loop reactor consisted of a Hastelloy autoclave of 1 dm^3 equipped with a magnetically driven stirrer and connected from the bottom to a tubular reactor (L = 26 cm; ID = 2 cm) where the catalyst was packed and its upper part was connected to the top of the vessel itself. The reagents were fed through a pump that allowed also their recycle in the tubular reactor. Two thermocouples with thermoregulators allowed the control of the temperature respectively of the liquid and of the vapor inside the vessel, heated through an oil thermostat, while another one was placed at the exit of the packed bed reactor. A vacuum pump allowed to operate at reduced pressures controlled by a manometer and a condenser was connected to the batch reactor in order to remove the water formed during the reaction. This system configuration has the advantage that the catalyst was placed in the tubular reactor avoiding the separation step of the catalyst itself from the products, making the process easier.

3.4 Reaction procedure

Pelargonic acid was loaded inside the batch reactor through a pipe parallel to the tubular reactor in order to avoid the passage of the reagents in the reactor packed with the catalyst, previously dried in an oven at T = 333K, before the beginning of the reaction. The system was heated and when the temperature reached the set value, 2-ethylhexanol was added. From that moment, reagents flowed through the tubular reactor and, even if after the single passage the conversion was low, the liquid flowed more times through the tubular reactor packed with the catalyst, obtaining high conversion degrees at the end of the reaction. The presence of the vacuum pump allowed the removing of the water shifting the equilibrium towards the products and furthermore at the end of the reaction, the excess of alcohol was removed in order to obtain a pure product.

3.5 Analytical method

The analytical method used to determine pelargonic acid conversion was the same used for the kinetic study and it was already described in section 2.5.

3.6 Solvents synthesis: tests promoted by Amberlyst-15

Several sets of tests were made in order to synthesize the solvents and investigate the best experimental conditions to reach the highest conversion. Furthermore, experiments were also performed to test the catalyst stability evaluating the final conversion in its re-uses.
Amberlyst-15 properties were reported in Table 4 in section 2.2 while information about the swelling can be found in section 2.4.

The first set was made to investigate catalyst reusability and the experimental conditions are reported in Table 19. A blank test was made in the same conditions to investigate the autocatalytic contribution of the pelargonic acid itself.

Table 19. First tests set conditions.

T_{BR} [K]	383
T_{TR} [K]	373
v [rpm]	600
EtHex/PA [mol/mol]	1.2:1
Q [m^3/s]	$1.67 \cdot 10^{-6}$
w_{cat} [g]	25
t [h]	5

Samples were withdrawn each hour to follow the reaction trend. A comparison between the blank test and the four reuses tests were reported in Figure 41.

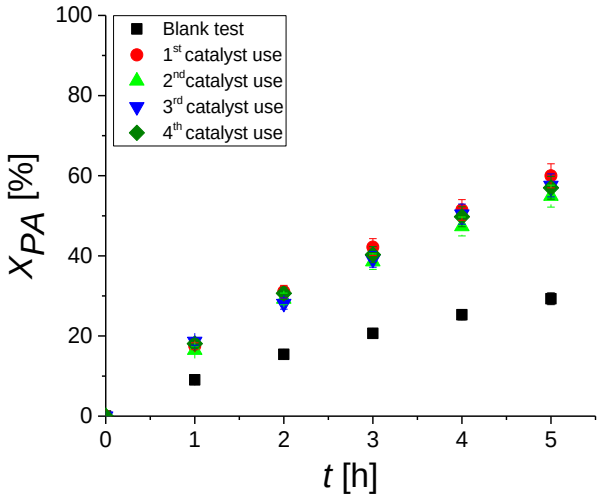

Figure 41. First set of Amberlyst-15 re-use tests.

From Figure 41, it is possible to appreciate that the catalyst could be re-used without losses in its activity. In fact, after four tests the reached conversion was always the same.

In the second set of tests, the recycle volumetric flow and alcohol/acid molar ratio effects on the final PA conversion were investigated (see Table 20 for the experimental conditions).

Table 20. Second tests set conditions.

Test	T_{BR} **[K]**	T_{TR} **[K]**	v **[rpm]**	**EtHex/PA [mol/mol]**	Q **[m³/s]**	w_{cat} **[g]**	t **[h]**
1	383	373	600	1.2:1	$1.67 \cdot 10^{-6}$	33	6
2	383	373	600	1.2:1	$1.11 \cdot 10^{-6}$	33	6
3	383	373	600	1.2:1	$5.56 \cdot 10^{-7}$	33	6
4	383	373	600	2:1	$1.67 \cdot 10^{-6}$	33	6

The results (Figure 42) showed that a little improvement derived from the volumetric flow increase. Since the use of high flows limited the possible presence of fluid-solid mass transfer limitation all other tests were conducted fixing $Q = 1.67 \cdot 10^{-6}$ m³/s.

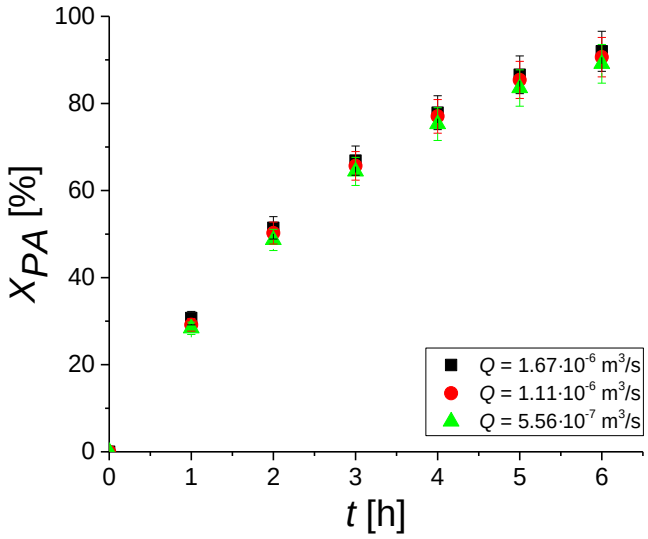

Figure 42. Recirculation volumetric flow effect tests.

Similar results, instead, were obtained increasing reactants molar ratio (Figure 43), hence in the subsequent experiments, EtHex/PA was set equal to 1.2:1 mol/mol.

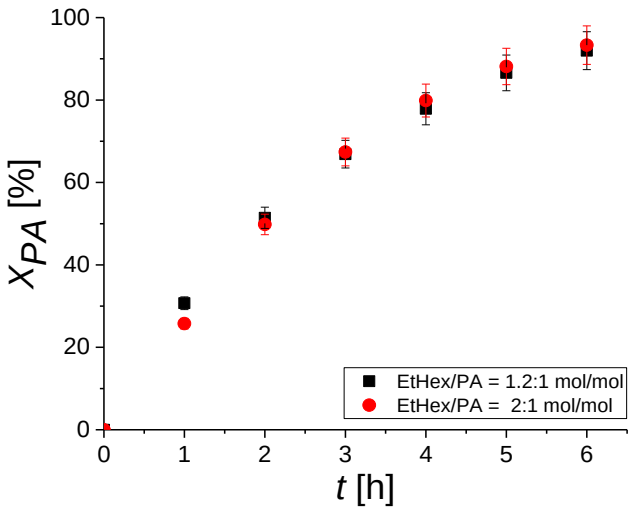

Figure 43. Reactants molar ratio effect tests.

Several tests were made in the same conditions, reported in Table 21, using a higher catalyst amount in order to produce solvents to be tested in inks formulations.

Table 21. Solvents synthesis reaction conditions.

T_{BR} [K]	383
T_{TR} [K]	373
v [rpm]	600
EtHex/PA [mol/mol]	1.2:1
Q [m^3/s]	$1.67 \cdot 10^{-6}$
w_{cat} [g]	50
t [h]	6

Figure 44 showed the reached conversion of about 95 %, at the end of each test, demonstrating the catalyst stability without losses in its activity.

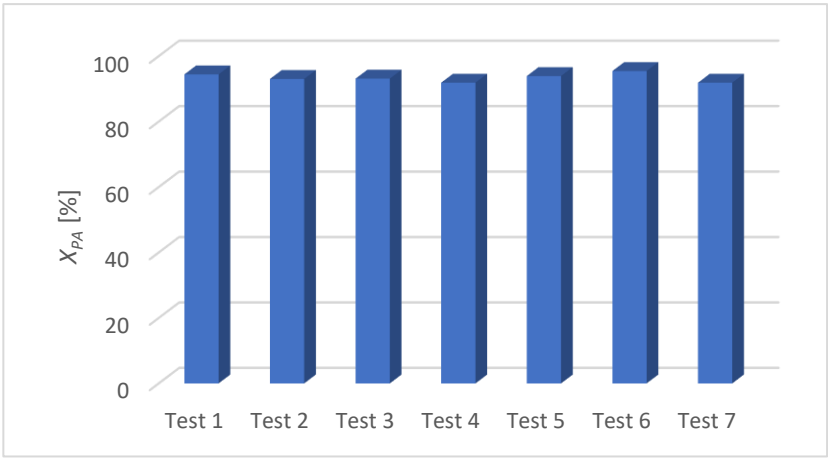

Figure 44. Solvents synthesis promoted by Amberlyst-15.

^{1}H-NMR analysis was made to verify the purity and confirm the absence of residual alcohol in the final product. A spectrum of one of the obtained products is reported in Figure 45.

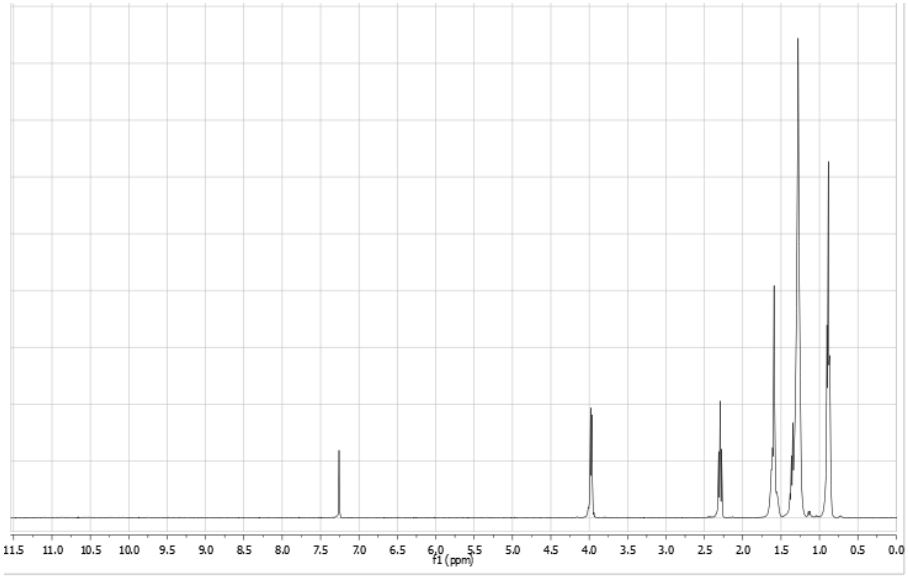

Figure 45. ^{1}H-NMR spectrum of the product.

3.7 Solvents characterization and printing inks formulation

The effectiveness of these solvents in the field of the inks was already known from the literature [2], therefore the synthesized solvents were tested in the formulation of inks for offset printing applications. Inks are generally composed by a vehicle, constituted by 43-45% w/w of resin dissolved in a solvent, a pigment and additives. Solvents together with the resin were loaded in a tank under stirring in order to dissolve the resin itself. The properties of the tested solvents were comparable, and a resin amount of 43% w/w was dissolved at 373 K for 1 h. This result confirmed what is reported in the literature [2] about the excellent properties of these solvents compared to other used and proposed products. In fact, the available commercial solvents, such as mineral oil, palmitic acid esters and triglyceride, don't show good properties in the dissolution of the resin. These solvents need high temperatures, up to 120 °C and higher time, up to 4 hours compared to solvents derived from pelargonic acid and 2-ethylhexanol which, instead, are able to dissolve the resin at lower temperature, 80 °C and up to 30 minutes [2]. Inks were prepared stirring the above-mentioned components for about 30 min and successively in order to obtain pigment particles smaller than 10 μm, a three-cylinder machine was used. The rheological properties of the tested formulations were investigated to determine fundamental parameters in these materials. Tan δ, namely the ratio between elastic and anelastic module of the material, viscosity, yield value and tack are reported in Table 24, where the formulation 1 and 2, characterized by the same composition, were obtained by using respectively solvents 1 and 2 (see Figure 44).

Table 24. Rheological parameters of the formulations.

Parameter	Formulation 1	Formulation 2
Viscosity [Poise]	220 ± 20	250 ± 20
Tan δ [-]	3,1 ± 0,1	3,0 ± 0,1
Yield value [Dyne/cm^2]	13500 ± 2000	15500 ± 2000
Tack [-]	14 ± 1	15 ± 1

The main parameters of the printing inks formulations were compared with the typical values reported in the literature [2]. In particular, Tan δ value should be included in a range between 2 and 4, viscosity between 200 and 300 Poise, yield value between 12000 and 15000 Dyne/cm^2 and tack between 14 and 18 [2]. As visible in Table 24, the obtained results were included in the ideal range values confirming the good properties of the synthesized products.

References

1. Benessere, V., Cucciolito, M. E., De Luca, A., Di Serio, M., & Ruffo, F. Compositions containing fatty acid esters of vegetable origin as solvents. WO 2018/142320 (2018).
2. Benessere, V., Cucciolito, M. E., De Santis, A., Di Serio, M., Esposito, M., Melchiorre, M., Nugnes, F., Paduano, L. & Ruffo, F. A Sustainable Process for the Production of Varnishes Based on Pelargonic Acid Esters. *JAOCS, J. Am. Oil Chem. Soc.* **96**, 443–451 (2019).

Chapter 4 – Ketalization reaction: Catalytic screening and batch kinetic study

4.1 Overview

In this chapter, the attention moved to a different reaction of increasing importance for the obtainable products in the industrial sector. The experimental investigation started with the kinetic study of the ketalization between glycerol and acetone to obtain solketal, promoted by an iron(III) complex. Industrially, this reaction is very interesting due to the huge amount of available glycerol derived from biodiesel production. After this, the attention was focused on the central point of this thesis part which is the study of the ketals from levulinic acid. First of all, a catalytic screening was made and then, the catalyst with the best performances was employed in a batch kinetic study to investigate the effect of different experimental conditions on the reaction rate in order to obtain kinetic and thermodynamic parameters.

4.2 Chemicals

Reagents used in the experiments were glycerol (purity ≥ 99.5%), acetone (purity ≥ 99.5%) and ethyl levulinate (purity 99%) purchased by Merck. Sulfuric acid 98% w/w, Amberlite IR120, Amberlyst-15, Dowex 50WX8 were purchased by Merck while all the zeolites by Alfa Aesar.
Amberlite IR120 and Amberlyst-15 properties are reported in Table 4 (section 2.2) while those of Dowex 50WX8 and zeolites respectively in Tables 25 and 26.

Table 25. Dowex 50WX8 properties.

	Dowex 50WX8
Particle size [µm]	50-100
Crosslinking degree [%]	8
Acid sites concentration [meq/g]	4.83
Surface area [m^2/g]	0.23
ρ_P [kg/m^3]	800

Table 26. Zeolites characteristics.

Catalyst	**SiO_2:Al_2O_3 [mol/mol]**	**Surface area [m^2/g]**
Zeolite Y, hydrogen	80:1	780
Zeolite ZSM-5, ammonium	200-400:1	400
Zeolite beta, hydrogen	360:1	620
Zeolite mordenite, ammonium	20:1	500

4.3 Experimental setup and reaction procedure

The experimental setup used both for the catalytic screening and for the kinetic study was already described in section 2.3 and represented in Figures 8 and 9.

The procedure followed for the reaction between glycerol and acetone consisted of loading about 180 g of the reactant's mixture in the reactor, while the catalyst (iron(III) complex) was dissolved in about 20 g of acetone and it was loaded in the syringe.

The reactor was pressurized with nitrogen (5 bar) to avoid the partition of the lowest boiling component between the gas and liquid phases and it was heated up to the set value. When the system reached the desired temperature, the catalyst was added into the reactor and this was considered the starting point of the reaction. Further details can be found in publication **II**.

In the case of the reaction between ethyl levulinate and glycerol, the same procedure was followed with the difference that ethyl levulinate and catalyst were loaded in the reactor while glycerol and part of ethyl levulinate in the syringe. At the temperature set value, the syringe content was loaded in the reactor. From that moment, samples were withdrawn at regular intervals to follow the reaction kinetics.

4.4 Analytical method

^{1}H-NMR was the method used for the analysis of the samples both in the ketalization of glycerol with acetone and ethyl levulinate. In the first case D_2O was used as solvent and the glycerol conversion was calculated from the integration of the signals of methyl groups between 1.55 and 1.35 ppm (labeled with A in Figures 46 and 47) compared with the signals between 4.55 and 3.50 ppm (labeled with B in Figures 46 and 47) referred to the proton of the glyceryl group of both glycerol and the two products, solketal and the six membered ketal. The selectivity toward solketal, instead, was determined by integrating the signals of a methyl of the six membered ketal at 1.51 ppm (indicated with number 2 in Figures 46 and 47) and those of a methyl of solketal at 1.41 ppm (indicated with number 1 in Figures 46 and 47). Other details are reported in publication **II**.

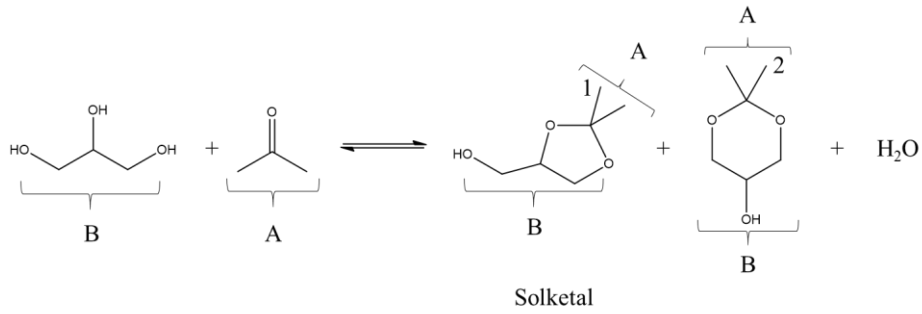

Figure 46. Glycerol ketalization with acetone.

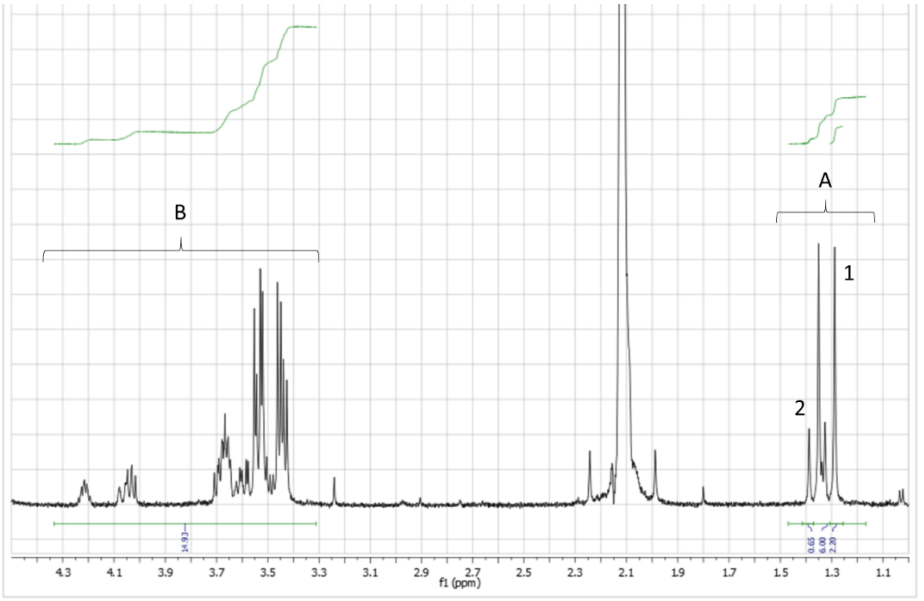

Figure 47. ^{1}H-NMR spectrum of the mixture of the glycerol ketalization reaction with acetone.

Glycerol conversion and solketal selectivity were obtained from Eq. 23.

$$X_{Gly} = \frac{5I_A}{6I_B}$$
$$\phi_{Solketal} = 1 - \frac{I_2}{I_1} \quad (23)$$

In the second case, instead, $CDCl_3$ was used as solvent and the conversion was calculated by integrating the signals of methyl groups of the two diastereoisomers between 1.42 and 1.32 ppm (indicated with letter A in Figures 48 and 49) and the signal of the terminal methyl groups of both reactants and products at the chemical shift between 1.32 and 1.20 ppm (indicated with letter B in Figures 48 and 49).

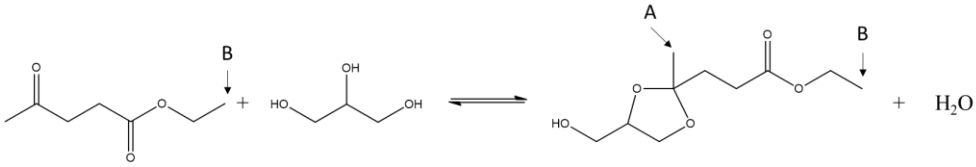

Figure 48. Glycerol ketalization with ethyl levulinate.

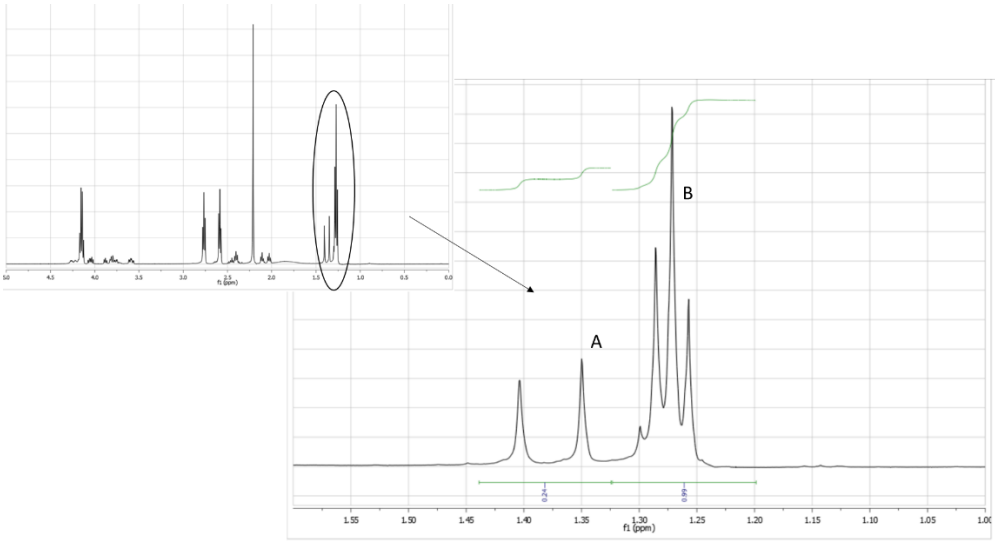

Figure 49. ^{1}H-NMR spectrum of the mixture of the glycerol ketalization reaction with ethyl levulinate.

The molar fraction of the obtained product (X) was determined with the Eq. 24.

$$X = \frac{I_A}{I_B} \tag{24}$$

4.5 Batch kinetic investigation of glycerol ketalization with acetone

Kinetic tests were performed in the presence of an iron(III) complex ($FeCl_3$(1-NO_2) as homogeneous catalyst. This catalyst showed very promising properties and it showed a high selectivity toward solketal, as reported also from the literature [1]. Details on the catalyst can be found in publication **II**.

Several tests were made changing the experimental conditions, reported in Table 27.

Table 27. Experimental conditions for glycerol ketalization with acetone.

Test	***v* [rpm]**	***T* [K]**	**Ac/Gly [mol/mol]**	**ρ_B [kg/m^3]**
1	400	323	4:1	-
2	600	323	4:1	1.39
3	400	323	4:1	1.39
4	400	323	4:1	2.62
5	400	323	4:1	0.67
6	400	323	4:1	0.33
7	400	323	4:1	0.08
8	400	323	4:1	0.04
9	400	323	4:1	0.02
10	400	313	4:1	0.02
11	400	303	4:1	0.02
12	400	303	4:1	0.04
13	400	303	4:1	0.08
14	400	303	4:1	0.25

The effect of different experimental conditions on the reaction rate (i.e. stirring rate, temperature and catalyst load) was investigated.

Tests at different stirring rate were conducted to evaluate the occurring of liquid-liquid mass transfer limitation since the glycerol and acetone were poorly miscible at acetone/glycerol molar ratio equal to 4:1. The two tests at 400 and 600 rpm gave similar results both in terms of glycerol conversion and solketal selectivity confirming the absence of the liquid-liquid mass transfer limitation.

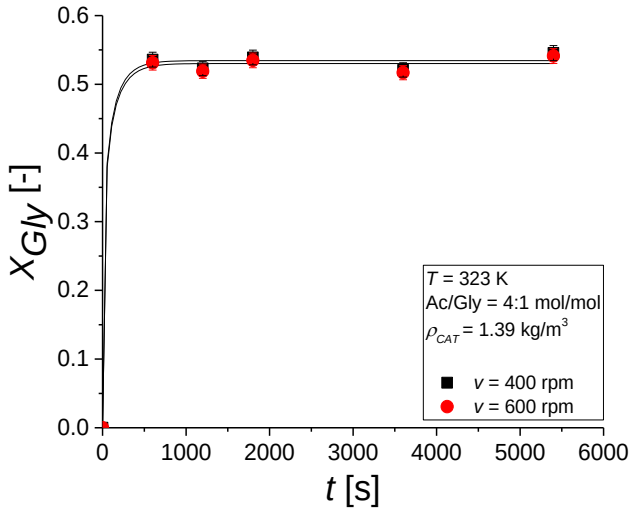

A.

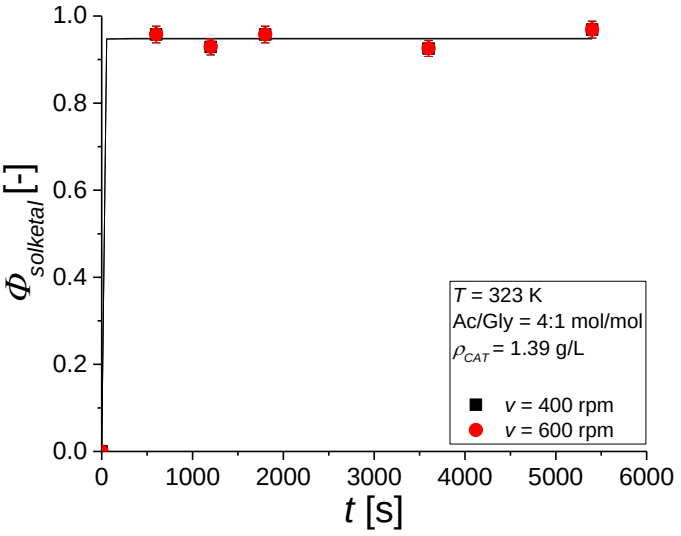

B.

Figure 50. Stirring rate effect. A. Glycerol conversion. B. Selectivity toward solketal.

From Figure 50B, it can be note that the solketal selectivity is about 1 due to the thermodynamic stability of solketal itself respect to the six membered by-product, hence its formation was preferred. Temperature effect was tested at three different

values showing that by increasing its value, glycerol conversion increased too while selectivity toward solketal was always similar (Figure 51).

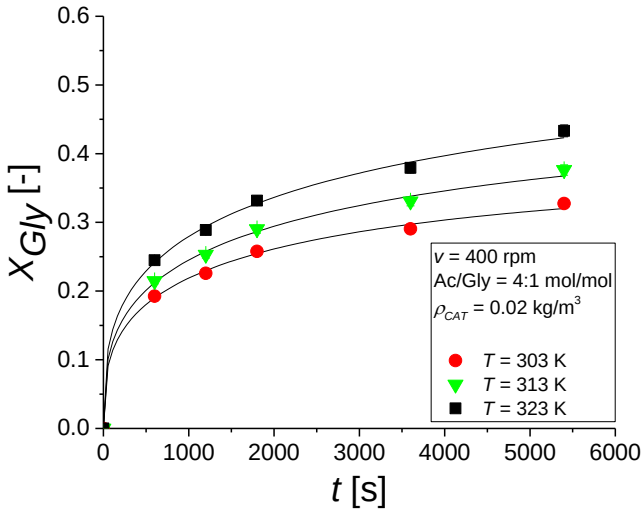

A.

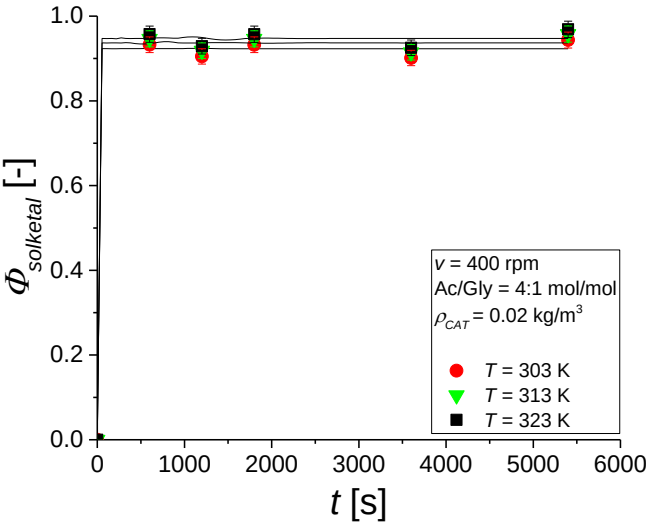

B.

Figure 51. Temperature effect. A. Glycerol conversion. B. Selectivity toward solketal.

As for catalyst load effect, two sets of tests were made at two different temperatures (T = 323 K and T = 303 K). First of all, a blank test was conducted to verify the contribution of the autocatalysis on the reaction rate. The results, reported in Figure 52, showed that the glycerol conversion was next to zero confirming that this effect could be considered negligible. Glycerol conversion reached in experiments performed at T = 323 K was always similar except for tests with a catalyst load equal to 0.04 kg/m^3 and 0.02 kg/m^3.

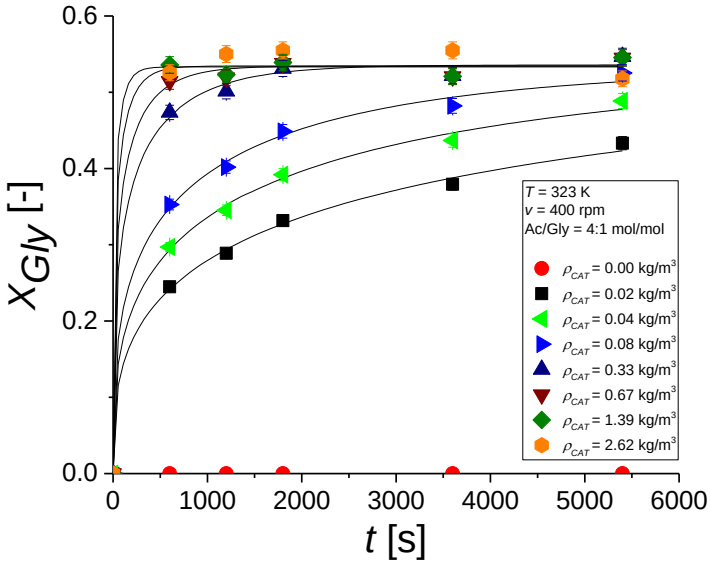

A.

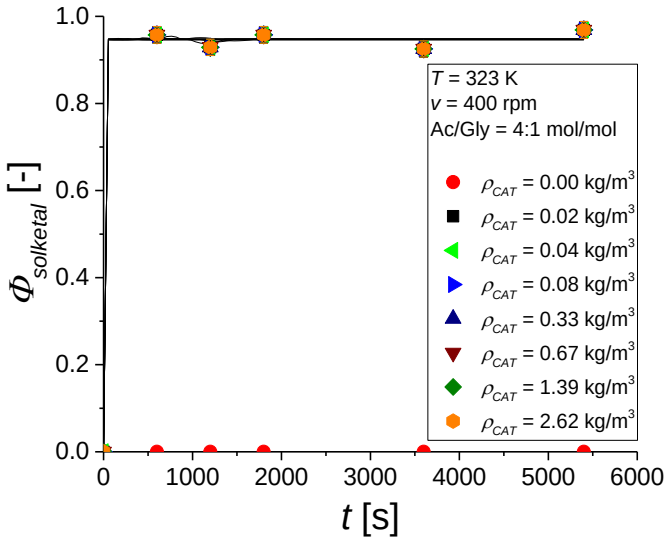

B.

Figure 52. Catalyst load effect for tests performed at T = 323 K. A. Glycerol conversion. B. Selectivity toward solketal.

From Figure 52A, it was possible to see that over 0.67 kg/m^3, glycerol conversion was no longer affected by catalyst load probably because the dehydration became the limiting step which was independent of the catalyst itself (see Figure 54). Glycerol conversion was lower in the case of tests conducted at lower temperature, as demonstrated from Figure 53A. In terms of selectivity toward solketal, instead, similar results were obtained both in tests at T = 323 K and T = 303, as reported in Figures 52B.

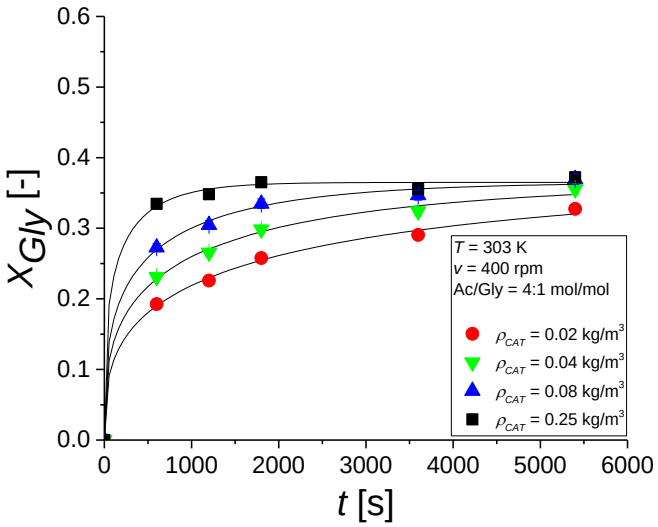

A.

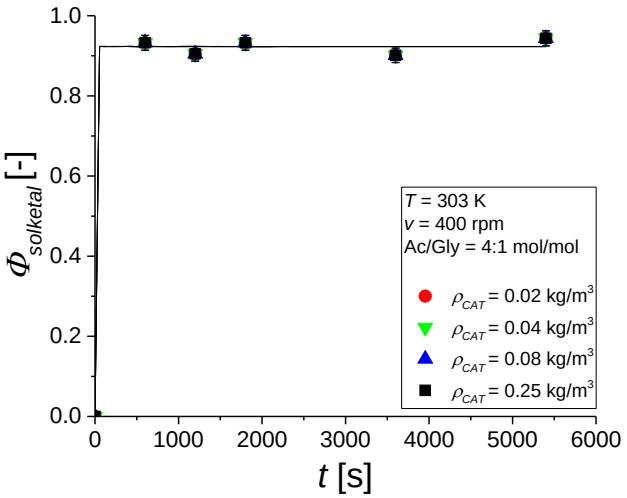

B.

Figure 53. Catalyst load effect for tests performed at T = 303 K. A. Glycerol conversion. B. Selectivity toward solketal.

A reaction mechanism was hypothesized based on three steps: firstly, the activated form of the catalyst, indicated as Fe*Cl_3(1-NO_2), was obtained through the carbonyl oxygen of acetone coordination to the metal. The second step consisted of the reaction between the activated form of the catalyst and glycerol to give solketal through the ring closure and water release. The third step consisted of the same reaction of the step 2 but in this case the six membered by-product was obtained. Details about the above described mechanism was reported in publication **II**. The three reactions of this mechanism can be represented as follows.

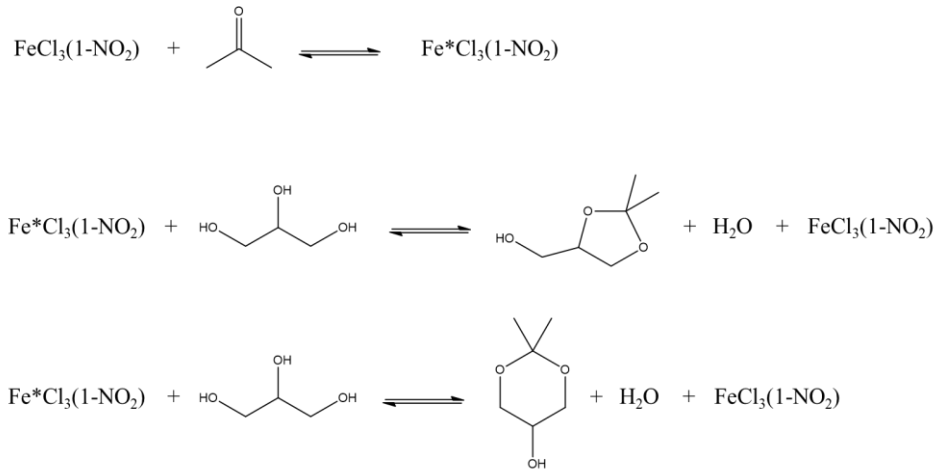

Figure 54. Glycerol ketalization with acetone reaction mechanism.

The experimental data were interpreted by a kinetic model based on the described reaction mechanism. Reaction rates were expressed as reported in Eqs. 25-27.

$$r_1 = k_1\left(c_{FeCl_3(1-NO_2)}c_{Ac} - \frac{1}{K_1}c_{Fe^*Cl_3(1-NO_2)}\right) \quad (25)$$

$$r_2 = k_2\left(c_{Fe^*Cl_3(1-NO_2)}c_{Gly} - \frac{1}{K_2}c_{FeCl_3(1-NO_2)}c_{solketal}c_{H_2O}\right) \quad (26)$$

$$r_3 = k_3 \left(c_{Fe^*Cl_3(1-NO_2)} c_{Gly} - \frac{1}{K_2} c_{FeCl_3(1-NO_2)} c_{BP} c_{H_2O} \right) \quad (27)$$

A modified Arrhenius (Eq. 28) and van't Hoff (Eq. 29) equations were considered to express the dependency with temperature. Reference temperature (T_{ref}) was set at 303 K.

$$k = k_{ref} \exp\left(-\frac{Ea}{R} \left(\frac{1}{T} - \frac{1}{T_{ref}} \right) \right) \quad (28)$$

$$K = K_{ref} \exp\left(-\frac{\Delta_r H}{R} \left(\frac{1}{T} - \frac{1}{T_{ref}} \right) \right) \quad (29)$$

The mass balance, considering the variation with time of the composition of each component was reported in Eq. 30.

$$\frac{dc_i}{dt} = \nu_i r \quad (30)$$

To simulate the experimental data, a simplified model was developed neglecting the by-product reaction since it was demonstrated that the selectivity toward solketal was close to 1. Furthermore, it was verified that the non-activated form of the catalyst only existed for short times of the reaction while, on the contrary, the activated form increased (Figure 55). This result allowed to consider in the kinetic model the catalyst only in its activated form.

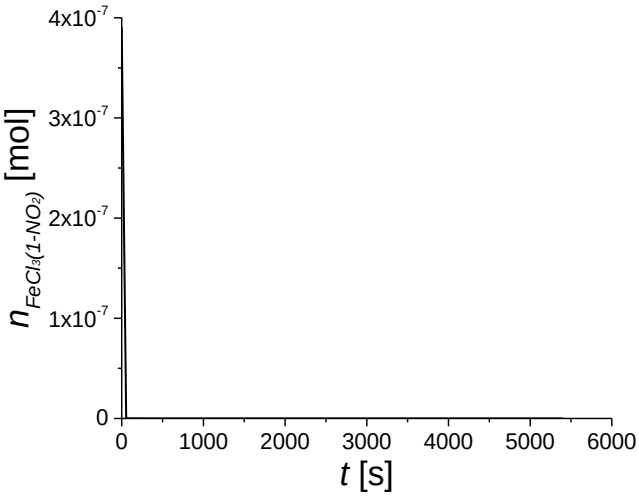

A.

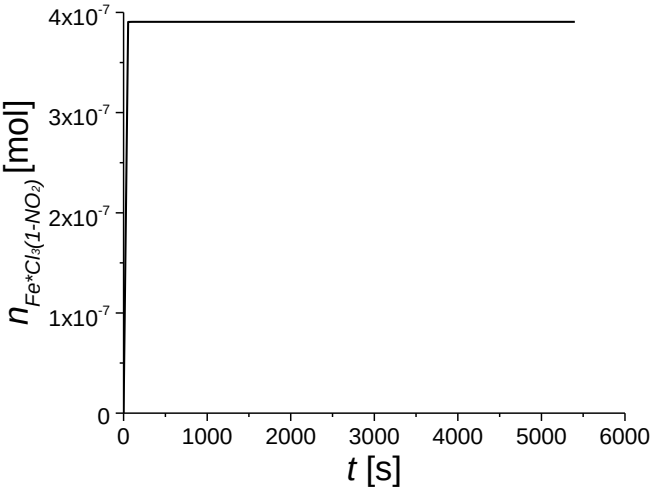

B.

Figure 55. Non-activated (A) and activated (B) catalyst form in the reaction time.

The kinetic model fitted well the experimental data as visible from Figures 50-53 and from the parity plots in Figure 56 where all the data are included in an error range of ±5% both for glycerol conversion and solketal selectivity.

A.

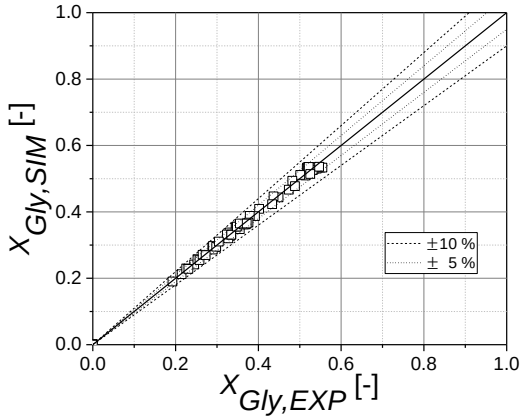

B.

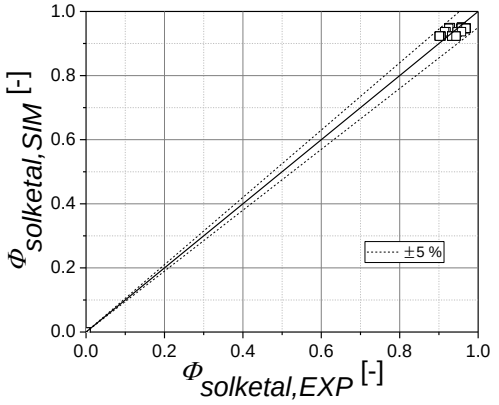

Figure 56. Parity plot including all the collected experimental data for glycerol conversion (A) and solketal selectivity (B).

Kinetic and thermodynamic parameters were calculated from the parameters estimation and the results are reported in Table 28.

Table 28. Parameter estimation results.

Parameter	Value	95% CI	Units
$\Delta_r H_1$	30	1	kJ/mol
$\Delta_r H_2$	16.4	0.5	kJ/mol
E_{a1}	13.0	0.5	kJ/mol
E_{a2}	64.0	2	kJ/mol
E_{a3}	63.0	3	kJ/mol
$K_{ref,1}$	0.55	0.05	-
$K_{ref,2}$	0.10	0.02	-
$K_{ref,3}$	$8.1 \cdot 10^{-3}$	$0.1 \cdot 10^{-3}$	-
$k_{ref,1}$	620	10	$(m^3/mol)\ s^{-1}$
$k_{ref,2}$	$14.0 \cdot 10^{7}$	$0.2 \cdot 10^{7}$	$(m^3/mol)\ s^{-1}$
$k_{ref,3}$	$42.0 \cdot 10^{5}$	$0.2 \cdot 10^{5}$	$(m^3/mol)\ s^{-1}$

4.6 Glycerol ketalization with ethyl levulinate: catalytic screening

As anticipated in section 4.1, the attention will be focused now on the glycerol ketalization with ethyl levulinate.

In order to identify the catalysts with the best performance in this reaction, a catalytic screening was made. H_2SO_4 was used as reference homogeneous catalyst while ion exchange resins, zeolites and a synthetic catalyst (H_2WO_4/SiO_2) were tested as heterogeneous catalysts.

The experimental conditions are reported in Table 29.

Table 29. Catalytic screening experimental conditions.

Test	Catalyst	ν [rpm]	T [K]	EtLev/Gly [mol/mol]	ρ_B [kg/m^3]
1	H_2SO_4	600	353	1:1	5.7
2	Amberlyst-15	600	353	1:1	23.0
3	Amberlite IR120	600	353	1:1	23.0
4	Dowex 50WX8	600	353	1:1	23.0
5	Zeolite Y, hydrogen	600	353	1:1	2.9
6	Zeolite ZSM-5, ammonium	600	353	1:1	2.9
7	Zeolite beta, hydrogen	600	353	1:1	2.9
8	Zeolite mordenite, ammonium	600	353	1:1	2.9
9	H_2WO_4/SiO_2	600	353	1:1	11.5

The equilibrium constant was determined for all the used catalysts in order to compare their performances. In the following figures, the graphical results are reported.

The equilibrium conversion reached in the presence of the homogeneous catalyst (H_2SO_4) was about 31%. In Figure 57, a comparison between the three ion exchange resins was reported. It is possible to see that Amberlite IR120 and Amberlyst-15 were very similar reaching a conversion of 22% and the apparent thermodynamic plateau after about 60 min of reaction. The same time for the apparent thermodynamic plateau was visible also for Dowex 50WX8 but the reached conversion was higher and equal to 25%. It is clear that the equilibrium constant depends exclusively by the temperature value and despite the operative temperature was the same in each test, the obtained results were different. The reason of this behavior in the presence of heterogeneous catalysts, can be found in the different concentration of the reactants in the liquid bulk compared to the concentration inside the catalysts.

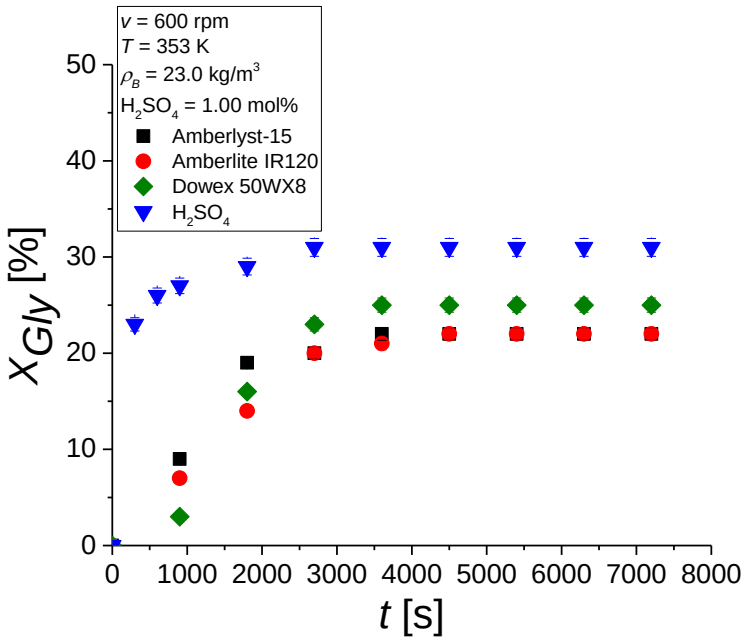

Figure 57. Comparison between ion-exchange resins and sulfuric acid in the glycerol ketalization reaction with ethyl levulinate.

The comparison between the different zeolites were showed in Figure 58. Among them, zeolite Y, hydrogen and zeolite beta, hydrogen resulted to be the best. In particular, zeolite Y, hydrogen reached the apparent thermodynamic plateau only after 20 min of reaction with a conversion of 27% while very similar results were obtained with zeolite beta, hydrogen which reached the plateau after 45 min with a conversion equal to 25%. In the case of zeolite ZSM-5, ammonium a maximum conversion of 21% was obtained and the plateau after 90 min of reaction while zeolite mordenite, ammonium didn't show promising performances. The reason could be probably found in the possibility that ammonium ion occupied the catalyst sites making it less active.

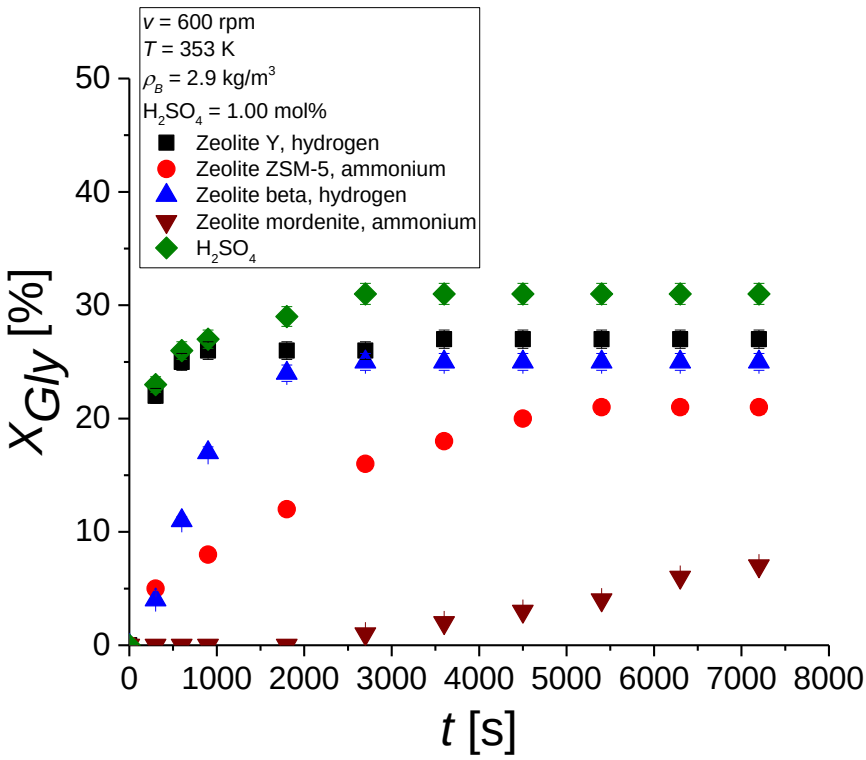

Figure 58. Comparison between zeolites and sulfuric acid in the glycerol ketalization reaction with ethyl levulinate.

Finally, tungstic acid supported on silica was also tested but it didn't show good performances as it needed long reaction time to reach the equilibrium and a lower conversion was reached, as reported in Figure 59. The reason of its low activity could be the operative temperature since this catalyst is active at higher temperatures [2] which promote the formation of Brønsted acid sites.

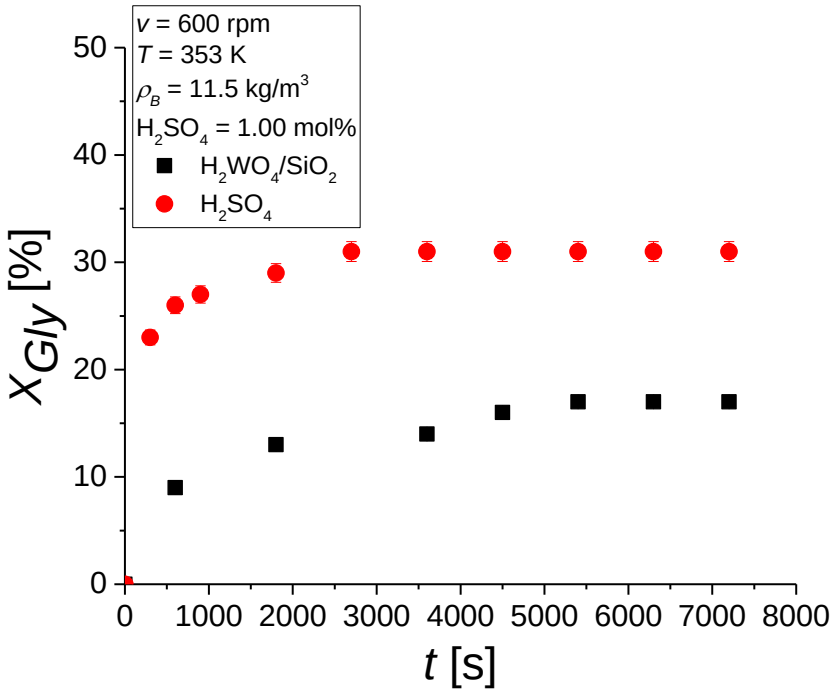

Figure 59. Comparison between H_2WO_4/SiO_2 and sulfuric acid in the glycerol ketalization reaction with ethyl levulinate.

The equilibrium constant was calculated in all the described cases except for the two reactions (zeolite mordenite, ammonium and H_2WO_4/SiO_2) where the plateau was not reached in the considered reaction time. The results are reported in Table 30.

Table 30. Equilibrium constant results.

Catalyst	Equilibrium constant
Amberlyst-15	0.08
Amberlite IR120	0.08
Dowex 50WX8	0.11
Zeolite Y, hydrogen	0.13
Zeolite ZSM-5, ammonium	0.07
Zeolite beta, hydrogen	0.11
H_2SO_4	0.20

The reference value resulted from the test promoted by H_2SO_4 since it is a homogenous catalyst and it didn't suffer problems connected with the different affinity with the liquid components.

It can be hypothesized, also based on similar investigations reported in the literature [3], that for the catalysts whose values differed from the real one, the partition of the reactants between the liquid bulk and the solid must be considered and consequently the difference in the concentration of the reactants themselves led to a different equilibrium value. For the resins, characterized by a Brønsted acidity, the TOF value was calculated and a linear trend was found with the active sites concentration (Figure 60). The same evaluation was not possible in the case of zeolites because of the absence of this value in the literature.

Table 31. Resins TOF values results.

Catalyst	Reaction mixture pH	Active sites concentration [meq/g]	TOF [h^{-1}]
Amberlyst-15	0.98	4.53	1288
Amberlite IR120	0.99	4.40	1152
Dowex 50WX8	0.95	4.83	1357

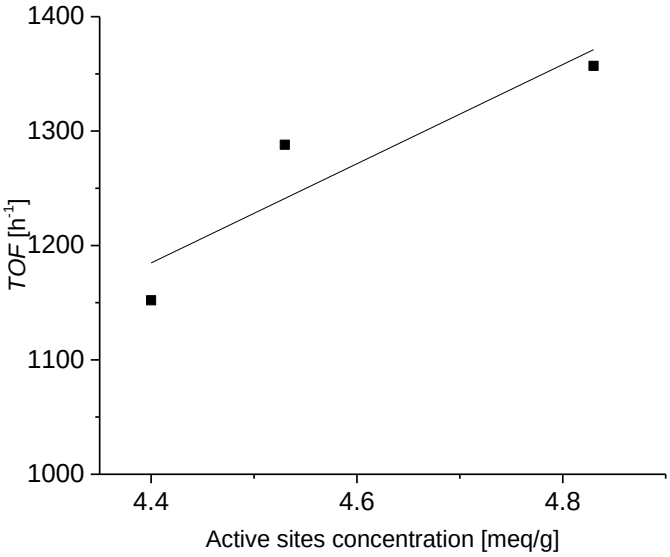

Figure 60. Resins TOF values vs Active sites concentration.

For the zeolites, a preliminary evaluation could be done considering the surface area and comparing the initial reaction rate, $\left(\frac{dX}{dt}\right)$, to the surface area itself (Table 32). Usually zeolites with a higher surface area result to be more active.

Table 32. Comparison of the reaction rate and surface area of zeolites.

Catalyst	Surface area [m_2/g]	Initial reaction rate $\left(\frac{dX}{dt}\right)$
Zeolite Y, hydrogen	780	2.5
Zeolite ZSM-5, ammonium	400	0.5
Zeolite beta, hydrogen	620	1.2
Zeolite mordenite, ammonium	500	0.08

From these values, it can be seen that as the surface area increased, the initial reaction rate increased as well excepted zeolite mordenite, ammonium. In order to better understand the reason of this results it is necessary to include in a future investigation also the data related with the acidity of the zeolite itself.
From the catalytic screening, it resulted that Dowex 50WX8 was the best among the resins together with zeolite beta, hydrogen and zeolite Y, hydrogen. The last one was chosen as the first catalyst to be tested in the batch kinetic investigation, discussed in the next section.

4.7 Glycerol ketalization with ethyl levulinate: batch kinetic investigation

Kinetic tests were performed in the presence of zeolite Y, hydrogen as catalyst varying the experimental conditions reported in Table 33.

Table 33. Experimental conditions for glycerol ketalization with ethyl levulinate promoted by zeolite Y, hydrogen.

Test	ν [rpm]	T [K]	EtLev/Gly [mol/mol]	ρ_B [kg/m^3]
1	200	353	1:1	2.9
2	600	353	1:1	2.9
3	1000	353	1:1	2.9
4	600	343	1:1	2.9
5	600	323	1:1	2.9
6	600	353	1:1	1.2
7	600	353	1:1	0.6
8	600	353	5:1	0.6
9	600	353	7.5:1	0.6

First of all, the presence of the external mass transfer limitation was investigated by performing tests at different stirring rate.

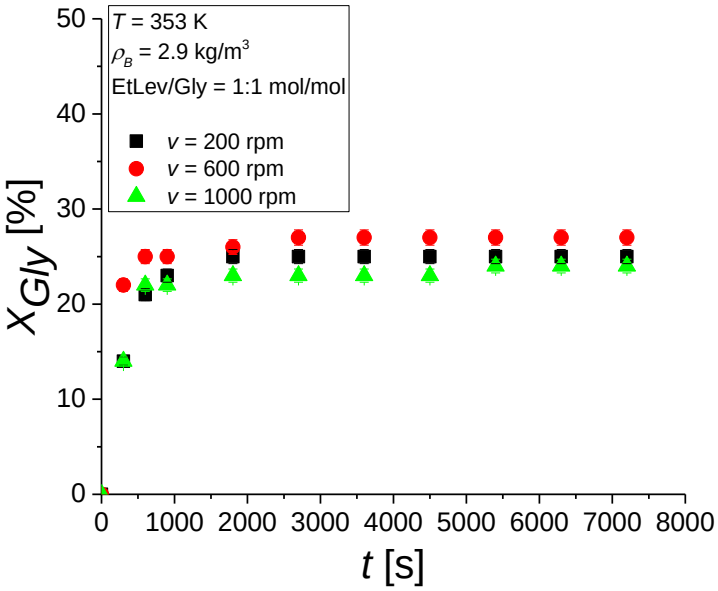

Figure 61. Stirring rate effect for the glycerol ketalization with ethyl levulinate promoted by zeolite Y.

Results showed that comparable reaction rates were obtained varying the stirring rate hence this implied that the reaction was not limited by fluid-solid mass transfer limitation. Experiments were made at three different temperatures and, as expected, the reaction rate increased by increasing temperature value reaching similar results for tests made at T = 343 K and 353 K.

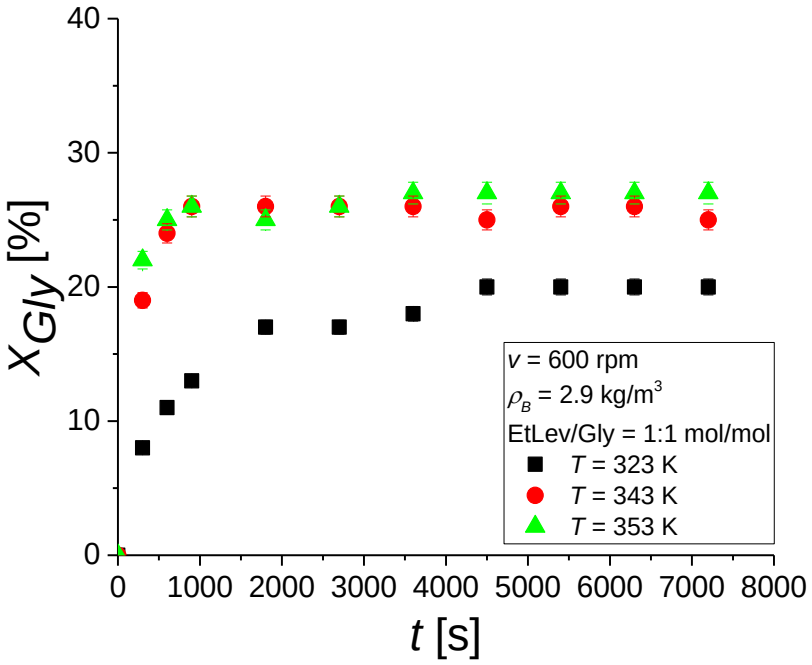

Figure 62. Temperature effect for the glycerol ketalization with ethyl levulinate promoted by zeolite Y.

From these tests, an apparent value of the activation energy could be estimated using the linearized Arrhenius equation, already reported in Eq. 18. The reaction enthalpy, instead, was evaluated using the linearized van't Hoff equation reported in Eq. 19. The obtained values are reported in Table 34.

Table 34. Parameter estimated for tests promoted by zeolite Y.

Parameter	Value	Error	Unit
E_a	30	6	kJ/mol
$\Delta_r H$	21	9	kJ/mol

The catalyst load effect on the reaction rate was showed in Figure 63 where it can be note that with a catalyst load higher than 1.2 kg/m^3, the intraparticle mass transfer limitation became relevant. It can be expected that by increasing the

catalyst load also the reaction rate increases. In this case, instead, it is possible to see that a further increase of the catalyst load no longer affects the reaction rate since the intraparticle mass transfer limitation effect is predominant on the reaction kinetics.

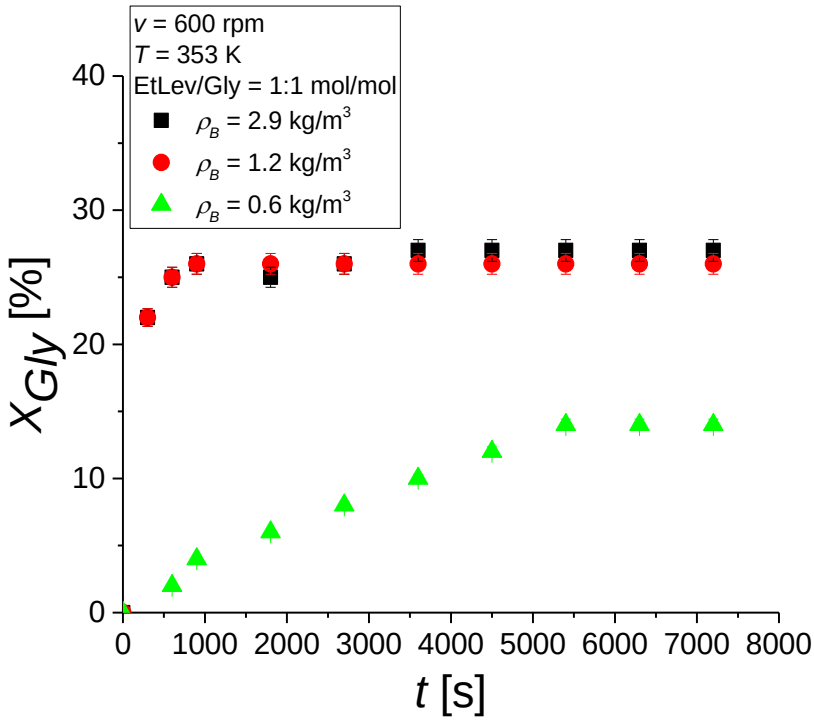

Figure 63. Catalyst load effect for the glycerol ketalization with ethyl levulinate promoted by zeolite Y.

In order to determine the proportionality coefficient, a relation between the reaction rate and the catalyst load can be express as follows obtaining a value equal to 0.5 (see Figure 64).

$$r_{obs} = r \cdot \rho_B^n \tag{31}$$

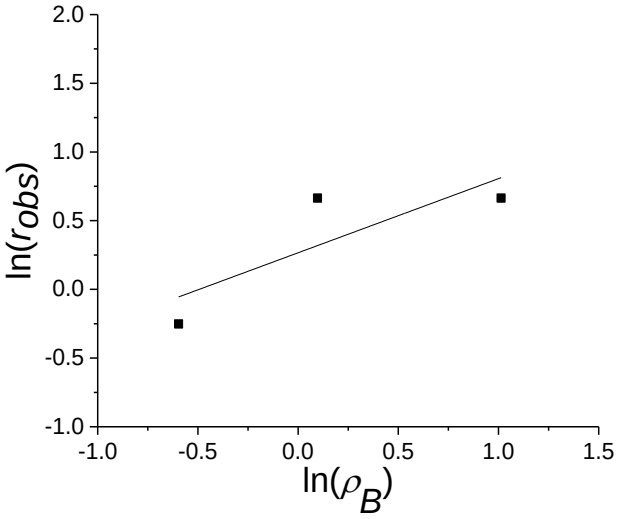

Figure 64. Proportionality coefficient determination for the glycerol ketalization with ethyl levulinate promoted by zeolite Y.

Finally, the ethyl levulinate/glycerol molar ratio effect on the reaction rate was evaluated.

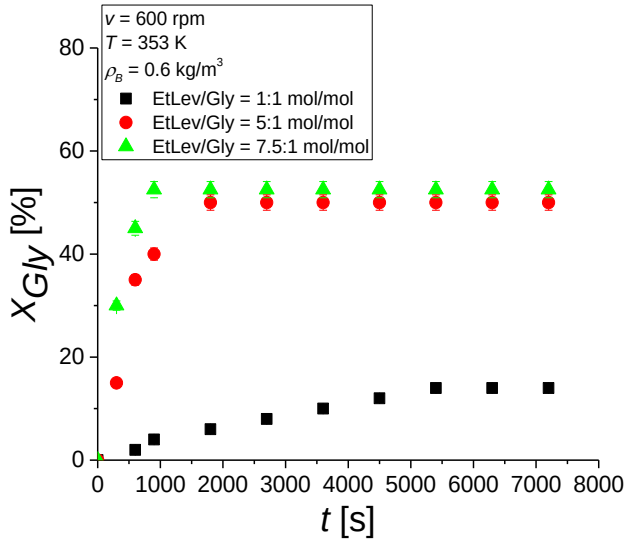

Figure 65. Reactants molar ratio effect for the glycerol ketalization with ethyl levulinate promoted by zeolite Y.

The results in Figure 65 demonstrated that an increase in the reached conversion corresponded to a higher reactants molar ratio and this effect was less evident for the ethyl levulinate/glycerol ratio equal to 5:1 and 7.5:1 mol/mol.
The present kinetic investigation is still ongoing and it will continue testing also the other promising catalysts as resulted from the catalytic screening.

References

1. Esposito, R., Raucci, U., Cucciolito, M.E., Di Guida, R., Scamardella, C., Rega, N. & Ruffo, F. Iron(III) Complexes for Highly Efficient and Sustainable Ketalization of Glycerol: A Combined Experimental and Theoretical Study. *ACS Omega* **4**, 688-698 (2019).
2. Vitiello, R., Tesser, R., Russo, V., Turco R., Andini, S. & Di Serio, M. Loop reactor modeling for lubricant synthesis. *Chem. Eng. J.* **329**, 295-304 (2017).
3. Russo, V., Rossano, C., Salucci, E., Tesser, R., Salmi, T. & Di Serio, M. Intraparticle diffusion model to determine the intrinsic kinetics of ethyl levulinate synthesis promoted by Amberlyst-15. *Chem. Eng. Sci.* **228**, 115974 (2020).

Conclusion

The topic of this thesis was divided into three main part: the first one was focused on the kinetic investigation in batch and continuous apparatus of the pelargonic acid esterification with 2-ethylhexanol promoted by different catalysts. As for the batch investigation, the first one was homogeneous (sulfuric acid) while the other heterogenous catalysts were Amberlite IR120, Amberlyst-15 and H_2WO_4/SiO_2. Different experimental conditions were varied in order to evaluate their effect on the reaction rate. In the presence of heterogeneous catalysts, it was demonstrated that an internal mass transfer limitation occurred. The experimental data were elaborated with dedicated kinetic models considering all the phenomena involved in the reaction network in order to estimate the thermodynamics and kinetic parameters. The two resins, Amberlite IR120 and Amberlyst-15 were also tested in a packed bed reactor to validate the results obtained in the batch investigation and, also in this case, a kinetic model was developed. Amberlyst-15 is characterized by larger pores allowing an easier access to the reactant's molecules inside the catalyst structure compared to Amberlite IR120. This implied the better behavior of the Amberlyst-15, visible also in the continuous experiments. In the case of Amberlite IR120 an higher intraparticle mass transfer limitation occurred and this phenomenon was found also in the case of H_2WO_4/SiO_2. This can be the reason why with this catalyst there was not an improvement in the reaction rate by increasing the catalyst amount. In order to better understand this behavior, further investigations will be made in the future also to develop a kinetic model to simulate the experimental data. Furthermore, since this catalyst is stable and active up to 200 °C, other tests will be made at higher temperatures and it can be tested also in a continuous apparatus.

The second part of the thesis was focused on the synthesis of solvents to be used in the formulation on inks for offset prints applications through the esterification

of pelargonic acid with 2-ethylhexanol. The reaction was promoted by Amberlyst-15 and also the stability of the catalyst was tested, obtaining good results both in terms of catalyst activity and product characteristics. A conversion higher than 95 % was reached in each re-use test, demonstrating the catalyst stability. The rheological characterization, based on the determination of the fundamental parameters of the final products, confirmed their excellent properties since the obtained results were included in the ideal range values also reported in the literature.

Finally, the aim of third part was the investigation of the ketalization reaction. A kinetic study was made on the glycerol ketalization with acetone using an iron(III) complex as catalyst and a kinetic model was developed to interpret the experimental data obtaining a good agreement between the experimental data themselves and the simulated curves. After that, the attention moved to the glycerol ketalization with ethyl levulinate. Firstly, a catalytic screening was made in order to identify the most promising catalysts. Ion exchange resins (Amberlite IR120, Amberlyst-15 and Dowex 50WX8), zeolites and H_2WO_4/SiO_2 were tested. Dowex 50WX8 resulted to be the most interesting among the resins, while Y-zeolite and beta zeolite were the most active zeolites. Y-zeolite was chosen to be used in a batch kinetic investigation. A preliminary evaluation of the thermodynamic and kinetic parameters was made. An intraparticle mass transfer limitation occurred in the considered reaction system and a reliable kinetic model will be develop taking into account all the phenomena to simulate the experimental data. Furthermore, the kinetic investigation of this reaction will continue in the next future using also the other promising catalysts (Dowex 50WX8 and beta zeolite) tested in the catalytic screening.

List of symbols

A	Reactor cross sectional area [m^2]
a_{sp}	Specific external surface area [m^2/m^3]
c_i	Concentration of component *i* [mol/m^3]
$c_{i,s}$	Concentration of component *i* in the solid phase [mol/m^3]
$D_{e,i}$	Effective diffusivity of component *i* [m^2/s]
D_i	Molecular diffusivity of component *i* [m^2/s]
D_z	Axial dispersion coefficient [m^2/s]
Ea	Activation energy reaction [kJ/mol]
Ea_A	Activation energy of the esterification reaction promoted by Amberlite IR120 [kJ/mol]
$Ea_{A\text{-}15}$	Activation energy of the esterification reaction promoted by Amberlyst-15 [kJ/mol]
Ea_H	Activation energy of the esterification reaction promoted by H_2SO_4 [kJ/mol]
I_A, I_B, I_1, I_2,	Integral of ^{1}H-NMR signals [-]
ID	Reactor internal diameter [cm]
K	Equilibrium constant [-]
K_{ref}	Reference equilibrium constant [-]
k	Kinetic constant of the reaction [$(m^3/mol)\ s^{-1}$]
k_{ref}	Reference kinetic constant of the reaction [$(m^3/mol)\ s^{-1}$]

k_A	Kinetic constant of the esterification reaction promoted by Amberlite IR120 and Amberlyst-15 [$(m^3/kg)(m^3/mol)s^{-1}$]
$k_{A,ref}$	Reference kinetic constant of the esterification reaction promoted by Amberlite IR120 [$(m^3/kg)(m^3/mol)s^{-1}$]
$k_{A\text{-}15,\ ref}$	Reference kinetic constant of the esterification reaction promoted by Amberlyst-15 [$(m^3/kg)(m^3/mol)s^{-1}$]
k_H	Kinetic constant of the esterification reaction promoted by H_2SO_4 [$(m^3/mol)^2s^{-1}$)]
$k_{H,ref}$	Reference kinetic constant of the esterification reaction promoted by H_2SO_4 [$(m^3/mol)^2s^{-1}$)]
k_s	Fluid-solid mass transfer coefficient [m/s]
L	Reactor length [cm]
m_i	Partition coefficient for component *i* between the liquid and intraparticle phases [-]
M_i	Molecular weight of component *i* [g/mol]
Pe	Péclet number [-]
Q	Volumetric flowrate [m^3/s]
r_A	Rate of the reaction promoted by Amberlite IR120 and Amberlyst-15 [mol/(kg s)]
r	Rate of the reaction [$mol/(m^3\ s)$]
r_{obs}	Observed rate of the reaction [$mol/(m^3\ s)$]

r_H	Rate of the esterification reaction promoted by H_2SO_4 [mol/(m^3 s)]
R	Ideal gas constant [kJ/(K mol)]
R_P	Catalyst radius [m]
$R_{P,dry}$	Dry catalyst radius [m]
t	Time [s]
T	Temperature [K]
T_{ref}	Reference temperature [K]
u	Superficial velocity [m/s]
v	Stirring speed [rpm]
$V_{m,i}$	Molar volume of component I at boiling temperature in standard conditions from Le-Bas correlation [cm^3/mol]
w_{cat}	Catalyst mass [g]
x	Dimensionless particle radial coordinate [-]
X_{Gly}	Glycerol conversion degree [-]
X_{PA}	Nonanoic acid conversion degree [%]
$\Delta_r H$	Reaction enthalpy [kJ/mol]
ε	Void fraction [-]
ε_P	Catalyst porosity [-]
η	Catalyst form [mol]
μ_{mix}	Mixture viscosity [cP]
v_i	Stoichiometric coefficient of component *i* [-]

ρ_B	Catalyst bulk density [kg/m^3]
ρ_P	Catalyst density [kg/m^3]
τ_P	Catalyst tortuosity [-]
ϕ_{mix}	Mixture association factor of component *i* [-]
$\phi_{solketal}$	Selectivity towards solketal [-]

Abbreviations

Ac	Acetone
BP	By-product
BR	Batch reactor
CI	Confidence interval
EtHex	2-ethyl-1-hexanol
EtHex-PA	2-ethylhexylpelargonate
EtLev	Ethyl levulinate
EXP	Experimental data
Gly	Glycerol
PA	Pelargonic acid
SIM	Simulated data
TR	Tubular reactor

Publications

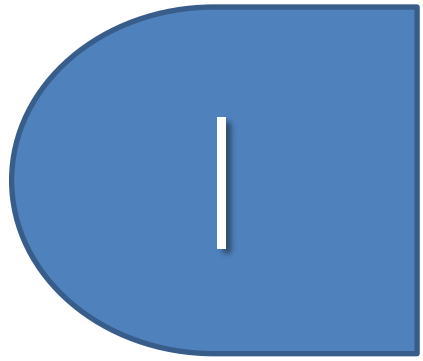

Chemical Engineering Journal 408 (2021) 127236

Contents lists available at ScienceDirect

Chemical Engineering Journal

journal homepage: www.elsevier.com/locate/cej

Investigation of the intrinsic reaction kinetics and the mass transfer phenomena of nonanoic acid esterification with 2-ethylhexanol promoted by sulfuric acid or Amberlite IR120

Vincenzo Russo [a,b], Francesco Taddeo [a], Tommaso Cogliano [a], Rosa Vitiello [a], Roberto Esposito [a], Riccardo Tesser [a], Tapio Salmi [b], Martino Di Serio [a,c,*]

[a] Department of Chemical Sciences, University of Naples Federico II, Via Cintia, IT-80126 Naples, Italy
[b] Laboratory of Industrial Chemistry and Reaction Engineering, Åbo Akademi, Piispankatu, FI-20500 Turku/Åbo, Finland
[c] International Research Organization for Advanced Science and Technology (IROAST), University of Kumamoto, JP-860-8555 Kumamoto, Japan

ARTICLE INFO

Keywords:
Nonanoic acid
Pelargonic acid
2-ethylhexanol
Esterification
Intraparticle diffusion
Modelling

ABSTRACT

Nonanoic acid is obtained as main coproduct in the synthesis of azelaic acid from oleic acid. The increase of azelaic acid production, being a monomer useful to synthesize biodegradable polyesters, lead to a high availability of nonanoic acid, that can be used as feedstock in esterification reactions to obtain lubricants and solvents. In this work, the esterification of nonanoic acid with 2-ethylhexanol to produce a solvent were conducted in a batch reactor in the presence of either a homogeneous (H_2SO_4) or an heterogenous catalyst (Amberlite IR120). The intrinsic reaction kinetics was investigated by considering all the physical and chemical phenomena occurring in the reaction network, leading to the determination of thermodynamic and kinetic parameters. The activation energy values of both catalysts are similar (≈60 kJ/mol) and the enthalpy value of $\Delta_r H = 10.3$ kJ/mol showed that the reaction is slightly endothermic. The reaction is shifted to the products as demonstrated by the reference equilibrium constant equal to 1.69 at 333 K. The obtained results will be useful to design industrial reactors.

1. Introduction

The reduced availability of fossil resources and the negative effects on the environment led to the development of chemical processes based on renewable raw material which predominantly consists of biomass [1,2]. Biomass includes all the organic material present on earth [3] and it is derived from crops and trees, agricultural food, wood, animal wastes and other waste materials [4].

Among the products obtainable from biomass, carboxylic acids have a great importance and their esterification is an industrially important reaction [5]. Esters produced from this reaction can be used as plasticizers, solvents and as biofuel additives [6].

For example, nonanoic acid esters are used for several applications such as cosmetics, pharmaceuticals, as intermediate for synthetic flavors [7].

Recently it was reported that 2-ethylhexylnonanoate (EtHex-NA) obtained by reaction of nonanoic acid and 2-ethylhexanol can be used as solvent in printing inks formulations, showing excellent properties respect to conventional used solvents [8].

Despite the industrial interest, no papers appeared in the literature about the investigation of the kinetics of such reaction. Esterification reactions conducted in the absence of catalysts are extremely slow and, in this case their rate depends on the autoprotolysis of the carboxylic acid [9]. Generally, a homogeneous or a heterogeneous catalyst is used to promote the rate of the reaction, leading to the reduction of the activation energy value [10]. Different catalysts can be used, such as homogeneous, heterogeneous catalysts or biocatalysts [11]. Industrially, the esterification of fatty acids with alcohols is performed in the presence of strong acid catalysts, for example sulfuric acid, hydrochloric acid and *p*-toluenesulfonic acid [12]. Sulfuric acid is widely used in this reaction because its acid strength involves the carboxylic groups protonation of the fatty acid [13]. However, homogeneous catalysts show several negative aspects, such as the formation of side products, equipment corrosion, acidic waste and difficult separation of the catalyst itself from the reaction mixture. Biocatalysts promote chemical transformations reaching the equilibrium with low reaction rates [11]. Therefore, an important alternative is represented by heterogeneous

* Corresponding author at: Department of Chemical Sciences, University of Naples Federico II, Via Cintia, IT-80126 Naples, Italy.
E-mail address: diserio@unina.it (M. Di Serio).

https://doi.org/10.1016/j.cej.2020.127236
Received 16 July 2020; Received in revised form 8 September 2020; Accepted 30 September 2020
Available online 6 October 2020

Nomenclature

List of symbols

$A_{j,i}$	Coefficient j of the viscosity function for component i
a_s	Specific external surface area [m^2/m^3]
c_i	Concentration of component i [mol/m^3]
$c_{i,s}$	Concentration of component i in the solid phase [mol/m^3]
$D_{e,i}$	Effective diffusivity of component i [m^2/s]
D_i	Molecular diffusivity of component i [m^2/s]
Ea_j	Activation energy of reaction j [kJ/mol]
K	Equilibrium constant [–]
K_{ref}	Reference equilibrium constant [–]
k_A	Kinetic constant of the reaction promoted by Amberlite IR120 [$(m^3/kg)(m^3/mol)s^{-1}$]
$k_{A,ref}$	Reference kinetic constant of the reaction promoted by Amberlite IR120 [$(m^3/kg)(m^3/mol)s^{-1}$]
k_H	Kinetic constant of the reaction promoted by H_2SO_4 [$(m^3/mol)^2s^{-1}$)]
$k_{H,ref}$	Reference kinetic constant of the reaction promoted by H_2SO_4 [$(m^3/mol)^2s^{-1}$)]
k_s	Fluid-solid mass transfer coefficient [m/s]
m_i	Partition coefficient for component i between the liquid and intraparticle phases [–]
M_i	Molecular weight of component i [g/mol]
r_A	Rate of the reaction promoted by Amberlite IR120 [mol/(kg s)]
r_H	Rate of the reaction promoted by H_2SO_4 [$mol/(m^3\ s)$]
R	Ideal gas constant [kJ/(K mol)]
R_P	Catalyst radius [m]
$R_{P,dry}$	Dry catalyst radius [m]
t	Time [s]
T	Temperature [K]
T_{ref}	Reference temperature (333 K) [K]
v	Stirring speed [rpm]
V_{H2O}	Water volume [m^3]
$V_{H2O,max}$	Maximum water volume up taken by the resin [m^3]
$V_{m,i}$	Molar volume of component I at boiling temperature in standard conditions from Le-Bas correlation [cm^3/mol]
w_{cat}	Catalyst mass [kg]
x	Dimensionless particle radial coordinate [–]
x_i	Molar fraction of component i [–]
X_{NA}	Nonanoic acid conversion degree [%]
y_{H2O}	Water volumetric fraction [–]

Greek Letters

α_{H2O}	Specific cater content of the resin [m^3/kg]
$\Delta_r H$	Reaction enthalpy [kJ/mol]
ε_P	Catalyst porosity [–]
η	Effectiveness factor [–]
μ_i	Viscosity of component i [cP]
μ_{mix}	Mixture viscosity [cP]
ν_i	Stoichiometric coefficient of component i [–]
ρ_B	Catalyst bulk density [kg/m^3]
$\rho_{EtHex\text{-}NA}$	Ester density [kg/m^3]
ρ_P	Catalyst density [kg/m^3]
τ_P	Catalyst tortuosity [–]
ϕ_i	Association factor of component i [–]
ϕ_{mix}	Mixture association factor of component i [–]

Abbreviations

CI	Confidence interval
EtHex	2-ethyl-1-hexanol
EtHex-NA	2-ethylhexylnonanoate
EXP	Experimental data
NA	Nonanoic acid
SIM	Simulated data

catalysts as they can be easily separated and re-used with respect to the homogeneous ones [14]. An important characteristic of the heterogeneous catalysts is water resistance which is the byproduct in the esterification reaction. The most used heterogeneous catalysts in esterification reactions of organic acids with alcohols are ion-exchange resins functionalized with sulfonic acid groups such as Amberlyst, Dowex, Nafion and Purolite classes [15]. In the previous literature there are few works on the kinetics of nonanoic acid (NA) with different types of alcohols. Sharma et al. [9] investigated the esterification of nonanoic acid with methanol in a batch reactor in the presence of different types of heterogeneous catalysts such as Dowex 50Wx2, Amberlyst 35 and Amberlyst 15. In this case, results show that with Amberlyst 15 and Dowex 50Wx2 similar nonanoic acid conversion is achieved and it is higher than the other one reached using Amberlyst 35. In other papers, Amberlyst 15 was adopted to promote the esterification of nonanoic acid with ethanol [16] and 1-propanol [7] obtaining satisfactory results. The choice of the alcohol, linear or branched, low or high molecular weight, strictly influences the performance of the final product.

Amberlite IR120 was used in several esterification reactions, e.g Izci et al. [17] and Altiokka et al. [18] investigated the esterification of acetic acid with isobutanol using Amberlite IR120. This catalyst was used in some other cases such as the esterification of acetic acid with isoamyl alcohol [19]; Merchant et al. studied the esterification of different types of acids with ethanol [20].

Thus, the aim of this work is to investigate the kinetics of this reaction performing experiments in batch reactors first in the presence of an homogeneous catalyst (H_2SO_4) and subsequently with an heterogeneous catalyst (Amberlite IR120) to evaluate the effects of different experimental conditions (i.e. temperature, stirring rate, catalyst load and reactants molar ratio) on the reaction rate making a comparison between the results obtained from the two different cases.

To describe the collected data, it was necessary to measure both viscosity and density of the product, not available in the literature, data essential when calculating the reaction volume and the diffusivity of each component when simulating intraparticle mass balance equations. The kinetic experimental data were described with dedicated models to retrieve kinetic and thermodynamic parameters useful to design larger scale reactors.

2. Experimental section

2.1. Materials and method

Chemicals used in the experiments are nonanoic acid (purity $\geq$ 96%), 2-ethylhexanol (purity $\geq$ 99%), sulfuric acid (98% w/w), Amberlite IR120. All the reactants were purchased from by Merck while Amberlite IR120 from Rohm and Haas and its characteristics taken from the catalyst data sheet are reported in Table 1.

2.2. 2-ethylhexylnonanoate density and viscosity measurements

Measuring or estimating the dependence on the viscosity and density of the temperature is surely a key issue in the determination of the reaction kinetics as both parameters play an important effect on the reaction rate (as it will be seen later). The mentioned functionalities were evaluated for each component present in the reaction system, based on the empirical expression [21]:

$$\mu_i = exp\left(A_{1,i} + \frac{A_{2,i}}{T}\right) \quad (2)$$

$$\rho_i = B_{1,i}T + B_{2,i} \quad (3)$$

The coefficients of the Eqs. (2) and (3), for nonanoic acid, 2-ethylhexanol and water were determined by parameter estimation on the data generated using ChemCAD data bank [22] and, in the case of water density also from Perry and Green handbook [23]. No data were found in the literature for 2-ethylhexylnonanoate, thus in the present paper we have measured both density and viscosity values with temperature.

The experiments were conducted on products obtained in the Run A2 of Table 2, after recovering of excess of alcohol by distillation. The composition of the purified product sample was (98% 2-ethylhexylnonanoate, 2% nonanoic acid, 2-ethylhexanol <0.05).

Density was measured using a graduated cylinder in a temperature-controlled water bath. A precise amount of ester, synthesized in the present work, was weighed and it was put into the cylinder. The volume of the ester was measured at different temperatures from which it was possible to determine density values.

Viscosity of the 2-ethylhexylnonanoate was determined using a capillary viscometer Cannon–Fenske in which the ester synthesized in the present work was put. The viscometer was placed in a controlled temperature water bath and the tests were made at different temperature.

The error on the experimental measurements was estimated by conducting the same experiment three times. An average error of 2% was obtained.

2.3. Swelling tests using Amberlite IR120

The shape and dimension of catalysts particle can have an important influence of reaction rate because the mass transfer phenomena. Swelling phenomena can occur when a heterogeneous catalyst, such as an ion exchange resin, is used. In this work, dry Amberlite IR120 was placed into four cylinders and nonanoic acid, 2-ethylhexanol, ester and water were respectively added. It was measured the volume occupied by the resin before and after adding the liquid. Moreover, an additional test was conducted to evaluate the volume of water adsorbed per mass of catalyst, by putting in contact 10 g of catalyst and adding under stirring water drop by drop from a graduated cylinder, until the permanence of not adsorbed water on the resin's surface.

2.4. Reactor setup and procedure of kinetic experiments

Nonanoic acid esterification, both with homogeneous and heterogeneous catalysts, was performed in a Hastelloy autoclave, with a nominal volume of 0.3L, equipped with a magnetically driven stirrer, whose impeller was regulated at different values through a dedicated control system. A thermoregulator connected to a heating jacket allowed to keep the reaction temperature at the set value. An amount of 200 g solution was weighted in the reactor, together with the resin (sulfuric acid was added after the heating through an external loading syringe working at 10 bar). The system was pre-heated at the desired temperature level after vessel pressurization to 5 bar to avoid the partition of the light components between the gas and liquid phases. A sample was collected at $t = 0$ to measure the conversion degree after the pre-heating time (see Table 2). Samples of 1 cm^3 were withdrawal at periodic times and the reactions are prolonged till measuring the thermodynamic plateau.

Table 1
Amberlite IR120 properties.

	Value	Units
Particle size	620–830	μm
Crosslinking degree	8	%
Acid sites concentration	4.40	meq/g
Surface area	1.53	m^2/g
$R_{P,dry}$	$3.62 \cdot 10^{-4}$	m
ϵ_P	0.55	–
τ_P	5.00	–
ρ_P	1518	kg/m^3

Table 2
Operation conditions for both Blank (B), catalyzed by sulfuric acid (H) and Amberlite IR120 (A) kinetic experiments. Nonanoic acid conversions were measured at time zero, meaning when the system reached the set value of temperature.

Run	ν [rpm]	T [K]	EtHex/NA [mol/mol]	$X_{NA,0}$ [%]	H_2SO_4 [mol %]	ρ_B [kg/m^3]
B1	800	323	5:1	0	–	–
B2	800	333	5:1	0	–	–
B3	800	343	5:1	0	–	–
B4	800	353	5:1	0	–	–
B5	800	353	2.5:1	0	–	–
B6	800	353	1:1	0	–	–
H1	800	313	5:1	0	1.0	–
H2	800	323	5:1	0	1.0	–
H3	800	333	5:1	0	1.0	–
H4	800	343	5:1	0	1.0	–
H5	800	333	5:1	0	0.5	–
H6	800	333	5:1	0	0.25	–
A1	200	363	5:1	0.8	–	16.9
A2	400	363	5:1	1.5	–	16.9
A3	600	363	5:1	0.6	–	16.9
A4	800	363	5:1	2.8	–	16.9
A5	600	353	5:1	3.2	–	16.9
A6	600	343	5:1	3.2	–	16.9
A7	600	363	5:1	2.7	–	10.6
A8	600	363	5:1	5.1	–	4.2
A9	600	363	2.5:1	3.8	–	16.9
A10	600	363	1:1	3.6	–	16.9

Several experiments were conducted in absence of catalyst, to evaluate the autocatalytic effect of the system (Blank experiments). The operation conditions for blank and catalyzed tests are reported in Table 2, labelled with the B letter.

Experiments were conducted in the presence of sulfuric acid, varying in this case temperature, molar ratio between the reactants and catalyst load. The summary of the adopted conditions is reported in Table 2, labeling the experiments with letter H.

Finally, experiments were conducted in the presence of Amberlite IR120. Before being used, the catalyst was pretreated in an oven at 333 K to remove water adsorbed in its pores. In this case, also the influence of the stirring rate was studied. The operation conditions are listed in Table 2, labeling the tests with letter A.

Samples were analyzed via acid-base titration, using NaOH/EtOH 0.1 M solution and phenolphthalein as indicator [24]. No byproduct was observed in any case, demonstrated via GC-FID analysis. A fused silica capillary column 30 m × 0.32 mm ID × 0.26 μm (Supelco SLB-IL60) was used for the analysis. The injector and detector temperatures were of 300 °C and 1 μL of sample was injected. The oven temperature was varied from 100 °C up to 300 °C with a rate of 10 °C/min.

The error on the experimental data was estimated by conducting the same experiment three times. An average error of 2.5% was obtained.

3. Results and discussion

3.1. Density and viscosity measurements

The density and viscosity data generated with CHEMCAD database [22] (nonanoic acid (NA), 2-ethylhexanol (EtHex) and water), Perry and Green handbook (for water density only) [23] and experimentally measured (2-ethylhexylnonanoate, EtHex-NA) are reported in Fig. 1A and 1B respectively. The data were fitted using Eqs. (2)–(3) (see Fig. 1) and the parameters reported in Table 3.

The experimental values of density and viscosity measured in this paper for 2-ethylhexylnonanoate are reported in Fig. 1 and Table S1 of supplementary material.

3.2. Swelling tests using Amberlite IR120

Amberlite IR120 radius is the double than the dry one in the presence of water, while the liquid take-up can be considered negligible when putting the resin in contact with either the reactants or the ester.

To describe the liquid take-up as the composition changes, Eq. (4) was considered, where the particle radius varies linearly with the amount of water generated by the reaction (V_{H2O}) divided by the maximum amount of water uptaken by the resin ($V_{H2O,\max}$).

$$\begin{cases} R_P = R_{P,dry}\left(1+\dfrac{V_{H_2O}}{V_{H_2O,max}}\right), & V_{H_2O} \leqslant V_{H_2O,max} \quad (a) \\ R_P = 2R_{P,dry}, & V_{H_2O} > V_{H_2O,max} \quad (b) \end{cases} \tag{4}$$

As revealed, when water is not formed (i.e. $t = 0$), the particle has a radius equal to its dry version (see Table 1 for details). When the amount of water generated by the chemical reaction is lower than the maximum amount of water that can be up taken by the resin, a linear trend of the particle radius increase is considered. When the maximum water content is reached, the radius of the particle is double than the dry one, to respect the 100% uptake of water that was measured from the take-up experiments. Attention must be paid as Eq. 4a becomes Eq. 4b when $V_{H2O} = V_{H2O,\max}$.

The volume of water changing with time and the maximum volume of water that can be up taken by the resin were calculated as in Eqs. (5) and (6).

$$V_{H_2O} = y_{H_2O} V \tag{5}$$

$$V_{H_2O,max} = w_{cat}\alpha_{H_2O} \tag{6}$$

Where α_{H2O} was measured experimentally as the ratio between the maximum volume of water taken up referred to the catalyst mass. The obtained value is $\alpha_{H2O} = 1.50{\cdot}10^{-3}$ m^3/kg.

The readers must be aware that no liquid–liquid partition was observed when withdrawing the samples with the experimental time. A liquid–liquid separation is observed when cooling the product mixture at the end of the reaction at room temperature.

3.3. Blank tests

A first set of experimental tests was made without catalysts in order to investigate the possible autocatalysis effect of the nonanoic acid itself [14]. Tests were conducted at different temperatures and reactants molar ratio (see Fig. S1 in supplementary material). The influence of autocatalysis in the adopted reaction condition is very low: after 5 h of reaction the nonanoic acid conversion is always less than 5%.

Table 3
Viscosity and density parameters for the four chemical components involved in the esterification reaction. *Parameters and equation reported in Eqs. (2) and (3).

Component (i)	$A_{1,i}$	$A_{2,i}$	$B_{1,i}$	$B_{2,i}$
NA	−6.15 ± 0.05	2415 ± 5	−0.87 ± 0.01	1164 ± 0.3
EtHex	−8.12 ± 0.01	2981 ± 3	−0.88 ± 0.01	1095 ± 5
EtHex-NA	−5.32 ± 0.14	1993 ± 4	−0.82 ± 0.02	1093.4 ± 0.5
H_2O	−6.20 ± 0.08	1823 ± 4	−0.269 ± 0.001	1075.2 ± 0.3

3.4. Nonanoic acid esterification kinetics promoted by sulfuric acid

3.4.1. Experimental results

Experiments were performed with homogeneous catalyst (H_2SO_4), investigating different operation conditions (i.e. temperature and catalyst load).

Tests at different temperatures were performed to evaluate its effect on the reaction rate and to determine equilibrium constants, using a molar ratio 5:1 (alcohol/acid). The obtained results are reported in Fig. 2.

In Fig. 2, it can be observed that the reaction rate increases by increasing the temperature reaching the equilibrium for the runs at lower temperature at very long reaction time, hence to be sure about the equilibrium values it was necessary to extend experiments duration overnight. The equilibrium value is slightly favored by increasing the reaction temperature.

A second set of experiments was conducted at 333 K with molar ratio 5:1 (alcohol/acid) changing catalyst load, see Fig. 3A.

It is possible to observe that by increasing sulfuric acid amount reaction rate increases as well. As for the discussed previous tests, also in this case equilibrium was reached after long reaction time (about 24 h). These tests allow to determine the reaction order with respect to the catalyst, multiplying the experimental time for the catalyst percentage [14]. From Fig. 3B, were the conversion is reported as function of the reaction time multiplied for concentration of sulfuric acid (mol %), it is possible to observe that experimental data overlap; this implies that reaction kinetics is of the first order respect to the sulfuric acid concentration [14].

3.4.2. Kinetic modelling

The experimental data collected for the esterification reaction promoted by sulfuric acid, were described by a kinetic model based on the

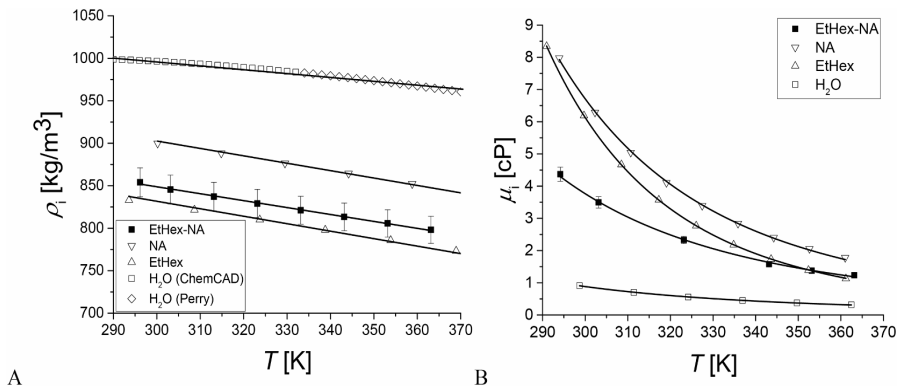

Fig. 1. Physical-chemical data measured for 2-ethylhexylnonanoate (■) and estimated for nonanoic acid (▽), 2-ethylhexanol (△), water from ChemCAD database [22] (□) and from Perry [23] (◇): A. density, B. viscosity. Symbols are experimental data; lines are calculated values.

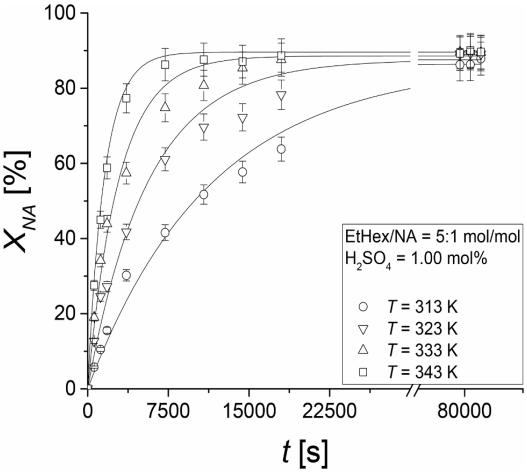

Fig. 2. Temperature effect for sulfuric acid catalyzed tests (Run H1-H4 of Table 2). Dots are experimental data; lines are calculated with the model described in 3.4.2 paragraph.

Fisher esterification mechanism, where the reaction rate is given by a reversible second order expression, Eq. (7).

$$r_H = k_H c_{H_2SO_4}\left(c_{NA}c_{EtHex} - \frac{1}{K}c_{EtHex-NA}c_{H_2O}\right) \quad (7)$$

The dependency with temperature of both the kinetic and equilibrium constants are included in the model, using a modified Arrhenius and the Van't Hoff equations, Eqs. (8), (9).

$$k_H = k_{H,ref}\,exp\left(-\frac{Ea_H}{R}\left(\frac{1}{T}-\frac{1}{T_{ref}}\right)\right) \quad (8)$$

$$K = K_{ref}\,exp\left(-\frac{\Delta_r H}{R}\left(\frac{1}{T}-\frac{1}{T_{ref}}\right)\right) \quad (9)$$

Where the reference temperature was set at $T_{ref} = 333$ K.

The generic mass balance equation to describe the evolution with time of the composition of each component along the reaction time is given as in Eq. (10).

$$\frac{dc_i}{dt} = \nu_i r_H \quad (10)$$

The autocatalytic extent of the reaction was neglected as in the adopted reaction conditions its effect is rather low (see paragraph 3.3).

The parameter estimation was conducted on all the available data (Run H1-H6 of Table 2) simultaneously, retrieving both kinetic and thermodynamic parameters. The results of the estimation are given in Table 4 together with statistic information, while the fit can be appreciated in Figs. 2 and 3, dealing with the evolution with time of nonanoic acid conversion, and Fig. 4 where an overall parity plot is reported.

As revealed, the agreements are reasonable, as all the data are included in a window of error lower than 10%. The thermodynamic parameters confirm that the reaction is slightly endothermic, and the equilibrium constant is greater than one, thus the reaction is shifted through the products. An activation energy value of 60.8 kJ/mol was obtained. The parameters are consistent as characterized by a low confidence interval value and a very low correlation between each other (see Table 4).

3.5. Esterification kinetics promoted by Amberlite IR120

3.5.1. Experimental results

Experiments were performed with Amberlite IR120 as heterogeneous catalyst, investigating different operation conditions (i.e. stirring rate, temperature, catalyst load and reactants molar ratio).

Three runs at different stirring rate values (Run A1: 200 rpm; Run A2: 400 rpm; Run A3: 600 rpm) were performed in order to investigate the possible presence of external mass transfer limitation, Fig. 5. Similar results were obtained within the range 200–600 rpm. These results identify the absence of fluid–solid mass transfer limitation. Another test was performed at 800 rpm (Run A4) but lower nonanoic acid conversion degree values were reached because catalyst is confined on the reactor walls due to the high stirring rate (see Fig. 5).

Kinetic experiments were conducted by evaluating the effect of the Amberlite IR120 load on the reaction. By increasing the catalyst concentration, the reaction rate increases too, as it can be seen in Fig. 6.

Multiplying the reaction time for the Amberlite IR120 bulk density a

Table 4
Parameter estimation results for the experiments conducted in the presence of sulfuric acid. CI: confidence interval.

	Value	95% CI	Units	Correlation matrix			
				$\Delta_r H$	Ea_H	K_{ref}	k_{ref}
$\Delta_r H$	10.3	0.2	kJ/mol	1			
Ea_H	60.8	0.1	kJ/mol	−0.2	1		
K_{ref}	1.69	0.01	–	+0.3	−0.1	1	
$k_{H,ref}$	$9.04\cdot10^{-10}$	$0.01\cdot10^{-10}$	$(m^3/mol)^2 s^{-1}$	−0.1	+0.4	−0.2	1

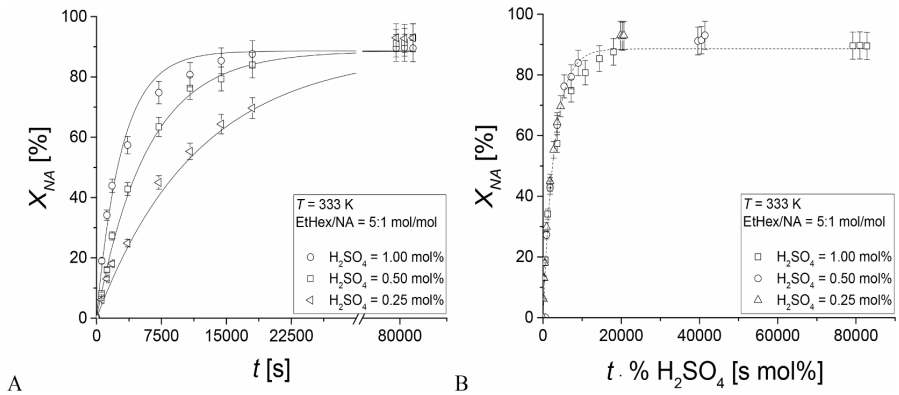

Fig. 3. A. Catalyst load effect for sulfuric acid catalyzed experiments (Run H3, H5, H6 of Table 2). Dots are experimental data; lines are calculated with the model described in 3.4.2 paragraph. B. Reaction time normalized per sulfuric acid percentage. Dots are experimental data, dashed line the calculated values.

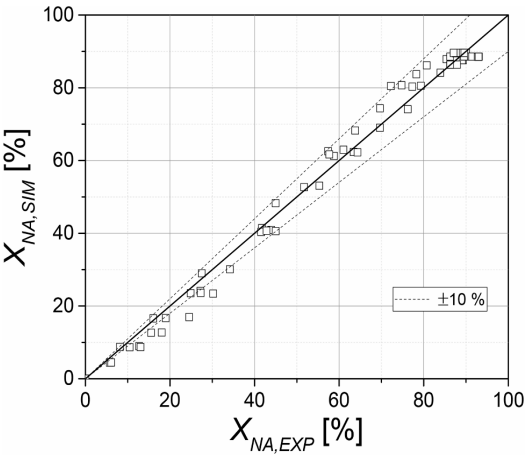

Fig. 4. Parity plot for the kinetic experiments catalyzed by sulfuric acid.

bad overlap of the experimental data was obtained, indicating that the apparent reaction order is different than unity (Fig. 7A). For this reason, we varied the exponent till reaching a good overlap between the data. The result was a power of 0.5 (Fig. 7B). Thus, the order of the reaction kinetics with respect to the catalyst concentration is 0.5. A value lower than unity usually implies that internal mass transfer limitation occurs. For instance, it was recently demonstrated that levulinic acid esterification with ethanol, promoted by Amberlite IR120 [25], did not suffer of intraparticle mass transfer limitations as the size of the molecules are surely smaller than the ones used in the present paper, i.e. molecules branched or characterized by long carbon chains.

For this reason, the experimental data were interpreted using a mathematical model considering intraparticle diffusion phenomena.

Experiments, conducted changing alcohol/acid molar ratio, demonstrate that conversion degree increases by increasing reactants molar ratio, Fig. 8.

Experiments were conducted at different temperatures. The results are reported in Fig. 9. The results showed that by increasing the temperature, an increase of the reaction rate was observed. The equilibrium plateau is temperature dependent, showing an increasing value as temperature increases, confirming the endothermic behavior of the esterification reaction.

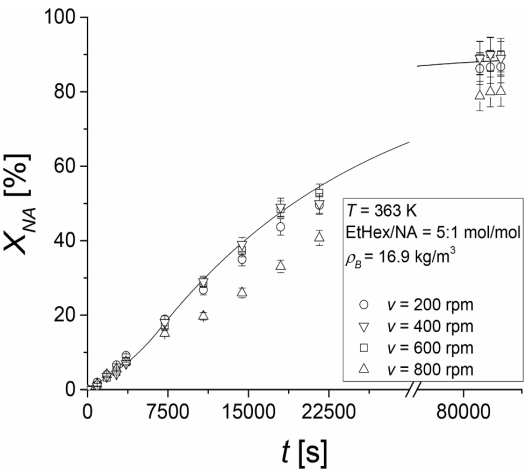

Fig. 5. Stirring rate effect for Amberlite IR120 catalyzed tests (Run A1-A4 of Table 2) T = 363 K, EtHex/NA = 5:1 mol/mol, ρ_B = 16.9 kg/m^3.

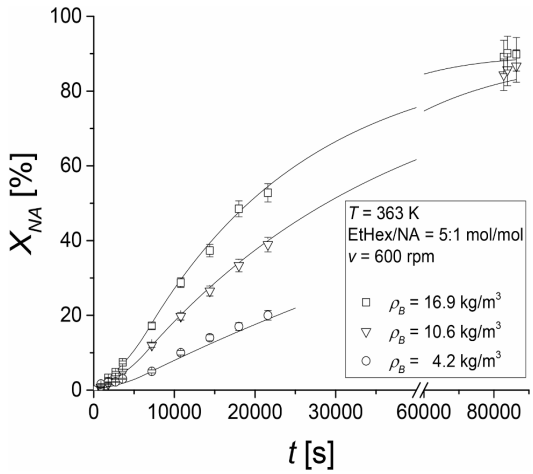

Fig. 6. Catalyst load effect for Amberlite IR120 catalyzed tests (Runs A3, A7, A8 of Table 2), fixing T = 363 K, EtHex/NA = 5:1 mol/mol, v = 600 rpm. Dots are experimental data; lines are calculated with the model described in 3.5.2 paragraph.

Moreover, having a closer look at the experimental data collected at reaction times lower than 10000 s, a sort of induction period is always present, that was totally absent for the experiments conducted in the presence of sulfuric acid. This apparent induction time is surely independent on the fluid–solid mass transfer as the experiments were conducted at a sufficiently high enough stirring rate to exclude it. Thus, this peculiar effect can be described only in terms of intraparticle mass balance limitation, i.e. the influence of either the particle radius value changing with the liquid phase composition or the physic-chemical characteristics of the liquid mixture. This aspect will be deepened in the kinetic modelling paragraph, reported below.

3.5.2. Kinetic modelling

As for the kinetic modelling of the homogenously catalyzed reaction, also for the elaboration of the experimental data collected in the presence of Amberlite IR120 we neglected the autocatalytic effect. In this case, the reaction rate expression can be written as in Eq. (11).

$$r_A = k_A\left(c_{NA}c_{EtHex} - \frac{1}{K}c_{EtHex-NA}c_{H_2O}\right) \tag{11}$$

It is important to underline that the equilibrium constant value and the related enthalpy change were already been estimated in the previous section, as they are independent on the choice of the catalyst. Thus, we have fixed the numerical values of both K_{ref} and $\Delta_r H$ as the ones reported in Table 4.

Also in this case, the modified version of the Arrhenius equation was adopted, Eq. (12).

$$k_A = k_{A,ref}exp\left(-\frac{Ea_A}{R}\left(\frac{1}{T}-\frac{1}{T_{ref}}\right)\right) \tag{12}$$

Where the reference temperature was set at T_{ref} = 333 K.

As it was demonstrated that intraparticle mass transfer limitation occurs (Fig. 7), thus an intraparticle mass balance equation must be considered. In Eq. (13), a dimensionless form of the classical mass balance equation for the intraparticle diffusion model in a spherical particle is reported.

$$\varepsilon_P\frac{\partial c_{i,s}}{\partial t} = \frac{D_{e,i}}{R_P^2}\left(\frac{\partial^2 c_{i,s}}{\partial x^2}+\frac{2}{x}\frac{\partial c_{i,s}}{\partial x}\right)+\nu_i r_A \rho_P \tag{13}$$

Writing the intraparticle mass balance equation in a dimensionless

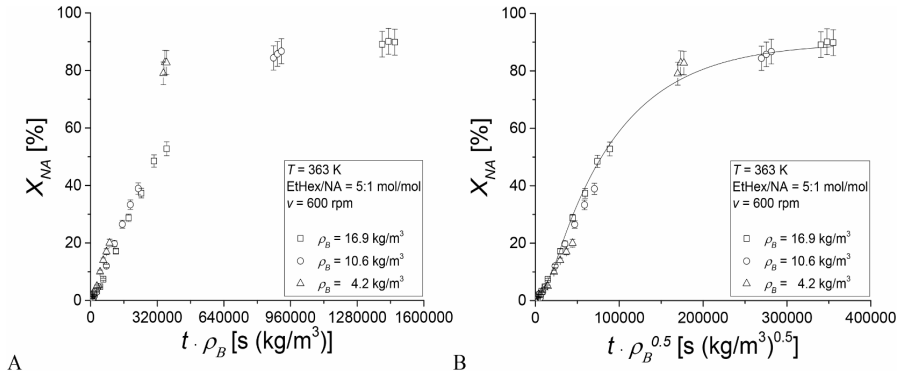

Fig. 7. Catalyst load effect for Amberlite IR120 catalyzed tests (Runs A3, A7, A8 of Table 2), fixing $T = 363$ K, EtHex/NA = 5:1 mol/mol, $v = 600$ rpm. Reaction time is multiplied for Amberlite IR120 bulk density (A) and for the square root of Amberlite IR120 bulk density (B). Dashed line is the simulation result, dots the experimental data.

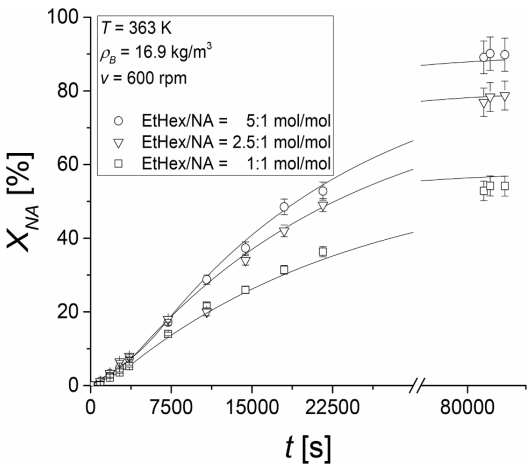

Fig. 8. Reactants molar ratio effect for Amberlite IR120 catalyzed tests (Runs A3, A9, A10 of Table 2), fixing $T = 363$ K, $\rho_B = 16.9$ kg/m^3, $v = 600$ rpm. Symbols are experimental data; lines are calculated with the model described in 3.5.2 paragraph.

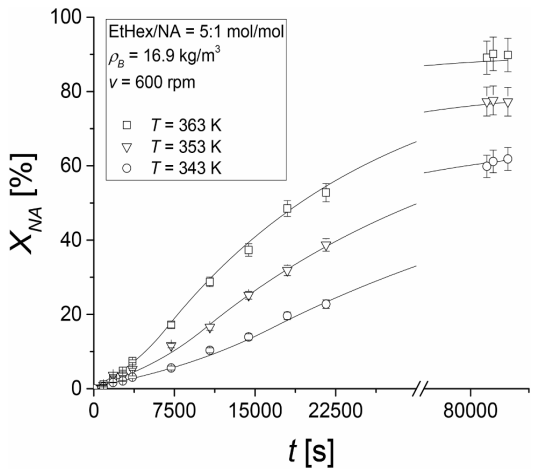

Fig. 9. Temperature effect for Amberlite IR120 catalyzed tests, fixing EtHex/NA = 5:1 mol/mol, $\rho_B = 16.9$ kg/m^3, $v = 600$ rpm (Runs A3, A5, A6 of Table 2). Dots are experimental data; lines are calculated with the model described in 3.5.2 paragraph.

form allows to solve a technical problem. As a matter of fact, as the reaction proceeds, the system changes in composition and water is formed. From data obtained as described in paragraph 3.2 no swelling of resin was observed with the organic components of reaction mixture while Amberlite IR120 swallows in the presence of water. This means that the particle radius changes as a function of the liquid phase composition. For this reason, the higher integration extreme of the particle radial coordinate changes with time. Numerically it is not possible to solve a situation as such. Writing the mass balance in dimensionless form, the particle radius is placed outside from the differential terms, thus it is possible to use the functionalities reported in paragraph 3.2.

Effective diffusivity was calculated in agreement with Eq. (14).

$$D_{e,i} = D_i \frac{\varepsilon_P}{\tau_P} \tag{14}$$

Catalyst porosity and tortuosity are given in Table 1. Where the molecular diffusivity D_i stands for the diffusivity of each component, obtained from the Wilke and Chang equation valid for a multicomponent system, Eq. (15) [22].

$$D_i = 7.4 \cdot 10^{-12} \frac{T(\phi_{mix} M_i)^{0.5}}{\mu_{mix} V_{m,i}^{0.5}} \tag{15}$$

Where, $\phi_{mix}$is the association factor of the mixture calculated as in Eq. (16).

$$\phi_{mix} M_i = \sum_{i=1, j \neq i}^{N_c} x_{i,j} \phi_i M_i \tag{16}$$

Where, $\phi_i$is the association factor of each component (see Table 5).

The viscosity of the mixture was evaluated by weighting the viscosity of each component by its molar fraction, Eq. (17).

$$ln(\mu_{mix}) = \sum_{i=1}^{N_c} x_i ln(\mu_i) \tag{17}$$

The viscosities of pure components were calculated using the Eq. (2)

Molar volumes were calculated in agreement with Le-Bas correlation [21], values reported in Table 5.

To solve the intraparticle mass balance equation, two boundary conditions were used for both the center of the particle and the surface of

the catalyst, Eqs. (18),19.

$$\left.\frac{\partial c_{i,s}}{\partial x}\right|_{x=0} = 0 \tag{18}$$

$$\left.\frac{D_{e,i}}{R_P}\frac{\partial c_{i,s}}{\partial x}\right|_{x=1} = k_s a_s\left(c_i - m_i c_{i,s}|_{x=1}\right) \tag{19}$$

As revealed, a symmetry condition was adopted as boundary condition in the particle center, while a continuity equation between the bulk liquid phase and the surface of the catalyst is considered at $x = 1$.

Where m_i represent the partition coefficient of component i between the bulk fluid and intraparticle phases. It is important to underline that when adoption ion exchange resins as heterogeneous catalysts, partition phenomena always occur between the fluid bulk and the intraparticle phases, as the resin show a higher affinity towards specific chemical components [26]. As demonstrated in our previous paper, long chained molecules or branched molecules show a lower affinity than water. Thus, the concentration of each component inside the resin can be different than the concentration in the bulk liquid phase. For the mentioned reason, we assumed partition coefficients similar to the ones we found previously in the esterification of fatty acids, where water was demonstrated to accumulate inside the resin four times than branched and long chained components. For the mentioned reasons, we assumed that $m_{NA} = m_{EtHex} = m_{Et\text{-}Hex\text{-}NA} = 1$ and $m_{H2O} = 0.25$.

As the fluid–solid mass transfer is fast enough to not affect reaction rate in agreement with the experimental observations reported in Fig. 5, a sufficiently high value was imposed for $k_s a_s$.

The liquid bulk phase concentrations were computed by writing a generic mass balance equation, where the accumulation term is considered equal to the mass transfer flux to the catalyst surface, Eq. (20).

$$\frac{dc_i}{\partial t} = -k_s a_s\left(c_i - m_i c_{i,s}|_{x=1}\right)\frac{\rho_B}{\rho_P} \tag{20}$$

Where the catalyst bulk density is defined as the mass of catalyst loaded in the reactor divide by the liquid volume.

All the additional physical–chemical properties needed for the computations are provided in Table 5 [21].

All the experimental data were elaborated with the proposed mathematical model by using gPROMS Model Builder v.4.0 software [27]. In Table 6, the results obtained from the parameter estimation and the correlation matrix are reported. The errors of the parameters fall into the 95% confidence interval. The enthalpy of the reaction and the activation energy were fixed as the ones obtained using sulfuric acid as catalyst. As revealed, the activation energy obtained for the Amberlite IR120 catalyzed system is similar to the obtained using sulfuric acid, as the esterification reaction is catalyzed by the protons, independently on their source. The reference kinetic constants of both systems are in a ratio of $k_{H,ref}/k_{A,ref} = 26$, as the acid sites concentration is lower for Amberlite IR120 than for sulfuric acid where protons are promptly available.

A sensitivity study on the partition coefficients was conducted showing that by varying m_{H2O} in a range between 0.125 and 0.35, the obtained kinetic constants fall within the confidence interval. Thus, our assumption can be considered valid.

The comparison between the experimental data and the simulated curves using the values obtained from the parameter estimation shows a good agreement, as it is possible to see from the Figs. 5–9, where the evolution of nonanoic acid conversion with time is reported.

Finally, from the parity plot in Fig. 10 it is possible to see that all the experimental data collected in the experiments fall into an error range of about ± 20%.

To show the influence of the intraparticle mass transfer limitation, the effectiveness factor was calculated as in Eq. (21).

$$\eta = \frac{\int_0^1 r_A(x)\cdot x\cdot dx}{r_A|_{x=1}\int_0^1 x\cdot dx} \tag{21}$$

In Fig. 11 the simulation of both effectiveness factor, the particle radius and the mixture viscosity are reported, adopting the operation conditions of experiment A3. As revealed, η is maximum at the beginning of the reaction when particle radius is equal to the initial value, i.e. the lowest possible (Fig. 11A). As the radius increases up to the final wet value (Fig. 11B), the catalyst efficiency decreases, and it remains constant. Moreover, the viscosity of the solution decreases as the ester is formed (Fig. 11B).

The readers must be aware that the correct inclusion of the swelling phenomenon and the measurement of the viscosity data for the ester allowed the exact description of the initial slope of the conversion plots, that always showed an induction period (e.g. initial slopes of Figs. 5–9). Two competitive phenomena occur simultaneously: (i) the formation of water that increases the particle radius, leading to a longer diffusion path; (ii) the production of the ester and water that are both characterized by a lower viscosity value compared to the reactants, leading to an increase of the molecular diffusivity.

The first mentioned phenomenon is in contrast with the experimental observation, as longer diffusion paths would lead to an even longer induction period characterized by a lower rate of the increase of the conversion. The decrease of the viscosity of the liquid mixture, instead, is in line with the experimental observation. As a matter of fact, lower is the viscosity, higher the molecular diffusivity of the chemical compounds, leading to a fastening of the overall rate of the reaction network as intraparticle diffusion limitations start to be less

Table 5
Physical-chemical parameters for the four chemical components involved in the esterification reaction.

Component (i)	M_i [g/mol]	ϕ_i [–]	$V_{m,i}$ [cm^3/mol]
NA	158.23	1	223.8
EtHex	130.23	1	192.4
EtHex-NA	270.42	1	399.4
H_2O	18.01	2.6	18.4

Table 6
Results of parameter estimation based on all the experimental data collected in the presence of Amberlite IR120. CI: confidence interval.

	Value	95% CI	Units	Correlation matrix	
				Ea_A	$k_{A,ref}$
Ea_A	57.7	0.1	kJ/mol	1	
$k_{A,ref}$	$3.4\cdot10^{-11}$	$0.01\cdot10^{-11}$	$(m^3/kg)(m^3/mol)s^{-1}$	−0.5	1

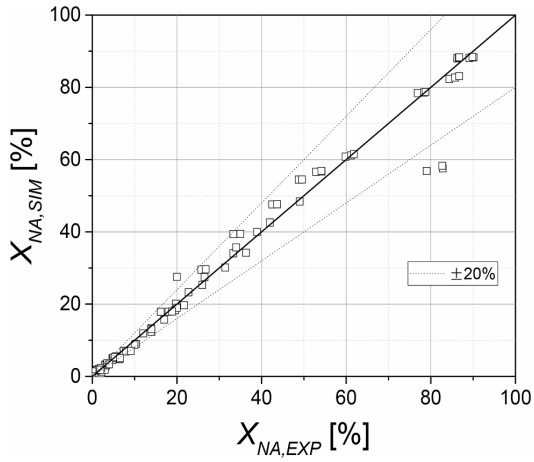

Fig. 10. Parity plot representing all the experimental data.

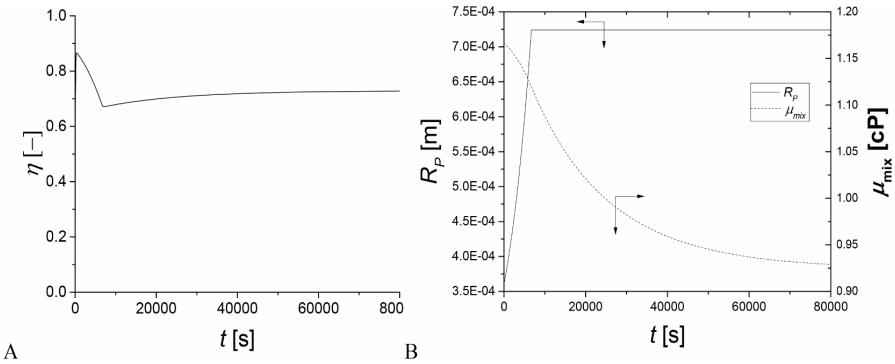

Fig. 11. A. Catalyst effectiveness factor vs reaction time; B. catalyst particles radius and liquid phase viscosity vs time.

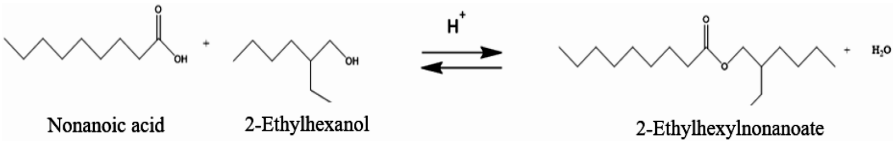

pronounced.

Moreover, we tried to neglect the particle radius dependency with water content, running a new parameter estimation. It was verified that the agreements were worse, as a too short induction time was simulated in any case. For the mentioned reasons we can conclude that to properly describe the physics and the chemistry of the investigated system both phenomena must be considered, and this is a clear novelty in the field of esterification reactions promoted by ion exchange resins.

The concept we drawn can be considered of high interest overall when facing with long-chained or highly branched carboxylic acids and alcohols.

4. Conclusions

The kinetics of the esterification reaction of the nonanoic acid with 2-ethylhexanol was investigated using sulfuric acid as homogeneous catalyst and Amberlite IR120 as heterogeneous catalyst. The density and viscosity of the product were measured with accuracy.

The activation energy values of both catalysts are similar (≈60 kJ/mol), as the reaction mechanism is the same. The thermodynamic parameters showed that the reaction is slightly endothermic, characterized by an enthalpy value of $\Delta_r H = 10.3$ kJ/mol, and a reference equilibrium constant at 333 K of 1.69, showing that the reaction is shifted to the products.

All the collected experimental data were elaborated with reliable reactor models which well interpreted the obtained results showing a good agreement between the experimental and the simulated curves.

Internal mass transfer limitation was observed experimentally and correctly described adopting intraparticle mass balance model, that allowed to properly describe quantitatively all the collected data in the presence of the heterogeneous catalyst.

The induction time present in every experiment conducted with Amberlite IR120 was properly simulated by taking into account both the particle radius dependency with water content and the liquid viscosity change with composition.

In perspectives, this work can be considered a good starting point to develop a pilot plant working in continuous operation, to maximize the productivity of the ester.

Declaration of Competing Interest

The authors declare that they have no known competing financial interests or personal relationships that could have appeared to influence the work reported in this paper.

Acknowledgements

Authors wish to thank European Union (FSE, PON Ricerca e Innovazione 2014-2020, Azione I.1 “Dottorati Innovativi con caratterizzazione Industriale”), for funding a Ph.D. grant to Francesco Taddeo. Federica Orabona is acknowledged for the experimental support.

Appendix A. Supplementary data

Supplementary data to this article can be found online at https://doi.org/10.1016/j.cej.2020.127236.

References

[1] C.-H. Zhou, X.i. Xia, C.-X. Lin, D.-S. Tong, J. Beltramini, Catalytic conversion of lignocellulosic biomass to fine chemicals and fuels, Chem. Soc. Rev. 40 (11) (2011) 5588, https://doi.org/10.1039/c1cs15124j.
[2] G.W. Huber, S. Iborra, A. Corma, Synthesis of transportation fuels from biomass: chemistry, catalysts, and engineering, Chem. Rev. 106 (9) (2006) 4044–4098.
[3] R.C. Saxena, D.K. Adhikari, H.B. Goyal, Biomass-based energy fuel through biochemical routes: a review, Renew. Sustain. Energy Rev. 13 (1) (2009) 167–178.
[4] B. Kamm, M. Kamm, P.R. Gruber, S. Kromus, Biorefinery systems - an overview, In: Biorefineries - Industrial Processes and Products: Status Quo and Future Directions, Eds. Wiley-VCH: Weinheim 1 (2008) 1–40.
[5] V.K.S. Pappu, V. Kanyi, A. Santhanakrishnan, C.T. Lira, D.J. Miller, Butyric acid esterification kinetics over Amberlyst solid acid catalysts: the effect of alcohol carbon chain length, Bioresour. Technol. 130 (2013) 793–797.
[6] V.V.S. Mbaraka, B. Shanks, Design of multifunctionalized mesoporous silicas for esterification of fatty acid, J. Catal. 229 (2) (2005) 365–373.
[7] M. Sharma, R.K. Wanchoo, A.P. Toor, Amberlyst 15 catalyzed esterification of nonanoic acidwith1-propanol: kinetics, modeling, and comparison of its reaction kinetics with lower alcohols, Ind. Eng. Chem. Res. 53 (2014) 2167–2174.
[8] V. Benessere, M.E. Cucciolito, A. De Santis, M. Di Serio, R. Esposito, M. Melchiorre, F. Nugnes, L. Paduano, F. Ruffo, A sustainable process for the production of varnishes based on pelargonic acid esters, J. Am. Oil Chem. Soc. 96 (4) (2019) 443–451.

[9] M. Sharma, R.K. Wanchoo, A.P. Toor, Adsorption and kinetic parameters for synthesis of methyl nonanoate over heterogeneous catalysts, Ind. Eng. Chem. Res. 51 (44) (2012) 14367–14375.
[10] S.Y. Chin, M.A.A. Ahmad, M.R. Kamaruzaman, C.K. Cheng, Kinetic studies of the esterification of pure and dilute acrylic acid with 2-ethylhexanol catalyzed by Amberlyst 15, Chem. Eng. Sci. 129 (2015) 116–125.
[11] K. Kaur, P. Jain, A. Sobti, A.P. Toor, Sulfated metal oxides: eco-friendly green catalysts for esterification of nonanoic acid with methanol, Green Process. Synth. 5 (2016) 93–100.
[12] Y. LIU, E. LOTERO, J. GOODWINJR, Effect of carbon chain length on esterification of carboxylic acids with methanol using acid catalysis, J. Catal. 243 (2) (2006) 221–228.
[13] Y. Jiang, J. Lu, K. Sun, L. Ma, J. Ding, Esterification of oleic acid with ethanol catalyzed by sulfonated cation exchange resin: experimental and kinetic studies, Energy Convers. Manag. 76 (2013) 980–985.
[14] V. Russo, V. Hrobar, P. Mäki-Arvela, K. Eränen, F. Sandelin, M. Di Serio, T. Salmi, Kinetics and Modelling of levulinic acid esterification in batch and continuous reactors, Top Catal. 61 (18-19) (2018) 1856–1865.
[15] M.A.A. Ahmad, S.Y. Chin, Screening of catalyst and important variable for the esterification of acrylic acid with 2 ethylhexanol, IOP Conf. Ser.: Mater. Sci. Eng. 206 (2017) 012064, https://doi.org/10.1088/1757-899X/206/1/012064.
[16] M. Sharma, A.P. Toor, R.K. Wanchoo, Reaction kinetics of catalytic esterification of nonanoic acid with ethanol over amberlyst 15, Int. J. Chem. React. Eng. 12(1) (2014) 451–463.
[17] A. Izci, F. Bodur, Liquid-phase esterification of acetic acid with isobutanol catalyzed by ion-exchange resins, React. Funct. Polym. 67 (2007) 1458–1464.
[18] M.R. Altıokka, A. Çıtak, Kinetics study of esterification of acetic acid with isobutanol in the presence of amberlite catalyst, Appl. Catal. A: Gen. 239 (1-2) (2003) 141–148.
[19] W. Osorio-Viana, M. Duque-Bernal, J. Fontalvo, I. Dobrosz-Gómez, M.Á. Gómez-García, Kinetic study on the catalytic esterification of acetic acid with isoamyl alcohol over Amberlite IR-120, Chem. Eng. Sci. 101 (2013) 755–763.
[20] S.Q. Merchant, K.A. Almohammad, A.A.M. Al Bassam, S.H. Ali, Biofuels and additives: comparative kinetic study of AmberliteIR 120-catalyzed esterification of ethanol with acetic, propanoic and pentanoic acids to produce eco-ethyl-esters, Fuel 111 (2013) 140–147.
[21] B.E. Poling, J.M. Prausnitz, J.P. O'Connell, The Properties of Gases and Liquids, McGrawHill, New York, 2000.
[22] ChemCAD v.7.0 https://www.chemstations.com/ (last visited 01/05/2020).
[23] R.H. Perry, D.W. Green, Perry's Chemical Engineers' Handbook, 7th ed., McGrawHill, New York, 1997, pp. 2–91, 2–93.
[24] M.R. Riazi, D. Chiaramonti, Biofuels Production and Processing Technology, CRC Press, Boca Raton, 2017.
[25] V. Russo, R. Tesser, C. Rossano, T. Cogliano, R. Vitiello, S. Leveneur, M. Di Serio, Kinetic study of Amberlite IR120 catalyzed acid esterification of levulinic acid with ethanol: from batch to continuous operation, Chem. Eng. J. 404 (2020) 126126.
[26] R. Tesser, L. Casale, D. Verde, M. Di Serio, E. Santacesaria, Kinetics and modeling of fatty acids esterification on acid exchange resins, Chem. Eng. J. 157 (2-3) (2010) 539–550.
[27] gPROMS Model Builder v. 4.0, https://www.psenterprise.com/.

II

catalysts

MDPI

Article

Kinetic Modeling of Solketal Synthesis from Glycerol and Acetone Catalyzed by an Iron(III) Complex

Francesco Taddeo, Roberto Esposito *, Vincenzo Russo * and Martino Di Serio

Department of Chemical Sciences, University of Naples Federico II, Complesso Universitario di Monte Sant'Angelo, 80126 Naples, Italy; francesco.taddeo@unina.it (F.T.); diserio@unina.it (M.D.S.)
* Correspondence: roberto.esposito@unina.it (R.E.); v.russo@unina.it (V.R.)

Abstract: In the last few years, the depletion of the fossil sources and their negative effect on the environment has led to find new alternatives; among these, biodiesel is considered one of the most promising for this purpose. Biodiesel can be produced from the transesterification of vegetable oils or animal fats, obtaining glycerol as a by-product. Glycerol can be used in different processes and one of the most interesting is the condensation with acetone to produce solketal. Among its applications, plasticizers, solvents, and pharmaceutical formulations are the most common. In this work, the attention was focused on the reaction between glycerol and acetone to give solketal promoted by an iron(III) complex. The reaction mechanism was hypothesized, and the kinetics was studied in a batch reactor. Finally, the thermodynamic and kinetic parameters were determined with a reliable model investigating the phenomena that occurred in the reaction network.

Keywords: solketal; kinetics; homogeneous catalysts; modeling; glycerol

Citation: Taddeo, F.; Esposito, R.; Russo, V.; Di Serio, M. Kinetic Modeling of Solketal Synthesis from Glycerol and Acetone Catalyzed by an Iron(III) Complex. *Catalysts* **2021**, *11*, 83. https://doi.org/10.3390/catal11010083

Received: 15 December 2020
Accepted: 7 January 2021
Published: 9 January 2021

1. Introduction

Nowadays, the economy is mainly based on petrochemical processes starting from fossil feedstock to obtain fine chemicals, polymers, and fuels [1].

The depletion of fossil resources has led to the search of new alternatives. Among them, biofuels, above all bio-ethanol and biodiesel [2], are considered as the most interesting to replace fossil fuels that are considered harmful to the environment as well as their non-renewable nature [3].

Biodiesel can be obtained through the transesterification of animal fats or vegetable oils with alcohols, usually methanol, in the presence of base catalysts [4], producing glycerol as a by-product [5]. The European Union has proposed the use of diesel mixed with biodiesel by 10% in the field of transportation, so an increasing production of biodiesel will be expected, and by 2020, glycerol production of 41.9 billion liters per year [3].

Glycerol can be used for several applications such as food, polymers, cosmetics, and pharmaceutical industries [6,7], but increasing biodiesel production has led to an excessive amount of glycerol in the market and a subsequent decrease in its commercial value [6,8]. The wide use of glycerol in such different fields is due to its properties; the three hydroxyl groups produce a solubility in water and alcohols, while an insolubility in hydrocarbons [2]. The high boiling point does not make it suitable for use in the mixture with gasoline [4]. An important application of glycerol is to produce value-added chemicals due to its biodegradable and nontoxic nature [9].

In addition, the conversion of wastes or by-products of industrial processes have a double advantage in terms of *Sustainability*. The use of waste or by-products of other bio-refineries allows for the restriction of production loops in line with the principles of a *Circular Economy*. At the same time, it is an example that biomass is a chemical platform capable of potentially replacing oil and petrochemicals. Many examples in this field already exist [10–15].

Glycerol is involved in several reactions to obtain ethers, esters, ketals, and acetals [4], but one of the most interesting processes for the conversion of glycerol is its condensation with acetone to produce solketal [1].

Solketal, known also as 4-hydroxymethyl-2,2-dimethyl-1,3-dioxolane, is used in many applications such as nontoxic solvents, plasticizers, suspending agents in pharmaceutical formulations [16], and has a high potential as fuel additives to increase ignitability and reduce particle emissions [17–19]. Furthermore, when it is added to gasoline and biodiesel formulation, it can improve their properties, satisfying the characteristics for flash point and oxidation stability [19]. The ketalization reaction to synthesize solketal is an equilibrium reaction, which has a low equilibrium constant [2,20]. One of the main drawbacks of this reaction is water production [21], so to shift the equilibrium to the solketal formation, an excess of acetone or the removal of water formed during the reaction is required [2,20]. However, another problem verified in this process is the poor miscibility of glycerol and acetone at 25 °C and 1 atm [2]. In this reaction, the selectivity toward the main product, the five membered molecule (solketal), is very high (about 98%) while that toward the six membered ring one, which is the by-product, is lower (about 2%) [22]. The production of glycerol ketals occurs in the presence of an acid catalyst, both heterogeneous and homogeneous [23].

Heterogeneous catalysts with the most promising performances are cation exchange resins such as Amberlyst-15, Amberlyst-36, zeolites, heteropolyacids, and sulfonic acid-modified mesostructured silicas [21,23,24].

Homogeneous catalysts show high efficiency, but are difficult to separate from the products and cannot be reused. Among them, Brønsted acids such as *p*-toluenesulfonic, sulfuric, and hydrochloric acid are used, but they cause the corrosion of reactors [16,21,22,25].

Switching to Lewis acid catalysis is a possible solution to overcome this drawback. This catalysis is widely used for the sustainable conversion of biomass and different metal salts and complexes can catalyze multiple transformations such as esterification, transesterification, oxidative cleavage of double bonds, and many others [26–32].

Ketalization of glycerol is one of these and Menezes et al. used a $SnCl_2$ catalyst, which shows good performances being easily recovered and reused without loss of activity [33]. Some of us proposed a class of homogeneous catalysts based on iron(III) complexes obtaining excellent results with a turn over frequency (TOF) of 10^5 h^{-1} by loading a very low catalyst amount (up to 10 ppm) [18,25].

Catalysts based on this non-noble, cheap, low toxic, and abundant metal can be a sustainable choice for the catalytic conversion of the biomass or derivatives [34]. At the same time, in order to scale up the process and move toward industrial applications, it is necessary to obtain the fundamental kinetic and catalytic parameters. Some examples of these basic investigations on this reaction, using different catalysts still exist [16,22,35,36].

In this work, a detailed kinetic study of solketal synthesis (Scheme 1), using a very promising homogeneous catalyst that was demonstrated to be very selective toward the solketal synthesis [18], an iron(III) complex, indicated as $FeCl_3$(1-NO_2) was made. The choice of this complex was guided by different factors: the high TOF showed in previous works [18,25]; the low hygroscopicity, high air-stability, and ease of handling of the material; and the presence of the pyridinimine ligand that allows for tunability of the acidity of the metal and can be the starting point for the synthesis of a supported homogeneous catalyst.

The reaction was conducted in a batch reactor investigating the effect of different operative conditions (e.g., temperature, catalyst load, and reactants' molar ratio) on the reaction rate. A mathematical model was developed to obtain the kinetic and thermodynamic parameters according to the collected experimental data.

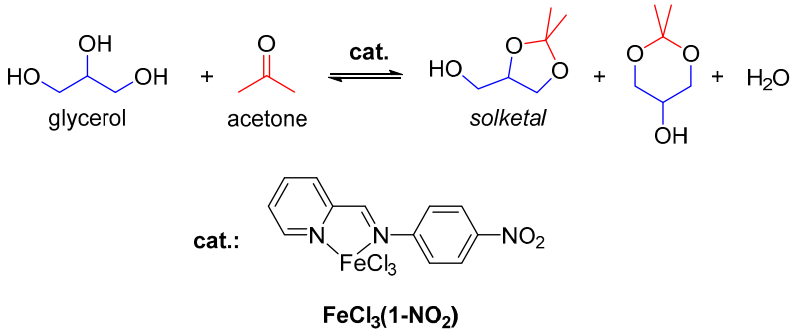

Scheme 1. Glycerol ketalization with acetone catalyzed by $FeCl_3(1\text{-}NO_2)$.

2. Results and Discussion

2.1. Kinetic Experiments of Glycerol Ketalization with Acetone Promoted by $FeCl_3(1\text{-}NO_2)$

Glycerol and acetone have been demonstrated to be rather immiscible when used in a 4:1 acetone/glycerol molar ratio [37,38], and it is important to verify if eventual liquid-liquid mass transfer limitations occur in the adopted experimental conditions. For this purpose, experiments were first conducted by varying the stirring rate. Similar results obtained at both 400 and 600 rpm for glycerol conversion and solketal selectivity implied the absence of liquid-liquid mass transfer limitation. The results are reported in Figure 1.

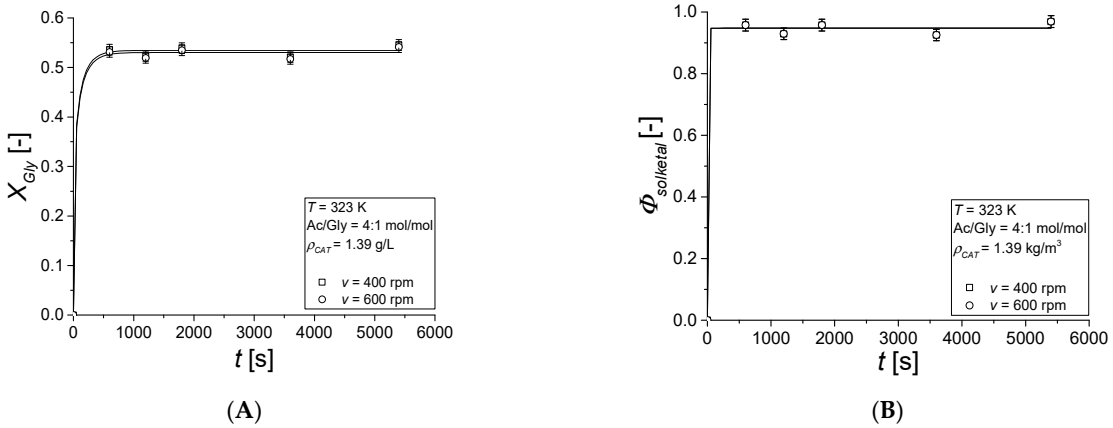

Figure 1. Stirring rate effect for catalyzed tests, fixing T = 323 K, Ac/Gly = 4:1 mol/mol, and ρ_{CAT} = 1.39 kg/m^3. (**A**) Glycerol conversion. (**B**) Selectivity toward solketal.

As revealed, the selectivity of this reaction was almost always near unity, as previously reported in the literature for the 5-membered acetal [16,39]. This aspect is mainly due to the thermodynamic stability of this compound compared to the 6-membered acetal and the mechanism favoring its production with respect to by-product.

Tests were performed at different temperatures (see Table 1 for details) to evaluate its effect on the reaction rate.

Table 1. Operation conditions for both blank (B) and catalyzed (C) kinetic experiments.

Run	v [rpm]	T [K]	Ac/Gly [mol/mol]	ρ_{CAT} [kg/m^3]
B	400	323	4:1	-
C1	600	323	4:1	1.39
C2	400	323	4:1	1.39
C3	400	323	4:1	2.62
C4	400	323	4:1	0.67
C5	400	323	4:1	0.33
C6	400	323	4:1	0.08
C7	400	323	4:1	0.04
C8	400	323	4:1	0.02
C9	400	313	4:1	0.02
C10	400	303	4:1	0.02
C11	400	303	4:1	0.04
C12	400	303	4:1	0.08
C13	400	303	4:1	0.25

From the experiments conducted at different temperature values, it can be verified that by increasing the temperature, the glycerol conversion also increased, while the solketal selectivity was similar in each test. The results are shown in Figure 2.

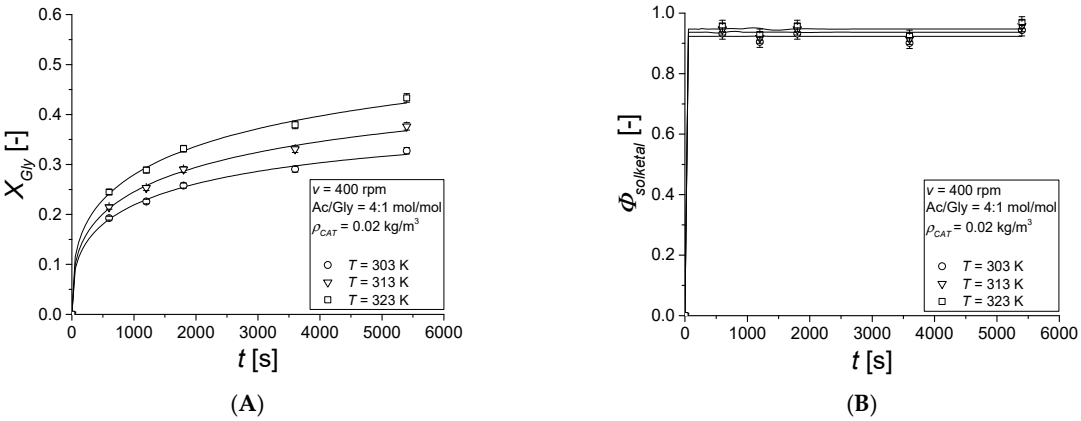

Figure 2. Temperature effect for catalyzed tests, fixing v = 400 rpm, Ac/Gly = 4:1 mol/mol, and ρ_{CAT} = 0.02 kg/m^3. (**A**) Glycerol conversion. (**B**) Selectivity toward solketal.

Two sets of experiments were made by evaluating the effect of the catalyst load on the reaction rate at two different temperature values. The first set was conducted at T = 323 K, while the second at T = 303 K.

The blank test (Table 1, Run B) showed that glycerol conversion was close to 0, so the reaction rate without a catalyst can be considered negligible.

For the experiments performed at 323 K, similar results were obtained in terms of glycerol conversion, except for those with a lower catalyst concentration (0.04 kg/m^3 and 0.02 kg/m^3) (see Figure 3A). It was possible to note that over the catalyst concentration of 0.33 kg/m^3, glycerol conversion became invariant with the catalyst load. This effect probably occurred because beyond a determined value of the catalyst load, the step of the

reaction catalyzed by $FeCl_3(1\text{-}NO_2)$ was no longer the limiting one, but the dehydration, which occurred independently of the catalyst, became the limiting step.

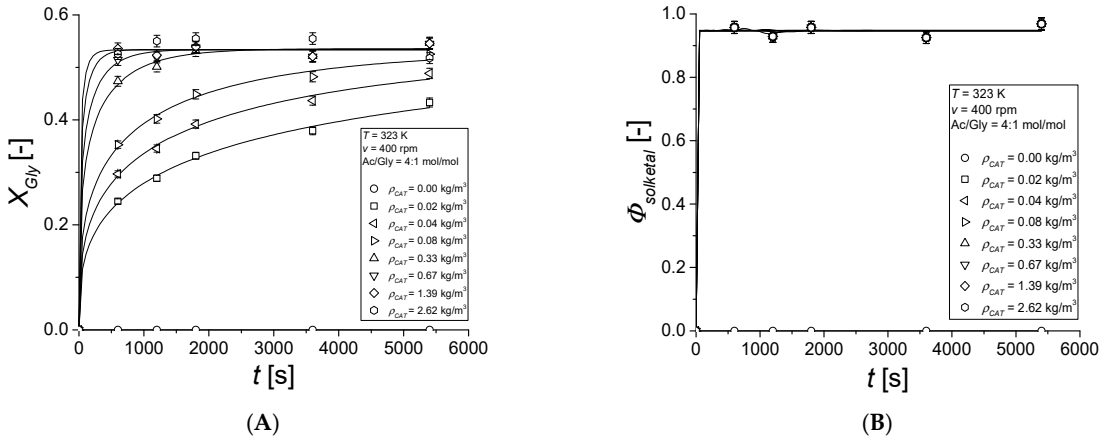

(**A**) (**B**)

Figure 3. Catalyst load effect for catalyzed tests, fixing v = 400 rpm, Ac/Gly = 4:1 mol/mol, and T = 323 K. (**A**) Glycerol conversion. (**B**) Selectivity toward solketal.

Lower conversion was reached in the experiments conducted at 303 K with respect to those performed at 323 K (Figure 4A). In both cases, similar values of solketal selectivity were obtained; a little variation occurred as the catalyst concentration changed, as reported in Figures 3B and 4B.

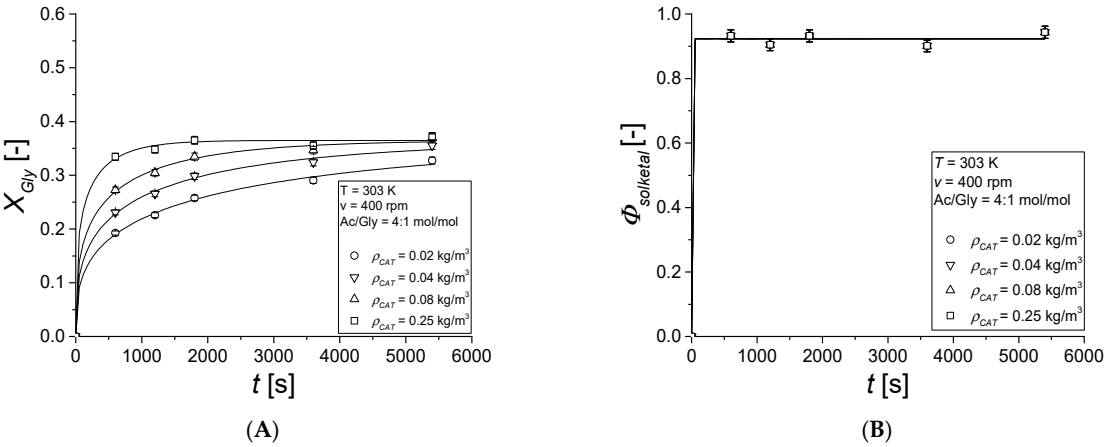

(**A**) (**B**)

Figure 4. Catalyst load effect for catalyzed tests, fixing v = 400 rpm, Ac/Gly = 4:1 mol/mol, and T = 303 K. (**A**) Glycerol conversion. (**B**) Selectivity toward solketal.

2.2. Kinetic Modeling

The hypothesized mechanism consisted of three reactions: (i) formation of the activated form of the iron-based catalyst ($Fe^*Cl_3(1\text{-}NO_2)$) by coordination of the carbonyl oxygen of acetone to the metal center; (ii) reaction between glycerol and the activated catalyst to obtain solketal through the nucleophilic attack of an oxygen of the glycerol to the carbonylic carbon of the coordinated acetone, the subsequent ring closure, and release of a molecule of water; and (iii) the analogous reaction between glycerol and the

activated catalyst to obtain the by-product. The scheme of this mechanism is reported below (Scheme 2).

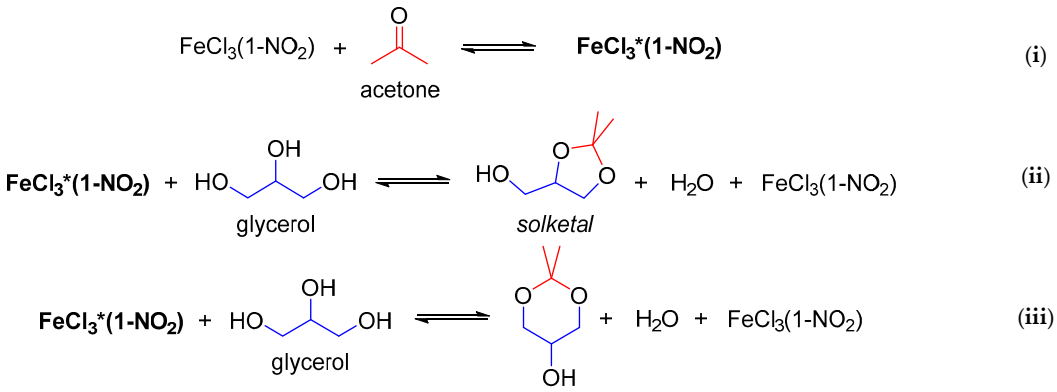

Scheme 2. Glycerol ketalization reaction scheme: (**i**) coordination of acetone to Fe(III) complex; (**ii**) glycerol ketalization to solketal; and (**iii**) glycerol ketalization to the by-product.

This mechanism is similar to that previously reported for a hexaaquairon(III) ion supported by a theoretical study [18] and is also in line with the mechanisms proposed in the literature for iron nitrate [40] and previously for others like Lewis acid catalysts [2].

The collected experimental data were interpreted with a reliable kinetic model considering the aforementioned mechanism. The reaction rates are expressed by Equations (1)–(3).

$$r_1 = k_1\left(c_{FeCl_3(1-NO_2)}c_{Ac} - \frac{1}{K_1}c_{Fe*Cl_3(1-NO_2)}\right) \quad (1)$$

$$r_2 = k_2\left(c_{Fe*Cl_3(1-NO_2)}c_{Gly} - \frac{1}{K_2}c_{FeCl_3(1-NO_2)}c_{solketal}c_{H_2O}\right) \quad (2)$$

$$r_3 = k_3\left(c_{Fe*Cl_3(1-NO_2)}c_{Gly} - \frac{1}{K_3}c_{FeCl_3(1-NO_2)}c_{BP}c_{H_2O}\right) \quad (3)$$

A modified Arrhenius and the van't Hoff equations (Equations (4) and (5)) were used in the model to express the relation between the kinetic and equilibrium constants and temperature for the three reactions reported in Scheme 2.

$$k = k_{ref}\exp\left(-\frac{Ea}{R}\left(\frac{1}{T} - \frac{1}{T_{ref}}\right)\right) \quad (4)$$

$$K = K_{ref}\exp\left(-\frac{\Delta_r H}{R}\left(\frac{1}{T} - \frac{1}{T_{ref}}\right)\right) \quad (5)$$

The reference temperature was fixed at T_{ref} = 303 K.

The mass balance equation, reported in Equation (6), was used in the model to describe the variation of each component with the reaction time.

$$\frac{dc_i}{dt} = \nu_i r \quad (6)$$

In Figures 1–4, it is possible to see the good agreement between the experimental and fitted data.

As reported in Figure 5A,B, the non-activated form of the catalyst disappeared for short times from the beginning of the reaction while at the same time, the amount of the catalyst in the activated form increased.

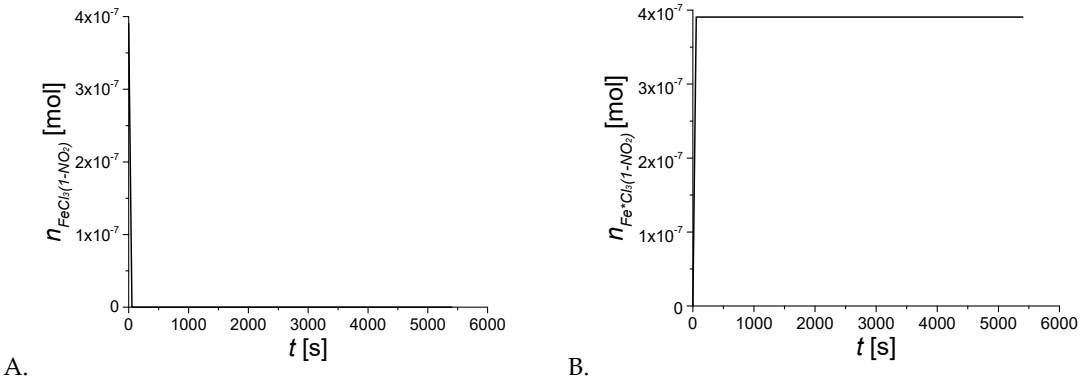

Figure 5. Catalyst forms vs. time. (**A**) Non-activated form. (**B**) Activated form.

Thanks to these results, it was possible to use a simplified model to estimate the kinetic and thermodynamic parameters neglecting the non-activated catalyst form. Furthermore, in this model, the reaction that led to the formation of the by-product (Equation (3)) was neglected since the selectivity toward solketal was close to the unity, as possible to see from Figures 1–4 and as already reported [18].

In Table 2, the kinetic and thermodynamic parameters obtained from the parameter estimation are listed.

Table 2. Parameter estimation results. CI: confidence interval at 95%.

	Value	95% CI	Units
$\Delta_r H_1$	30	1	kJ/mol
$\Delta_r H_2$	16.4	0.5	kJ/mol
Ea_1	13.0	0.5	kJ/mol
Ea_2	64	2	kJ/mol
Ea_3	63	3	kJ/mol
$K_{ref,1}$	0.55	0.05	-
$K_{ref,2}$	0.10	0.02	-
$K_{ref,3}$	8.1×10^{-3}	0.1×10^{-3}	-
$k_{ref,1}$	620	10	$(m^3/mol)\ s^{-1}$
$k_{ref,2}$	14.0×10^{7}	0.2×10^{7}	$(m^3/mol)\ s^{-1}$
$k_{ref,3}$	42.0×10^{5}	0.5×10^{5}	$(m^3/mol)\ s^{-1}$

From the parity plots reported in Figure 6A,B, it is possible to demonstrate that for both the glycerol conversion and solketal selectivity, all the data collected in the experiments fell in an error window of 5%.

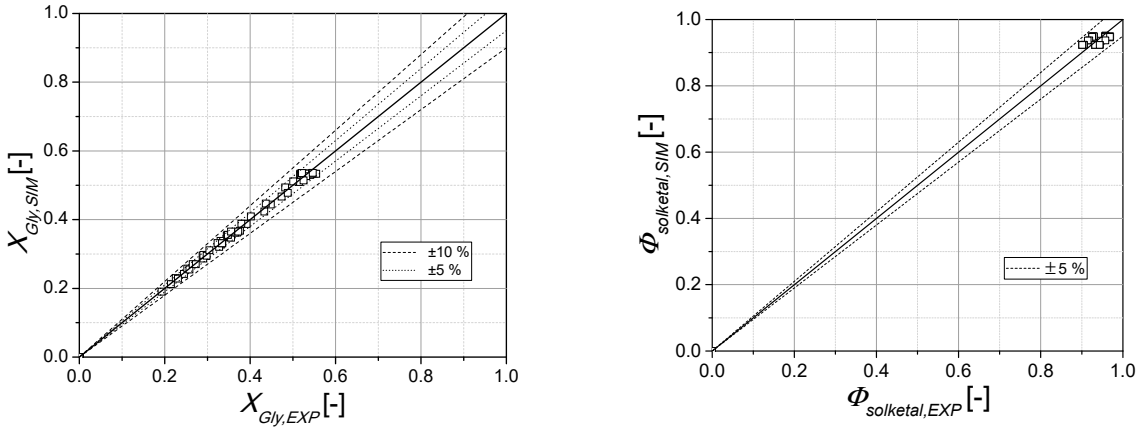

Figure 6. Parity plot for all the experimental data. (**A**) Glycerol conversion. (**B**) Solketal selectivity.

3. Materials and Method

3.1. Materials

All the reagents used in the kinetic experiments and for the catalyst preparation were purchased at the highest purity level by Merck KGAA, Darmstadt, Germany.

3.2. Catalyst Preparation

$FeCl_3$(1-NO_2): To a solution of 2-pyridinecarboxaldehyde (535 mg, 5.0 mmol) and 4-nitroaniline (771 mg, 5.0 mmol) in diethyl ether, anhydrous iron(III) chloride (810 mg, 5.0 mmol) was added. A yellow precipitate appeared, and the mixture was left at room temperature, under magnetic stirring for 30 min. After that time, the yellow solid was recovered by filtration, washed three times with diethyl ether, and finally dried in vacuum (90% yield). The compound was characterized by UV-Vis and IR, and the results compared with those reported in the literature [25]. UV-Vis in acetone: 363 nm (λ_{max}). Imine IR stretching (in nujol): 1626 cm^{-1}.

3.3. Reactor Setup and Procedure

The ketalization reaction was performed in a 0.3 L Hastelloy autoclave, equipped with a magnetically driven stirrer that allowed for the mixing of the reaction mixture with variable stirring through a control system. The reaction temperature was set and controlled through a thermoregulator connected to a heating jacket. In addition, a tank in which the catalyst was placed, was connected to the vessel. About 180 g of solution was weighed in the reactor, while the catalyst, dissolved in about 20 g of acetone, was loaded in the tank. The reactor was pre-heated at the desired temperature level and was pressurized with nitrogen to 5 bar to avoid the partition of the lowest boiling component between the gas and liquid phases. The catalyst solution was loaded into the vessel thanks to the nitrogen flow, after that, the desired temperature was reached. This time was considered as the starting point of the reaction and from this moment, samples were withdrawn at regular intervals to follow the reaction kinetics.

A first test (B in Table 1) was conducted in the absence of the catalyst, while the catalyzed experiments (listed with C in Table 1) were performed by varying stirring rate, temperature, and catalyst load.

Samples were analyzed through ^{1}H-NMR to evaluate the glycerol conversion and the selectivity toward solketal.

3.4. Analytical Method

Samples were analyzed by ^{1}H-NMR with a Bruker Avance Ultrashield (Bruker Corporation, Billerica, MA, USA) operating at a proton frequency of 400 MHz using D_2O as the solvent. The conversion was obtained by integrating the signals of methyl groups resonating at a chemical shift between 1.55 and 1.35 ppm (in red in Figure 7) and by comparing this integral (I_r) with the integral (I_b) of the signal resonating between 4.55 and 3.50 ppm (in blue in Figure 7), which corresponded to the signal of the proton of the glyceryl group of both the reactant (glycerol) and products (solketal and 2,2-dimethyl-1,3-dioxan-5-ol). The conversion (X_{Gly}) was calculated as follows:

$$X_{Gly} = \frac{5I_r}{6I_b} \tag{7}$$

The selectivity toward solketal was calculated comparing the integral (I_2) of signals resonating at 1.51 ppm (named 2 in Figure 7, corresponding to protons of a methyl of 2,2-dimethyl-1,3-dioxan-5-ol) and 1.41 ppm (named 1 in Figure 7, corresponding to protons of a methyl solketal). The selectivity ($\phi_{solketal}$) was calculated as follows:

$$\phi_{solketal} = 1 - \frac{I_2}{I_1} \tag{8}$$

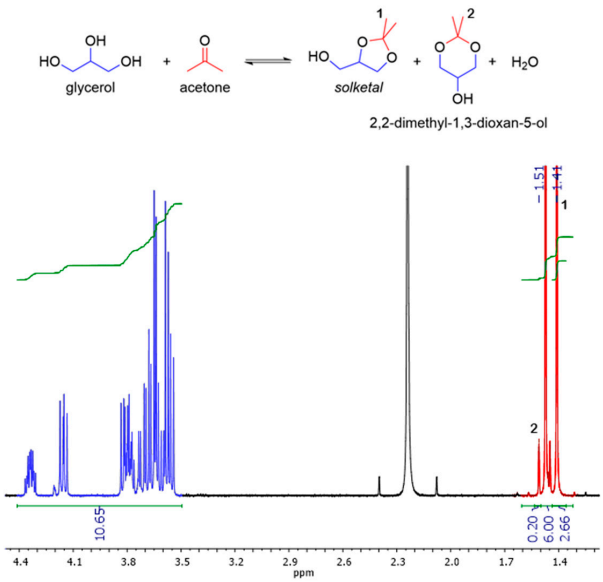

Figure 7. ^{1}H-NMR spectrum of a typical reaction mixture. In red, the integrals corresponding to the protons of the methyls of products, and in blue, the signals of the glyceryl portion of both the reactant and products.

4. Conclusions

The kinetics of the solketal synthesis promoted by an iron(III) complex was investigated. A reaction mechanism that consisted of three main steps was hypothesized as follows: (i) formation of the activated form of the iron-based catalyst ($FeCl_3$*(1-NO_2)); (ii) reaction between glycerol and the activated catalyst to obtain solketal; and (iii) reaction between glycerol and the activated catalyst to obtain the by-product. The reaction to obtain the by-product was neglected in the model since the selectivity toward solketal was close to the unity.

The activated form of the catalyst increased rapidly at the beginning of the reaction, while the non-activated form existed only in the first period from the beginning of the reaction itself.

The collected experimental data were elaborated with a reliable reactor model estimating the kinetic and thermodynamic parameters. The obtained results showed a good agreement between the experimental and the simulated curves.

Author Contributions: F.T.: Data curation, Formal analysis, Writing—original draft. R.E.: Conceptualization, Investigation, Supervision, Writing—review & editing. V.R.: Conceptualization, Investigation, Supervision, Writing—review & editing. M.D.S.: Project administration, Supervision, Writing—review & editing. All authors have read and agreed to the published version of the manuscript.

Funding: This research received no external funding.

Institutional Review Board Statement: Not applicable.

Informed Consent Statement: Not applicable.

Data Availability Statement: All the data of this study are presented within this paper itself and are openly available.

Acknowledgments: The authors wish to thank the European Union (FSE, PON Ricerca e Innovazione 2014-2020, Azione I.1 "Dottorati Innovativi con caratterizzazione Industriale") for funding a PhD grant to Francesco Taddeo. Roberto Esposito thanks the European Union and MIUR for funding through PON-AIM project code E61G19000090002, proposal code AIM1829571-1. Simone Silvestro is acknowledged for their experimental support.

Conflicts of Interest: The authors declare no conflict of interest.

Abbreviations

Ac	Acetone
BP	By-product
CI	Confidence interval
EXP	Experimental data
Gly	Glycerol
SIM	Simulated data
List of Symbols	**Explanation**
c_i	Concentration of component i [mol/m^3]
Ea	Activation energy of reaction [kJ/mol]
K	Equilibrium constant [-]
K_{ref}	Reference equilibrium constant [-]
k	Kinetic constant [(m^3/mol) s^{-1}]
k_{ref}	Reference kinetic constant [(m^3/mol) s^{-1}]
r	Rate of the reaction [mol/(m^3 s)]
R	Ideal gas constant [kJ/(K mol)]
t	Time [s]
T	Temperature [K]
T_{ref}	Reference temperature (303 K) [K]
v	Stirring speed [rpm]
X_{Gly}	Glycerol conversion degree [-]
Greek Letters	
$\Delta_r H$	Reaction enthalpy [kJ/mol]
η	Catalyst form [mol]
ν_i	Stoichiometric coefficient of component i [-]
ρ_{CAT}	Catalyst bulk density [kg/m^3]
$\phi_{solketal}$	Selectivity towards solketal [-]

References

1. Li, L.; Korányi, T.I.; Sels, B.F.; Pescarmona, P.P. Highly-efficient conversion of glycerol to solketal over heterogeneous Lewis acid catalysts. *Green Chem.* **2012**, *14*, 1611–1619. [CrossRef]
2. Nanda, M.R.; Zhang, Y.; Yuan, Z.; Qin, W.; Ghaziaskar, H.S.; Xu, C.C. Catalytic conversion of glycerol for sustainable production of solketal as a fuel additive: A review. *Renew. Sustain. Energy Rev.* **2016**, *56*, 1022–1031. [CrossRef]
3. Ilgen, O.; Yerlikaya, S.; Akyurek, F.O. Synthesis of Solketal from Glycerol and Acetone over Amberlyst-46 to Produce an Oxygenated Fuel Additive. *Period. Polytech. Chem. Eng.* **2016**, *61*, 144–148. [CrossRef]
4. Mota, C.J.A.; da Silva, C.X.A.; Rosenbach, N.; Costa, J.; Da Silva, F. Glycerin Derivatives as Fuel Additives: The Addition of Glycerol/Acetone Ketal (Solketal) in Gasolines. *Energy Fuels* **2010**, *24*, 2733–2736. [CrossRef]
5. Suriyaprapadilok, N.; Kitiyanan, B. Synthesis of Solketal from Glycerol and Its Reaction with Benzyl Alcohol. *Energy Procedia* **2011**, *9*, 63–69. [CrossRef]
6. Gui, Z.; Zahrtmann, N.; Saravanamurugan, S.; Reyero, I.; Qi, Z.; Bañares, M.A.; Riisager, A.; García-Suárez, E.J. Brønsted Acid Ionic Liquids (BAILs) as Efficient and Recyclable Catalysts in the Conversion of Glycerol to Solketal at Room Temperature. *Chem.* **2016**, *1*, 5869–5873. [CrossRef]
7. da Silva, G.P.; De Lima, C.J.B.; Contiero, J. Production and productivity of 1,3-propanediol from glycerol by Klebsiella pneuoniae GLC29. *Catal. Today* **2015**, *257*, 259–266. [CrossRef]
8. Royon, D.; Locatelli, S.; Gonzo, E. Ketalization of glycerol to solketal in supercritical acetone. *J. Supercrit. Fluids* **2011**, *58*, 88–92. [CrossRef]
9. Zhou, C.-H.; Beltramini, J.N.; Fan, Y.-X.; Lu, G.Q. (Max) Chemoselective catalytic conversion of glycerol as a biorenewable source to valuable commodity chemicals. *Chem. Soc. Rev.* **2008**, *37*, 527–549. [CrossRef]
10. Tuck, C.O.; Pérez, E.; Horváth, I.T.; Sheldon, R.A.; Poliakoff, M. Valorization of Biomass: Deriving More Value from Waste. *Science* **2012**, *337*, 695–699. [CrossRef]
11. Sheldon, R.A. Green chemistry and resource efficiency: Towards a green economy. *Green Chem.* **2016**, *18*, 3180–3183. [CrossRef]
12. Biermann, U.; Bornscheuer, U.; Meier, M.A.; Metzger, J.O.; Schäfer, H.J. Oils and Fats as Renewable Raw Materials in Chemistry. *Angew. Chem. Int. Ed.* **2011**, *50*, 3854–3871. [CrossRef] [PubMed]
13. Turco, R.; Tesser, R.; Cucciolito, M.E.; Fagnano, M.; Ottaiano, L.; Mallardo, S.; Malinconico, M.; Santagata, G.; Di Serio, M. Cynara cardunculus Biomass Recovery: An Eco-Sustainable, Nonedible Resource of Vegetable Oil for the Production of Poly(lactic acid) Bioplasticizers. *ACS Sustain. Chem. Eng.* **2019**, *7*, 4069–4077. [CrossRef]
14. Benessere, V.; Cucciolito, M.E.; De Santis, A.; Di Serio, M.; Esposito, R.; Melchiorre, M.; Nugnes, F.; Paduano, L.; Ruffo, F. A Sustainable Process for the Production of Varnishes Based on Pelargonic Acid Esters. *J. Am. Oil Chem. Soc.* **2019**, *96*, 443–461. [CrossRef]
15. Russo, V.; Taddeo, F.; Cogliano, T.; Vitiello, R.; Esposito, R.; Tesser, R.; Salmi, T.; Di Serio, M. Investigation of the intrinsic reaction kinetics and the mass transfer phenomena of nonanoic acid esterification with 2-ethylhexanol promoted by Sulfuric acid or Amberlite IR120. *Chem. Eng. J.* **2020**, 127236. [CrossRef]
16. Esteban, J.; Ladero, M.; García-Ochoa, F. Kinetic modelling of the solventless synthesis of solketal with a sulphonic ion exchange resin. *Chem. Eng. J.* **2015**, *269*, 194–202. [CrossRef]
17. Alsawalha, M. Catalytic Activity and Kinetic Modeling of Various Modules HZMS-5 and Treated MCM-41 Catalysts, for the Liquid-Phase Ketalization of Glycerol With Acetone. *Front. Chem.* **2019**, *7*, 799. [CrossRef]
18. Esposito, R.; Raucci, U.; Cucciolito, M.E.; Di Guida, R.; Scamardella, C.; Rega, N.; Ruffo, F. Iron(III) Complexes for Highly Efficient and Sustainable Ketalization of Glycerol: A Combined Experimental and Theoretical Study. *ACS Omega* **2019**, *4*, 688–698. [CrossRef]
19. Reddy, P.S.; Sudarsanam, P.; Mallesham, B.; Raju, G.; Reddy, B.M. Acetalisation of glycerol with acetone over zirconia and promoted zirconia catalysts under mild reaction conditions. *J. Ind. Eng. Chem.* **2011**, *17*, 377–381. [CrossRef]
20. Clarkson, J.S.; Walker, A.J.; Wood, M.A. Continuous Reactor Technology for Ketal Formation: An Improved Synthesis of Solketal. *Org. Process. Res. Dev.* **2001**, *5*, 630–635. [CrossRef]
21. Vicente, G.; Melero, J.A.; Morales, G.; Paniagua, M.; Martín, E. Acetalisation of bio-glycerol with acetone to produce solketal over sulfonic mesostructured silicas. *Green Chem.* **2010**, *12*, 899–907. [CrossRef]
22. Rossa, V.; Pessanha, Y.D.S.P.; Díaz, G.C.; Câmara, L.D.T.; Pergher, S.B.C.; Aranda, D.A.G. Reaction Kinetic Study of Solketal Production from Glycerol Ketalization with Acetone. *Ind. Eng. Chem. Res.* **2017**, *56*, 479–488. [CrossRef]
23. Maksimov, A.L.; Nekhaev, A.I.; Ramazanov, D.N.; Arinicheva, Y.; Dzyubenko, A.A.; Khadzhiev, S.N.; Maximov, A.L. Preparation of high-octane oxygenate fuel components from plant-derived polyols. *Pet. Chem.* **2011**, *51*, 61–69. [CrossRef]
24. Ferreira, P.; Fonseca, I.; Ramos, A.; Vital, J.; Castanheiro, J. Valorisation of glycerol by condensation with acetone over silica-included heteropolyacids. *Appl. Catal. B: Environ.* **2010**, *98*, 94–99. [CrossRef]
25. Esposito, R.; Cucciolito, M.E.; D'Amora, A.; Di Guida, R.; Montagnaro, F.; Ruffo, F. Highly efficient iron(III) molecular catalysts for solketal production. *Fuel Process. Technol.* **2017**, *167*, 670–673. [CrossRef]
26. Melchiorre, M.; Amendola, R.; Benessere, V.; Cucciolito, M.E.; Ruffo, F.; Esposito, R. Solvent-free transesterification of methyl levulinate and esterification of levulinic acid catalyzed by a homogeneous iron(III) dimer complex. *Mol. Catal.* **2020**, *483*, 110777. [CrossRef]

27. Esposito, R.; Melchiorre, M.; Annunziata, A.; Cucciolito, M.E.; Ruffo, F. Emerging catalysis in biomass valorisation: Simple Zn(II) catalysts for fatty acids esterification and transesterification. *ChemCatChem* **2020**, *12*, 5858. [CrossRef]
28. Benessere, V.; Cucciolito, M.E.; Dal Poggetto, G.; Di Serio, M.; Granados, M.L.; Ruffo, F.; Vitagliano, A.; Vitiello, R. Strategies for immobilizing homogeneous zinc catalysts in biodiesel production. *Catal. Commun.* **2014**, *56*, 81–85. [CrossRef]
29. Benessere, V.; Cucciolito, M.E.; Esposito, R.; Lega, M.; Turco, R.; Ruffo, F.; Di Serio, M. A novel and robust homogeneous supported catalyst for biodiesel production. *Fuel* **2016**, *171*, 1–4. [CrossRef]
30. Benessere, V.; Cucciolito, M.E.; De Santis, A.; Di Serio, M.; Esposito, R.; Ruffo, F.; Turco, R. Sustainable Process for Production of Azelaic Acid Through Oxidative Cleavage of Oleic Acid. *J. Am. Oil Chem. Soc.* **2015**, *92*, 1701–1707. [CrossRef]
31. Melchiorre, M.; Benessere, V.; Cucciolito, M.E.; Melchiorre, C.; Ruffo, F.; Esposito, R. Direct and Solvent-Free Oxidative Cleavage of Double Bonds in High-Oleic Vegetable Oils. *ChemistrySelect* **2020**, *5*, 1396–1400. [CrossRef]
32. Annunziata, A.; Esposito, R.; Gatto, G.; Cucciolito, M.E.; Tuzi, A.; Macchioni, A.; Ruffo, F. Iron(III) Complexes with Cross-Bridged Cyclams: Synthesis and Use in Alcohol and Water Oxidation Catalysis. *Eur. J. Inorg. Chem.* **2018**, *2018*, 3304–3311. [CrossRef]
33. Menezes, F.D.L.; Guimaraes, M.D.O.; da Silva, M.J. Highly Selective SnCl2-Catalyzed Solketal Synthesis at Room Temperature. *Ind. Eng. Chem. Res.* **2013**, *52*, 16709–16713. [CrossRef]
34. Du, H.; Deng, F.; Kommalapati, R.R.; Amarasekara, A.S. Iron based catalysts in biomass processing. *Renew. Sustain. Energy Rev.* **2020**, *134*, 110292. [CrossRef]
35. Moreira, M.; Faria, R.P.; Ribeiro, A.M.; Rodrigues, A.E. Solketal Production from Glycerol Ketalization with Acetone: Catalyst Selection and Thermodynamic and Kinetic Reaction Study. *Ind. Eng. Chem. Res.* **2019**, *58*, 17746–17759. [CrossRef]
36. Nanda, M.R.; Yuan, Z.; Qin, W.; Ghaziaskar, H.S.; Poirier, M.-A.; Xu, C.C. Thermodynamic and kinetic studies of a catalytic process to convert glycerol into solketal as an oxygenated fuel additive. *Fuel* **2014**, *117*, 470–477. [CrossRef]
37. Esteban, J.; García-Ochoa, F.; Ladero, M. Solventless synthesis of solketal with commercially available sulfonic acid based ion exchange resins and their catalytic performance. *Green Process. Synth.* **2017**, *6*, 79–89. [CrossRef]
38. Esteban, J.; Vorholt, A.J.; Behr, A.; Ladero, M.; Garcia-Ochoa, F. Liquid–Liquid Equilibria for the System Acetone + Solketal + Glycerol at (303.2, 313.2, and 323.2) K. *J. Chem. Eng. Data* **2014**, *59*, 2850–2855. [CrossRef]
39. Deutsch, J.; Martin, A.; Lieske, H. Investigations on heterogeneously catalysed condensations of glycerol to cyclic acetals. *J. Catal.* **2007**, *245*, 428–435. [CrossRef]
40. da Silva, M.J.; Rodrigues, A.A.; Pinheiro, P.F. Solketal synthesis from glycerol and acetone in the presence of metal salts: A Lewis or Brønsted acid catalyzed reaction? *Fuel* **2020**, *276*, 118164. [CrossRef]

La borsa di dottorato è stata cofinanziata con risorse del
Programma Operativo Nazionale Ricerca e Innovazione 2014-2020 (CCI 2014IT16M2OP005),
Fondo Sociale Europeo, Azione I.1 “Dottorati Innovativi con caratterizzazione Industriale”

UNIONE EUROPEA
Fondo Sociale Europeo

Ministero dell'Istruzione, dell'Università e della Ricerca

PON
RICERCA E INNOVAZIONE
2014 - 2020